Elsevier Editorial System(tm) for Renewable & Sustainable Energy Reviews
Manuscript Draft

Manuscript Number: RSER-D-18-03673R2

Title: Cyclic transient behavior of the Joule-Brayton based pumped heat electricity storage: Modeling and analysis

Article Type: Original Research Article

Section/Category: Energy Storage

Keywords: pumped heat electricity storage, pumped thermal electricity storage, Brayton, thermal energy storage, heat storage, energy storage

Corresponding Author: Professor Haisheng Chen,

Corresponding Author's Institution: Institute of Engineering Thermophysics, Chinese Academy of Sciences

First Author: Liang Wang

Order of Authors: Liang Wang; Xipeng Lin; Lei Chai; Long Peng; Dong Yu; Haisheng Chen

Abstract: Pumped heat electricity storage (PHES) has the advantages of a high energy density and high efficiency and is especially suitable for large-scale energy storage. The performance of PHES has attracted much attention which has been studied mostly based on steady thermodynamics, whereas the transient characteristic of the real energy storage process of PHES cannot be presented. In this paper, a transient analysis method for the PHES system coupling dynamics, heat transfer, and thermodynamics is proposed. Judging with the round trip efficiency and the stability of delivery power, the energy storage behavior of a 10 MW/4 h PHES system is studied with argon and helium as the working gas. The influencing factors such as the pressure ratio, polytropic efficiency, particle diameters, structure of thermal energy storage reservoirs are also analyzed. The results obtained indicate that, mainly owing to a small resistance loss, helium with a round-trip efficiency of 56.9% has an overwhelming advantage over argon with an efficiency of 39.3%. Furthermore, the increases in the pressure ratio and isentropic efficiencies improve the energy storage performance considerably. There also exit optimal values of the delivery compression ratio, particle sizes, length-to-diameter ratios of the reservoirs, and discharging durations corresponding to the maximum round-trip efficiency and preferable discharging power stability. The above can provide a basis for the optimal design and operation of the Joule-Brayton based PHES.

Response to Reviewers: Dear Editor,

We read the Editor’s and the reviewer’s comments carefully and response to the comments point by point accordingly in the following:

The editorial requirements 1) to 7) are as follows:
1) Submit the original manuscript showing clearly all textual changes using track changes. Just highlighting textual changes in yellow (or

other colour) is not acceptable. This includes all edits related to reviewer(s) comments and the Editorial points.
Reply: The revised draft based on the original manuscript with clearly all the changes using track changes will be submitted.

2) submit the clean revised version of the manuscript.
Reply: The clean revised version manuscript will be submitted.

3) Provide a 'Response to reviewers and Editor document' with a point by point response to each comment from the reviewer(s) and the Editor (i.e. points 1 to 7). Carefully and fully address the issues raised and refer to each comment from the reviewer(s) and the Editor clearly in the revised/edited/changed text in the marked-up copy of the original manuscript (e.g. line number X to Y on page X in the marked-up manuscript) in this response.
Reply: The reply letter with a point by point response to each comment from the reviewer(s) and the Editor will be submitted.

4) Read the 'Guide for Authors' at https://www.elsevier.com/journals/renewable-and-sustainable-energy-reviews/1364-0321/guide-for-authors very carefully. It is the sole responsibility of the author(s) to ensure that their article is correct and meets RSER style and format fully in terms of contents and layout (e.g. authorship, order of authorship, addresses, article structure, keywords, abbreviations, nomenclature, captions on figures and tables, acknowledgement of those that helped and or funded the research including datasets, references).
Reply: The authors have corrected the style and format fully in terms of contents and layout. Also the Elsevier Language Editing Services helped to correct the style and format of the manuscript.

5) Ensure that permission is attained for all copyrighted graphics, images, tables and/or figures. Note that for any figures, graphics or images published elsewhere by the author or others, the author(s) must arrange permission and this must be clearly stated in the 'Acknowledgements' section at the end of the article. If the author(s) cannot arrange permission, then the graphics, images, tables and or figure must be removed from the manuscript.
Reply: There are no copyrighted graphics, images, tables and or figure in this manuscript.

6) Check the English carefully for grammar, spelling and syntax. This is an English language journal. It is also not the role of reviewer(s), the Editor or indeed the publishing team to proof read the English, grammar and or syntax of a manuscript. The function of the reviewer(s) and an editor is to examine scope, robustness and technical content. Proof reading is the sole responsibility of the author(s), for example, articles are written in the first or third person and the use of "I," "we" or "they" should be avoided. Note if an article is revised and resubmitted with poor English, grammar and or syntax it will be rejected. Author(s) should get help from a colleague with better English, or alternatively a paid English language editing service of which there are many, could be arranged. For example, Elsevier offers author-paid language editing services via the Author Webshop, see http://webshop.elsevier.com/languageediting However, using an English language service (including Elsevier's) is NOT a guarantee that an article will be subsequently accepted for publication.

Reply: This manuscript has been edited by the Elsevier Language Editing Services to improve the English writing.

7) Check your manuscript for intentional or unintentional plagiarism of your own work or work by others elsewhere. All author(s) must read 'Ethics in publishing' in the 'Guide for Authors' and 'Publishing Ethics' at https://www.elsevier.com/about/our-business/policies/publishing-ethics and 'Ethical guidelines for journal publication' at https://www.elsevier.com/authors/journal-authors/policies-and-ethics The policy of RSER is to publish new and original work. Text, even in introductions, is the intellectual property of the original publication, and should never be used without clearly distinguishing that it is from another source (either by quotations or indentations). Author(s) cannot also reuse or recycle some (or indeed all) of their work published elsewhere as it is already covered by copyright. Each article should present some novelty and new result, and it is the Editor's opinion that this should be written in the author(s) own words. Unless the author(s) have a legitimate explanation for the large amount of textual overlap between their submitted manuscript and previously published work(s), an article will not be considered further for publication. All manuscripts submitted to RSER are checked for originality using the CrossRef Similarity Check database. For more information on CrossRef visit their website at http://www.crossref.org/crosscheck.html
Reply: The authors confirm that each part of this manuscript has not been published elsewhere.

Reviewers and/or Editors' comments:
Reviewer #1: This manuscript is resubmitted after a careful revising based on the comments from the first-round review. Therefore, I agree with the final publication.
Reply: The authors thank the reviewer's comments.

Reviewer #3: Accept as it is.
Reply: The authors thank the reviewer's comments.

Reviewer #4: This paper carried out transient simulation of pumped heat electricity storage system. The influences of different factors were investigated. However, the manuscript still has some drawbacks:
1. In the transient simulation of this paper, the author seems to set the pressure ratio of compressor a constant value (7, 10 or 13 as shown in Fig. 10). However, should the pressure ratio keep a constant during the transient process of charging or discharging?
Reply: The authors thank the reviewer's comments.
In this section, the compression ratio βc is set to 7, 10 and 13 in figure 10(b) where the expansion ratio βe is not constant value during the transient process of charging or discharging. Owing to the transient variation of the pressure loss in the hot reservoir and the cold reservoir, as shown in Fig 9(c), the expansion ratio βe changes transient over time and is less than the compression ratio βc.

2. The descriptions of models used in this paper are not clear. For example, the transient models of turbo machines are missing. The relationship between pressure ratio, mass flow rate and shaft speed during the transient process should be presented in the paper. And Eq. (15) and (16) should be explained in detail.
Reply: The transient models of turbo machines have been added in the text at section 3.2.1 as below. And the relationship of volume flow rate and

shaft speed during the transient process have been presented in the paper where the mass flow rate is set to a constant value in this study, please see equation (6).
In section 3.2.1, the following analysis have been added.
"During the charging and discharging process, temperatures and densities of the HR and CR outflow gas transiently vary leading to the variation of volume flow rates and rotation rates in the compressor and the expander. The unsteady variation of the turbo-machines shaft power P(t) owing to the inertia of rotors can be calculated by equation (5).
Where I is the moment of inertia of rotor and $\omega(t)$ is the angular velocity. The angular velocity is proportional to the volume flow rate Q(t) and inversely proportional to the gas density at the constant mass flow rate, with equation (6)
Where ωdes and Qdes are the angular velocity and the volume flow rate under the design condition, respectively."
In section 3.3, the following analysis have been added.
"For the PHES system, the transient specific energy performed during charging and delivered during discharging, with considering the unsteadiness of the compressor and expander, can be obtained using equation (17) and equation (18), respectively.
As shown in equation (5), the moment of inertia of the compressor and the expander are needed for calculating P(t), whereas there is no available compressor and expander for the 10MW PTES system. In this study, referring to the compressor and the expander in the 10MW Advanced compressed air energy storage, the moment of inertia of compressor and the expander rotor is taken 1800 kgm2 at the rated speed of 1500 rpm [42, 43]. Under the situations in this study, the maximum absolute value of angular acceleration of the expander rotor and the compressor rotor is 0.0063 rad/s2 and 0.0026 rad/s2 respectively, and the corresponding Pe(t) and Pc(t) is -3.47 kW and 0.36 kW, which are less than ±0.04% of the transient shaft power and can be neglected.
By bringing equation (3), (4) into equation (15), (16), and neglecting the unsteady variation of the turbine machines, the transient specific energy can be calculated using equation (19) for the charging process and equation (20)for the discharging process.
Where echr and edis are specific energy (J/kg) of shaft work during charging and discharging, Tc,in and Te,in are the inflow temperatures (K) of the compressor and the expander during charging, and the superscript 'denotes the discharging process."

3. The arrangement of this paper should be improved a lot. For example, the Section 3 is followed by Section 5. Section 6.1 is directly followed by Section 6.2.1. The Section 6.2 should be arranged before 6.2.1. And the paper is divided into too many sections, it would be better if the author can arrange it in 4 or 5 sections.
Reply: These mistakes have been corrected and the text has been rearranged in 5 sections.

Over all, as mentioned by other reviewers, the main problems of this paper are still the structure and writing. The author should take a positive attitude to improve the quality of this paper, or the paper is not suggested to be published on RSER journal.
Reply: The structure and writing of this paper has been revised carefully.

Reply letter regarding "Cyclic transient behavior of the Joule–Brayton based pumped heat electricity storage: Modeling and analysis"

Dear Editor,

We read the Editor's and the reviewer's comments carefully and response to the comments point by point accordingly in the following:

The editorial requirements 1) to 7) are as follows:

1) Submit the original manuscript showing clearly all textual changes using track changes. Just highlighting textual changes in yellow (or other colour) is not acceptable. This includes all edits related to reviewer(s) comments and the Editorial points.

Reply: The revised draft based on the original manuscript with clearly all the changes using track changes will be submitted.

2) submit the clean revised version of the manuscript.

Reply: The clean revised version manuscript will be submitted.

3) Provide a 'Response to reviewers and Editor document' with a point by point response to each comment from the reviewer(s) and the Editor (i.e. points 1 to 7). Carefully and fully address the issues raised and refer to each comment from the reviewer(s) and the Editor clearly in the revised/edited/changed text in the marked-up copy of the original manuscript (e.g. line number X to Y on page X in the marked-up manuscript) in this response.

Reply: The reply letter with a point by point response to each comment from the reviewer(s) and the Editor will be submitted.

4) Read the 'Guide for Authors' at https://www.elsevier.com/journals/renewable-and-sustainable-energy-reviews/1364-0321/guide-for-authors very carefully. It is the sole responsibility of the author(s) to ensure that their article is correct and meets RSER style and format fully in terms of contents and layout (e.g. authorship, order of authorship, addresses, article structure, keywords, abbreviations, nomenclature, captions on figures and tables, acknowledgement of those that helped and or funded the research including datasets, references).

Reply: The authors have corrected the style and format fully in terms of contents and layout. Also the Elsevier Language Editing Services helped to correct the style and format of the manuscript.

5) Ensure that permission is attained for all copyrighted graphics, images, tables and/or figures. Note that for any figures, graphics or images published elsewhere by the author or others, the author(s) must arrange permission and this must be clearly stated in the 'Acknowledgements' section at the end of the article. If the author(s) cannot arrange permission, then the graphics, images, tables and or figure must be removed from the manuscript.

Reply: There are no copyrighted graphics, images, tables and or figure in this manuscript.

6) Check the English carefully for grammar, spelling and syntax. This is an English language journal. It is also not the role of reviewer(s), the Editor or indeed the publishing team to proof read the English, grammar and or syntax of a manuscript. The function of the reviewer(s) and an editor is to examine scope, robustness and technical content. Proof reading is the sole responsibility of the author(s), for example, articles are written in the first or third person and the use of "I," "we" or "they" should be avoided. Note if an article is revised and resubmitted with poor English, grammar and or syntax it will be rejected. Author(s) should get help from a colleague with better English, or alternatively a paid English language editing service of which there

are many, could be arranged. For example, Elsevier offers author-paid language editing services via the Author Webshop, see http://webshop.elsevier.com/languageediting However, using an English language service (including Elsevier's) is NOT a guarantee that an article will be subsequently accepted for publication.

Reply: This manuscript has been edited by the Elsevier Language Editing Services to improve the English writing.

7) Check your manuscript for intentional or unintentional plagiarism of your own work or work by others elsewhere. All author(s) must read 'Ethics in publishing' in the 'Guide for Authors' and 'Publishing Ethics' at https://www.elsevier.com/about/our-business/policies/publishing-ethics and 'Ethical guidelines for journal publication' at https://www.elsevier.com/authors/journal-authors/policies-and-ethics The policy of RSER is to publish new and original work. Text, even in introductions, is the intellectual property of the original publication, and should never be used without clearly distinguishing that it is from another source (either by quotations or indentations). Author(s) cannot also reuse or recycle some (or indeed all) of their work published elsewhere as it is already covered by copyright. Each article should present some novelty and new result, and it is the Editor's opinion that this should be written in the author(s) own words. Unless the author(s) have a legitimate explanation for the large amount of textual overlap between their submitted manuscript and previously published work(s), an article will not be considered further for publication. All manuscripts submitted to RSER are checked for originality using the CrossRef Similarity Check database. For more information on CrossRef visit their website at http://www.crossref.org/crosscheck.html

Reply: The authors confirm that each part of this manuscript has not been published elsewhere.

Reviewers and/or Editors' comments:

Reviewer #1: This manuscript is resubmitted after a careful revising based on the comments from the first-round review. Therefore, I agree with the final publication.

Reply: The authors thank the reviewer's comments.

Reviewer #3: Accept as it is.

Reply: The authors thank the reviewer's comments.

Reviewer #4: This paper carried out transient simulation of pumped heat electricity storage system. The influences of different factors were investigated. However, the manuscript still has some drawbacks:

1. In the transient simulation of this paper, the author seems to set the pressure ratio of compressor a constant value (7, 10 or 13 as shown in Fig. 10). However, should the pressure ratio keep a constant during the transient process of charging or discharging?

Reply: The authors thank the reviewer's comments.

In this section, the compression ratio β_c is set to 7, 10 and 13 in figure 10(b) where the expansion ratio β_e is not constant value during the transient process of charging or discharging. Owing to the transient variation of the pressure loss in the hot reservoir and the cold reservoir, as shown in Fig 9(c), the expansion ratio β_e changes transient over time and is less than the compression ratio β_c.

2. The descriptions of models used in this paper are not clear. For example, the transient models of turbo machines are missing. The relationship between pressure ratio, mass flow rate and shaft speed during the transient process should be presented in the paper. And Eq. (15) and (16) should be explained in detail.

Reply: The transient models of turbo machines have been added in the text at section 3.2.1 as below. And the relationship of volume flow rate and shaft speed during the transient process have been presented in the paper where the mass flow rate is set to a constant value in this study, please see equation (6).

In section 3.2.1, the following analysis have been added.

"During the charging and discharging process, temperatures and densities of the HR and CR

outflow gas transiently vary leading to the variation of volume flow rates and rotation rates in the compressor and the expander. The unsteady variation of the turbo-machines shaft power P(t) owing to the inertia of rotors can be calculated by:

$$P(t) = -I \cdot \omega(t) \frac{\mathrm{d}\omega(t)}{\mathrm{d}t} \tag{5}$$

Where I is the moment of inertia of rotor and ω(t) is the angular velocity. The angular velocity is proportional to the volume flow rate Q(t) and inversely proportional to the gas density at the constant mass flow rate.

$$\omega(t) = \frac{\omega_{\mathrm{des}}}{Q_{\mathrm{des}}} Q(t) = \frac{\omega_{\mathrm{des}}\rho_{\mathrm{des}}}{\rho(t)} \tag{6}$$

Where ω_{des} and Q_{des} are the angular velocity and the volume flow rate under the design condition, respectively."

In section 3.3, the following analysis have been added.

"For the PHES system, the transient specific energy performed during charging and delivered during discharging, with considering the unsteadiness of the compressor and expander, can be obtained using equation (17) and equation (18), respectively.

$$e_{\mathrm{chr}}(t) = e_{\mathrm{c,chr}}(t) - e_{\mathrm{e,chr}}(t) + \frac{1}{\dot{m}c_{\mathrm{p}}}\left(P_{\mathrm{e}}(t) + P_{\mathrm{c}}(t)\right) \tag{17}$$

$$e_{\mathrm{dis}}(t) = e_{\mathrm{e,dis}}(t) - e_{\mathrm{c,dis}}(t) - \frac{1}{\dot{m}c_{\mathrm{p}}}\left(P_{\mathrm{e}}(t) + P_{\mathrm{c}}(t)\right) \tag{18}$$

As shown in equation (5), the moment of inertia of the compressor and the expander are needed for calculating P(t), whereas there is no available compressor and expander for the 10MW PTES system. In this study, referring to the compressor and the expander in the 10MW Advanced compressed air energy storage, the moment of inertia of compressor and the expander rotor is taken 1800 kgm^2 at the rated speed of 1500 rpm [42, 43]. Under the situations in this study, the maximum absolute value of angular acceleration of the expander rotor and the compressor rotor is 0.0063 rad/s^2 and 0.0026 rad/s^2 respectively, and the corresponding P_e(t) and P_c(t) is -3.47 kW and 0.36 kW, which are less than ±0.04% of the transient shaft power and can be neglected.

By bringing equation (3), (4) into equation (15), (16), and neglecting the unsteady variation of the turbine machines, the transient specific energy can be calculated as below:

For the charging process,

$$e_{\mathrm{chr}}(t)=T_{\mathrm{c,in}}(t)\cdot\left(r_{\mathrm{c}}(t)^{\kappa/\eta_{\mathrm{c}}}-1\right)-T_{\mathrm{e,in}}(t)\cdot\left(1-r_{\mathrm{e}}(t)^{-\kappa\eta_{\mathrm{e}}}\right) \tag{19}$$

For the discharging process,

$$e_{\mathrm{dis}}(t)=T'_{\mathrm{e,in}}(t)\cdot\left(1-r'_{\mathrm{e}}(t)^{-\kappa\eta_{\mathrm{e}}}\right)-T'_{\mathrm{c,in}}(t)\cdot\left(r'_{\mathrm{c}}(t)^{\kappa/\eta_{\mathrm{c}}}-1\right) \tag{20}$$

Where e_{chr} and e_{dis} are specific energy (J/kg) of shaft work during charging and discharging, $T_{\mathrm{c,in}}$ and $T_{\mathrm{e,in}}$ are the inflow temperatures (K) of the compressor and the expander during charging, and the superscript ‘denotes the discharging process.”

3. The arrangement of this paper should be improved a lot. For example, the Section 3 is followed by Section 5. Section 6.1 is directly followed by Section 6.2.1. The Section 6.2 should be arranged before 6.2.1. And the paper is divided into too many sections, it would be better if the author can arrange it in 4 or 5 sections.

Reply: These mistakes have been corrected and the text has been rearranged in 5 sections.

Over all, as mentioned by other reviewers, the main problems of this paper are still the structure and writing. The author should take a positive attitude to improve the quality of this paper, or the paper is not suggested to be published on RSER journal.

Reply: The structure and writing of this paper has been revised carefully.

*Marked Version of revised manuscript

Cyclic transient behavior of the Joule–Brayton based pumped heat electricity storage: Modeling and analysis

Liang Wang[1, 2], Xipeng Lin[1], Lei Chai[3], Long Peng[1], Dong Yu[1], Haisheng Chen[1, 2]

(1Institute of Engineering Thermophysics, Chinese Academy of Sciences, Beijing 100190, People's Republic of China; 2University of Chinese Academy of Sciences, Beijing 100049, People's Republic of China; 3RCUK National Centre for Sustainable Energy Use in Food Chain (CSEF), Brunel University London, Uxbridge, Middlesex UB8 3PH, United Kingdom)

*Corresponding author. Tel.: +86 10 82543148, E-mail: chen_hs@iet.cn

Abstract

Pumped heat electricity storage (PHES) has the advantages of a high energy density and high efficiency and is especially suitable for large-scale energy storage. The performance of PHES has attracted much attention which has been studied mostly based on steady thermodynamics, whereas the transient characteristic of the real energy storage process of PHES cannot be presented. In this paper, a transient analysis method for the PHES system coupling dynamics, heat transfer, and thermodynamics is proposed. Judging with the round trip efficiency and the stability of delivery power, the energy storage behavior of a 10 MW/4 h PHES system is studied with argon and helium as the working gas. The influencing factors such as the pressure ratio, polytropic efficiency, particle diameters, structure of thermal energy storage reservoirs are also analyzed. The results obtained indicate that, mainly owing to a small resistance loss, helium with a round-trip efficiency of 56.9% has an overwhelming advantage over argon with an efficiency of 39.3%. Furthermore, the increases in the pressure ratio and isentropic efficiencies improve the energy storage performance considerably. There also exit optimal values of the delivery compression ratio, particle sizes, length-to-diameter ratios of the reservoirs, and discharging durations corresponding to the maximum round-trip efficiency and preferable discharging power stability. The above can provide a basis for the optimal design and operation of the Joule–Brayton based PHES.

Key words: pumped heat electricity storage, pumped thermal electricity storage, Brayton, thermal energy storage, heat storage, energy storage

1 Introduction

The increase in energy consumption and the demand for decrease in carbon emission have result in great changes in the global energy structure owing to which the proportion of renewable energy usage has increased and that of fossil energy has gradually decreased [1]. From 2007 to 2017, the total renewable power capacity of non-hydropower renewables increased more than six-fold (that of solar energy and wind energy increased 48-fold and six-fold respectively) [1, 2]. In particular in 2017, renewable power accounted for 70% of net additions to the global power generation capacity and 26.5% of the global electricity production [1, 2]. However, the majority of renewable energy resources have inherent intermittency and instability characteristics, which results in the carryover of oscillation and unreliability to the power network. For example, 6% photovoltaic power and 12% wind power was wasted in China in 2017 [3]. Electrical energy Storage (EES) that converts electrical energy into another form of energy for storage and converts it back to electrical energy when required, is considered as one of the most promising solutions for increasing the penetration depth of renewable energy resources [4, 5]. Moreover, EES is an essential link in the energy supply chain, which provides services such as load leveling, peaking shaving, power quality improvement, and frequency regulation for the traditional power grid, thus improving the security and utilization rate of the power grid [6-8].

Nowadays, there exist various energy storage technologies and different criteria for their classification. Based on the form of energy storage in the system, the energy storage technologies can be mainly categorized into five classes: chemical (hydrogen and synthetic natural gas), electrical (capacitors and superconducting magnetic), electrochemical (classic batteries and flow batteries), mechanical (flywheels, adiabatic compressed air, pumped heat electrical storage, pumped hydro and cryogenic energy storage) and thermal (sensible heat, latent heat and thermochemical heat) [4, 5]. Each EES technology has a suitable range of applications (e.g. batteries, compressed air energy storage (CAES), and pumped hydro storage are suitable candidates for peak shaving; flywheels, super-capacitors and superconducting magnetic energy storage are suitable candidates for frequency regulation) depending on its advantages, drawbacks, and scales [4, 9].

Among the available storage technologies, only pumped hydro storage (PHS) and CAES are mature large-scale stand-alone electricity storage technologies that can be used to store power greater than 100 MW under commercial operation [4, 5, 10]. PHS is the most mature EES technology having a high capacity, long storage period, high efficiency and relatively low cost per unit of energy. To date, there are more than 300 facilities with a total power of over 170 GW in operation, which accounts for approximately 96% of the global energy storage capacity [4, 11]. The Bath County Pumped Storage Station in the USA is the largest PHS power station in the world which has a generation capacity of 3 GW and a storage capacity of 11 h [12]. CAES is another mature technology that is typically used for large scale energy storage. The operational CAES units in the world are 290 MW/2 h CAES in Huntorf, Germany with an underground storage cavern of approximately 310,000 m^3 and 110 MW/26 h CAES in McIntosh, Alabama, USA, with a cavern of approximately 500,000 m^3 [4, 5, 13]. The main barriers for PHS and CAES plants are similar, in that their construction requires appropriate geographical conditions for the huge volume of storage.

A category of novel energy storage technologies "pumped heat electricity storage (PHES)" was proposed, which is also called "pumped thermal electricity storage (PTES)" and "thermo-electrical energy storage (TEES)". During the charging process of the energy storage, heat is pumped from cold reservoirs (CRs) to hot reservoirs (HRs) via a heat pump circle and then stored; during the discharging process electricity is generated by the stored thermal energy through the heat-work conversion circle. Owning to the advantages of its high energy density and high efficiency, PHES has captured the attention of researchers as a promising technology for large-scale energy storage in recent years [14-31]. The categories of the PHES systems is mainly based on two types of reversible heat-work conversion circles thus far: The Joule–Brayton cycles [25-31] and the Rankine cycles [14-24].

The Rankine-cycle-based PHES system was first proposed by the ABB Company by the name of TEES [14, 15]. It mainly includes the transcritical CO_2 Rankine cycle, organic Rankine cycles (ORCs), and subcritical stream Rankine cycle. Morandin et al. studied a TEES system based on a transcritical CO_2 Rankine cycle with hot-water thermal storage and ice-cold storage, and then optimized the system with an achieved round-trip efficiency of 60% on using the pinch analysis approach [16, 17]. Kim et al. then presented an isothermal TEES system based on the transcritical CO_2 Rankine cycle wherein water was sprayed to cool/heat transcritical CO_2 directly, and it was found that the expansion work and efficiency were improved via the isothermal expansion owing to the high efficient heat transfer with the thermal storage tanks [18]. Abarr et al. proposed the use of a PTES and bottoming system based on the transcritical ammonia cycle connected to a natural-gas peak plant and the obtained result indicates that the stand-alone energy storage efficiencies is between 51%-66% with a stand-alone bottoming efficiency of 24% [19, 20]. Wang and Zhang proposed and analyzed a PHES based on the transcritical CO_2 heat pump cycle during charging and the cascaded system of the transcritical CO_2 Rankine cycle and the subcritical NH3 Rankine cycle utilizing liquid natural gas cold energy with a round-trip efficiency of up to 139% [21]. Steinmann developed the compressed heat energy storage (CHEST) concept based on stream Rankine cycles combined with sensible and latent heat storage with an estimated round-trip efficiency of 70% based on the isentropic efficiencies of 0.9 [22]. A PHES based on the ORC system with the integration of low-temperature heat was also studied. Jockenhöfer et al. found that the ORC-CHEST system could provide 1.25 times the net power with a heat resource temperature of 100°C and a maximum exergetic efficiency of 0.59 [23]. Frate et al. studied a PHES system comprising of a vapor-compression heat pump integrated with a low-grade heat source for charging and an ORC system for discharging and found that the achievable round-trip efficiency was 130% on using R1233zd at the heat source temperature of 110 °C and the isentropic efficiency was 0.8 [24].

Using a single-phase gas as the working fluid, the Joule–Brayton-cycle based PHES generally consists of cold (low-pressure) thermal energy storage (TES) reservoirs, hot (high-pressure) TES reservoirs, and compressor–turbine-pairs, wherein the CRs and HRs are generally comprise packed-bed solid thermal energy storage owning to its wide temperature range, high efficiency, and small pressure loss. Desrues et al. presented a PHES system based on the Joule–Brayton cycle consisting of two TES reservoirs connected by two compressor-turbine-pairs and two heat exchangers comprising argon as the working gas and obtained an optimized round-trip efficiency of 66.7% based on the turbo machines' polytrophic efficiency of 0.9 [25]. Ni and Caram analyzed the influence of gas and pressure ratios etc. through a simulation and found the efficiency of the turbomachinery to be the factor limiting the round-trip efficiency [26]. Howes from the company Isentropic introduced three prototype of PTES and proposed a 2 MW PTES system with heat and cold thermal storage temperatures of 500 °C and -160 °C having a round-trip efficiency of up to 72% [27]. White et al. found that the round-trip efficiency and energy storage density increase with the temperature ratio between the hot and cold TES [28]. McTigue et al. presented a PTES system based on the Joule–Brayton cycle with a buffer vessel and performed a theoretical analysis on the PTES system coupled with a packed bed model of the HRs and CRs [29]. Benato presented a Joule–Brayton PHES system with an electric heater settled after the compressor in order to maintain the hot–tank temperature during charging, and the performance and cost evaluation of such a system with different TES materials and different working gases was analyzed [30,31].

There are mainly three categories of TES technologies: sensible heat storage, latent heat storage, and chemical heat storage [32]. Among the TES technologies, packed bed sensible TES has been identified as the most suitable technology for the PHES system owing to its advantages of low cost, small pressure loss, wide applicable temperature range, and large heat transfer surface area that results in a small temperature difference, etc. [30].

The performance of a PHES comprising heat and cold packed–bed reservoirs of different materials was analyzed in terms of the round-trip efficiency [25, 29, 30], energy density [30, 31], and costs [30, 31]. However, there still exist defects in the published studies: (1) such a PHES comprising heat and cold packed-bed reservoirs have strong unsteady characteristics whereas the majority of the analyses on the PHES were performed using the stable thermodynamics method, (2) it is not based on continuous cycles, and the initial state of each cycle is strong related to the state at the end of last cycle for the continuous cycles, (3) it neglects the coupling effect of dynamics, heat transfer and thermodynamics, (4) it involves the oversimplification of heat exchangers, and (5) argon or air is used as the working fluid.

In this context, we make the first attempt to investigate the cyclic transient behavior of the Joule–Brayton PHES system. Specifically, on a 10 MW/4 h PHES system, a transient analysis method for the coupling of the dynamics, heat transfer and thermodynamics of the PHES system with the components including the compressor, expander, TES reservoirs and heat exchangers is proposed and solved numerically for multiple continuous cycles. The research presents a more realistic behavior that is close to the real cyclic operations of the Joule–Brayton PHES, wherein the working performance including both the round-trip efficiency and power attenuation during discharging can obtained. Helium is studied as a monoatomic molecular gas with a high energy density that can be used as the working gas. This paper is thus focused on the influencing mechanism of the parameters of the PHES system and the key components that are presented in figure 1.

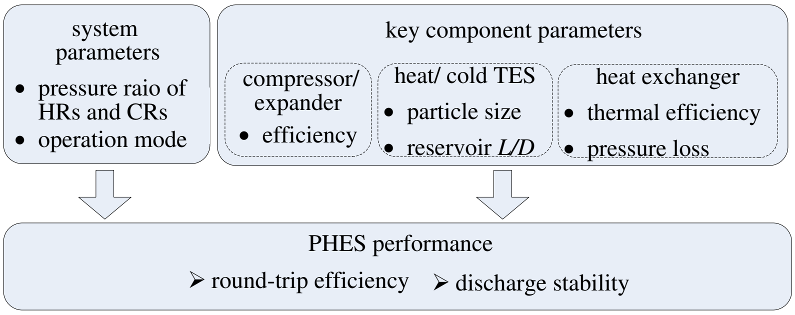

Fig.1. Parameters influencing on PHES performance

In the following, section 2 presents a detailed description of the Joule–Brayton based PHES system, section 3 describes the coupling analysis method of the PHES system and the components, ~~section 4 presents the reliability of the packed beds simulation, section 5~~and ~~–~~ introduces the parameters design of the 10 MW/4 h PHES system, section ~~6~~ 4 presents the results and findings, and the last section concludes the paper.

2 Description of Joule–Brayton based PHES system

Based on the PHES system proposed by White et al. [28], and McTigue et al. [29], the Joule–Brayton PHES discussed in this paper, as shown in figure 2, mainly consists of a cold (low–pressure) TES reservoir, a hot (high–pressure) TES reservoir~~s~~, two compressor–turbine–pairs(one for charging and the other for discharging) and two heat exchangers. The heat exchangers are required to remove surplus heat from the PHES system and stabilize the temperature variation in the packed–bed reservoirs during the charging process. A buffer vessel is also required to store/release gas in order to stabilize the system pressure during charging/discharging to balance the gas mass changes in the two reservoirs. During the charging and discharging processes, approximately 0.36% of the total flow rate of the gas is required to be exported to the buffer vessel through position 1 in figure 2 to maintain the system under a constant pressure. Furthermore, the same amount of gas returns the system through position 2 during the discharging process. Moreover, a different pressure ratio of the compressor and expander during the charging and discharging processes can be obtained by adjusting the buffer vessel, valves, and a pressure adjustment compressor coordinately during the idle period.

The working principal of the Joule–Brayton based PHES system is that during the charging process, the working gas driven by the compressor (for charging) goes through the HR, heat exchanger 2 (HX2), the expander (for charging), the CR and heat exchanger 1 (HX1) in the indicated direction of charging. During the charging process, the system operates as a heat pump wherein the heat is extracted from the CR to the HR while consuming electricity, and cold and heat thermal energy are stored in the CR and HR respectively. During discharging, the system operates as a heat engine with the working gas flowing along the indicated direction of discharge, which is opposite to direction of charging, when the heat returns from the HR to the CR in order to generate electricity.

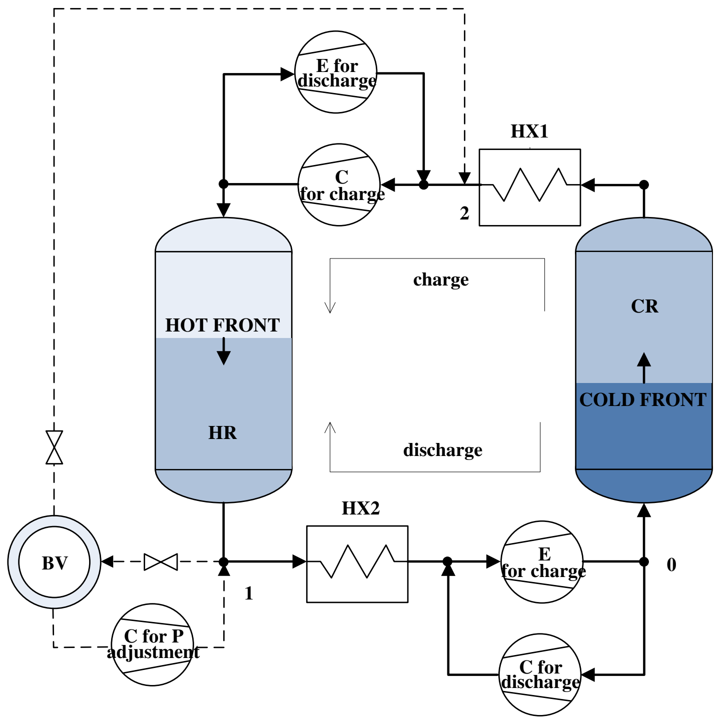

Fig.2. Layout of the PHES system. BV = buffer vessel; C = compressor; E = expander; HX = heat exchanger; CR = cold reservoir; HR = hot reservoir.

3 Methodology: coupling analysis of dynamics, transient heat transfer, and thermodynamics

Dynamics: In the PHES system, the compressor is the driving component of the gas flow, whereas the expander, the cold and hot storage reservoirs and the heat exchangers are the components that consume the mechanical energy of the gas during both the processes of charging and discharging. During the working process, the temperature profiles and thermophysical properties of the gas in the CR and HR are changing with time, thus resulting in a change in the pressure loss of the packed bed and leading to a pressure variation of the entire system. The pressure at point 1 during charging and at point 2 during discharging are maintained constant by the buffer vessel as shown in figure 3. *Heat transfer:* the transient temperature at the outflow of the CR and HR solved using the unsteady mass and energy conservation equations of the packed bed. *Thermodynamics:* For a fixed compression ratio of the compressor, the expansion ratio of the expander changes with time owing to the variation in the components' pressure loss. Along with the transient variation of the temperatures at the inlets and pressure ratios, the power and outflow temperatures of the compressor and the expander changes are time-varying. *Thermal properties:* The thermal properties of a gas, such as its density, thermal conductivity, and viscosity, have a great influence on the system performance. Moreover, the properties of the gas are obtained from the National Institute of Standards and Technology (NIST) database and updated in real-time during the solution procedure. Therefore, a coupling analysis including dynamics, transient heat transfer, thermodynamics and thermal properties is performed to obtain the transient behavior of the PHES system as shown in figure 3.

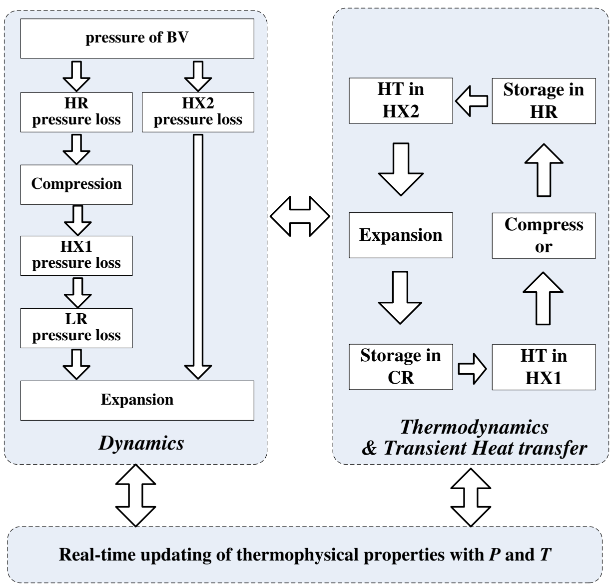

Fig.3. Coupling analysis of PHES during charging process

3.1 Dynamic conservation equation of PHES system

In the typically closed PHES system, the compressor provides the driving force of the expander and the gas flow in the components including the HR and CR and heat exchangers during both the charging and discharging processes. For the PHES system shown in figure 2, if we suppose that the total pressure at position 0 is P_0 during the charging and $p_0^{'}$ during the discharging respectively, we obtain:

$$\left(p_0 - \Delta p_{\mathrm{LP}} - \Delta p_{\mathrm{HX1}}\right)\beta_{\mathrm{c}} - \Delta p_{\mathrm{HP}} - \Delta p_{\mathrm{HX2}} - p_0\beta_{\mathrm{e}} = 0 \tag{1}$$

during the charging process and

$$p_0^{'}\beta_c^{'} - \Delta p_{\mathrm{HX2}}^{'} - \Delta p_{\mathrm{HP}}^{'} - \left(p_0^{'} + \Delta p_{\mathrm{LP}}^{'} + \Delta p_{\mathrm{HX1}}^{'}\right)\beta_{\mathrm{e}}^{'} = 0 \tag{2}$$

during the discharging process, wherein the superscript ‘denotes the discharging process. Δ~~P~~ p indicates the total pressure loss at each component, and β_{c} and β_{e} are the compression ratio and expansion ratio respectively.

3.2 Thermodynamics of PHES system

3.2.1 Compressor and expander

Taking into account the irreversibility loss of turbomachines, the polytropic process of compression and expansion occurs with the polytropic efficiencies η_{c} and η_{e} respectively. For the compressor

$$T_{\mathrm{c,out}} / T_{\mathrm{c,in}} = \beta_{\mathrm{c}}^{\kappa/\eta_c} \tag{3}$$

For the expander

$$T_{\mathrm{e,out}} / T_{\mathrm{e,in}} = \beta_{\mathrm{e}}^{-\kappa\eta_{\mathrm{e}}} \tag{4}$$

where the parameter κ is defined as $\kappa = (\gamma-1)/\gamma$ and γ is the specific heat ratio ($c_{\mathrm{p}}/c_{\mathrm{v}}$) of the gas [25, 33].

During the charging and discharging process, temperatures and densities of the HR and CR

outflow gas transiently vary leading to the variation of volume flow rates and rotation rates in the compressor and the expander. The unsteady variation of the turbo-machines shaft power P(t) owing to the inertia of rotors can be calculated by:

$$P(t) = -I \cdot \omega(t) \frac{\mathrm{d}\omega(t)}{\mathrm{d}t} \qquad (5)$$

Field Code Changed

Where I is the moment of inertia of rotor and ω(t) is the angular velocity. The angular velocity is proportional to the volume flow rate Q(t) and inversely proportional to the gas density at the constant mass flow rate.

$$\omega(t) = \frac{\omega_{\mathrm{des}}}{Q_{\mathrm{des}}} Q(t) = \frac{\omega_{\mathrm{des}} \rho_{\mathrm{des}}}{\rho(t)} \qquad (6)$$

Field Code Changed

Where ω_{des} and Q_{des} are the angular velocity and the volume flow rate under the design condition, respectively.

3.2.2 Packed bed heat/cold thermal energy storage reservoirs

The domains of the hot and cold thermal energy storage reservoirs are considered as cylindrical tanks, which include the packed bed of the TES particles and the heat transfer gas flowing through the void space. On assuming that the flow pattern is a 1D Newtonian plug flow, neglecting the temperature gradient in the radial direction and neglecting the heat loss through the well-insulated wall, the governing energy conservation equations of the unsteady two-phase model of such packed beds is given as follows.

For the fluid phase,

$$\varphi \frac{\partial \rho_g}{\partial t} + \frac{\partial G}{\partial x} = 0 \qquad (\cancel{5}7)$$

$$\frac{\partial T_{g}}{\partial t}+\frac{G}{\rho_{g}\varphi}\frac{\partial T_{g}}{\partial x}=\frac{h_{v}}{\rho_{g}c_{p,g}\varphi}\left(T_{s}-T_{g}\right)$$ (~~6~~8)

For the solid phase,

$$\frac{\partial T_{s}}{\partial t}=\frac{h_{v,eff}}{\rho_{s}c_{s}(1-\varphi)}\left(T_{g}-T_{s}\right)+\frac{k_{s,eff}}{\rho_{s}c_{s}(1-\varphi)}\frac{\partial^{2}T}{\partial x^{2}}$$ (~~7~~9)

where $h_{v,eff}$ is the effective volumetric heat transfer coefficient on considering the internal heat conduction resistance in a solid (for a Biot number smaller than 100) having the relationship with the volumetric heat transfer coefficient $h_v = h_p 6(1\text{-}\varphi)/d$. The volumetric heat transfer coefficient of Chandra's equation is used which fits well with the experimental results under both low and high pressures [35, 36]

$$h_{v,eff}=\begin{cases} h_{v} & \text{for } Bi\le 0.1 \\ \dfrac{1}{\dfrac{1}{h_{v}}+\dfrac{d_{p}^{2}}{60k_{s}\left(1-\varphi\right)}} & \text{for } 0.1<Bi\le 100 \end{cases}$$ (~~8~~10)

$$h_{v}=1.45\frac{Re^{0.7}k_{g}}{d^{2}}$$ (11~~9~~)

where the characteristic length for the Biot number is $d_p/6$ [37].

$$Bi=\frac{h_{p}d_{p}}{6k_{s}}$$ (12~~0~~)

$k_{s,eff}$ is the effective thermal conductivity for the non-contiguous spherical particles in a dispersion medium given by [38, 39]:

$$\frac{k_{s}-k_{s,eff}}{k_{s}-k_{g}}\left(\frac{k_{s,eff}}{k_{g}}\right)^{-\frac{1}{3}}=\varphi$$ (13~~1~~)

which is solved by performing iteration.

The dramatic temperature changes dramatically in the packed beds would lead to a change in the volume flow rate and thermoproperty of the gas in the packed bed. In this paper, the packed bed is divided into n sections along the axis, and the pressure drop across the packed bed and each section are given by the Ergun equation shown as below [34].

$$\Delta p\left(i\right)=\frac{\Delta L\cdot G^{2}}{\rho(i)\cdot d}\left(1.75\frac{1-\varphi}{\varphi^{3}}+150\frac{1-\varphi}{\varphi^{3}}\frac{\mu(i)}{Gd}\right)$$ (14~~2~~)

$$\Delta p=\sum_{i=1}^{n}\Delta p(i)$$ (15~~3~~)

where Δp and $\Delta p(i)$ are the pressure drop across the packed bed and the pressure drop across the i_{th} section, respectively, and ΔL ($\Delta L = L/n$) is the length of each section.

3.2.3 Heat exchanger

In the PHES system, the heat exchangers play important roles including removing the surplus heat and stabilizing the temperature fluctuations from the HR and CR during the charging process. Water from the cooling towers is usually selected as an efficient cooling media for heat exchangers having a temperature approximately about 2–5° C higher than the ambient temperature. As the heat capacity of the cooling water is greater than that of the gas and on ignoring the influence of the heat exchanger heat capacity, the outflow temperature from the heat exchanger can be obtained as follows.

$$T_{\mathrm{g,o}}\left(t\right)=T_{\mathrm{g,i}}\left(t\right)-\varepsilon\frac{\dot{m}_{\mathrm{g}}c_{\mathrm{p,g}}}{\dot{m}_{\mathrm{w}}c_{\mathrm{p,w}}}\left(T_{\mathrm{g,i}}\left(t\right)-T_{\mathrm{w,i}}\right)$$ (16~~4~~)

where $\dot{m}$ and c_{p} are the mass flow rate and heat capacity ~~of the water and gas~~, and ε is the heat exchanger effectiveness.

3.3 Systemic analyses of PHES system

For the PHES system, ~~In the gas temperature and pressure variation in the PHES system, t~~the transient specific ~~shaft work~~energy performed during charging and delivered during discharging, with considering the unsteadiness of the compressor and expander, can be obtained using equation

Formatted: Font: Not Bold, Not Italic

Formatted: Font: Not Bold

(~~15~~17) and equation (18~~6~~), respectively.

$$e_{\mathrm{chr}}(t)=e_{\mathrm{c,chr}}(t)-e_{\mathrm{e,chr}}(t)+\frac{1}{\dot{m}c_{\mathrm{p}}}\left(P_{\mathrm{e}}(t)+P_{\mathrm{c}}(t)\right) \tag{17}$$

$$e_{\mathrm{dis}}(t)=e_{\mathrm{e,dis}}(t)-e_{\mathrm{c,dis}}(t)-\frac{1}{\dot{m}c_{\mathrm{p}}}\left(P_{\mathrm{e}}(t)+P_{\mathrm{c}}(t)\right) \tag{18}$$

Formatted: Right

Field Code Changed

Formatted: Right

Field Code Changed

As shown in equation (5), t~~T~~he moment of inertia~~parameters~~ of the compressor and the expander are needed for calculating P(t), whereas there is no available compressor and ~~the~~ expander for the 10MW PTES system. In this study, referring to the compressor and the expander in the 10MW Advanced compressed air energy storage, the moment of inertia of compressor and the expander rotor is taken 1800 kgm^2 at the rated speed of 1500 rpm~~, referring to the compressor and the expander in the 10MW Advanced Compressed air energy storage~~ [42, 43]. ~~Among~~Under the situations ~~of~~in this study, the maximum absolute value of angular acceleration of the expander rotor and the compressor rotor is 0.0063 rad/s^2 and 0.0026 rad/s^2 respectively, and the corresponding P_{e}(t) and P_{c}(t) is -3.47 kW and 0.36 kW, which ~~is~~are less than ±0.04% of the transient shaft power and can be negligible.

By bringing equation (3), (4) into equation (15), (16), and neglecting the unsteady variation of the turbine machines, the transient specific energy~~the transient shaft work~~ can be calculated as below:

For the charging process,

$$\cancel{e_{\mathrm{chr}}(t)=T_{\mathrm{c,in}}(t)\cdot\left(r_{\mathrm{c}}(t)^{\kappa/\eta_{\mathrm{c}}}-1\right)+T_{\mathrm{e,in}}(t)\cdot\left(r_{\mathrm{e}}(t)^{-\kappa\eta_{\mathrm{e}}}-1\right)}$$

$$e_{\mathrm{chr}}(t)=T_{\mathrm{c,in}}(t)\cdot\left(r_{\mathrm{c}}(t)^{\kappa/\eta_{\mathrm{c}}}-1\right)-T_{\mathrm{e,in}}(t)\cdot\left(1-r_{\mathrm{e}}(t)^{-\kappa\eta_{\mathrm{e}}}\right) \tag{19~~5~~}$$

Field Code Changed

For the discharging process,

$$\cancel{e_{\mathrm{dis}}(t)=T'_{\mathrm{c,in}}(t)\cdot\left(1-r'_{\mathrm{c}}(t)^{\kappa/\eta_{\mathrm{c}}}\right)+T'_{\mathrm{e,in}}(t)\cdot\left(1-r'_{\mathrm{e}}(t)^{-\kappa\eta_{\mathrm{e}}}\right)}$$

$$e_{\mathrm{dis}}(t)=T_{\mathrm{e,in}}^{'}(t)\cdot\left(1-r_{\mathrm{e}}^{'}(t)^{-\kappa\eta_{\mathrm{e}}}\right)-T_{\mathrm{c,in}}^{'}(t)\cdot\left(r_{\mathrm{c}}^{'}(t)^{\kappa/\eta_{\mathrm{c}}}-1\right) \qquad (20\cancel{16})$$

Where e_{chr} and e_{dis} are specific energy (J/kg) of shaft work during charging and discharging, $T_{\mathrm{c,in}}$ and $T_{\mathrm{e,in}}$ are the inflow temperatures (K) of the compressor and the expander during charging, and the superscript ‘denotes the discharging process.

On assuming no mechanical loss, the round-trip coefficient of the PHES system is obtained on using the quotient of the net delivered shaft work during the discharging process and the consumed shaft work during the charging process, as shown in equation (21~~17~~)

$$\chi=\frac{\text{net work output}}{\text{net work input}}=\frac{\int_{\mathrm{dis}}\dot{m}_{\mathrm{dis}}c_{\mathrm{p}}e_{\mathrm{dis}}(t)\,\mathrm{d}t}{\int_{\mathrm{chr}}\dot{m}_{\mathrm{chr}}c_{\mathrm{p}}e_{\mathrm{chr}}(t)\,\mathrm{d}t} \qquad (\cancel{17}21)$$

where $\dot{m}$ is the mass flow rate though the compressors and expanders.

The stability of the delivery power is another important factor affecting for the energy storage system. In this paper, the offset ratio of the delivery power is increased to evaluate the stability which is defined as the ratio of the offset range of the delivery power to the maximum value during the delivery period, as presented in equation (22~~18~~).

$$\theta=\frac{\mathrm{Max}\left(e_{\mathrm{dis}}(t)\right)-\mathrm{Min}\left(e_{\mathrm{dis}}(t)\right)}{\mathrm{Max}\left(e_{\mathrm{dis}}(t)\right)} \qquad (\cancel{18}22)$$

For the PHES system, a smaller offset ratio indicates a more stable delivery power during the discharging process.

In order to validate the transient equation of the packed beds, the numerical simulations of the TES process of the crushed steatite (magnesium silicate rock) packed beds are performed by solving equations (~~5~~7)–(13~~1~~) with the parameters used in reference [44~~2~~] and [45~~3~~]. The temperature dependence of the heat capacity of the crushed steatite ($Mg_3Si_4O_{10}(OH)_2$) is

Field Code Changed

taken in to consideration in the simulation [40]. The temperature profiles along the axial distance of the packed beds of the simulated and experimental results are shown in figures 4 (a) and 4(b); it can be observed that an obvious thermocline occurs during the charging process and the simulated profiles fit well with the experimental results which proves the accuracy of the simulation method [42, 43].

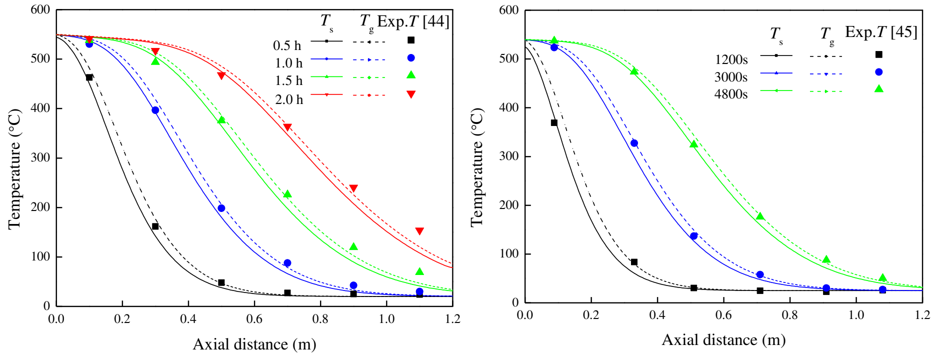

(a) with Meier et al.'s study [~~42~~44] (b)with Hänchen et al.'s study [~~43~~45]

Fig.4. Comparison between the simulation and experimental results of the temperature profiles in the packed beds

~~5~~3.4 Parameters design of the 10 MW/4 h PHES system

Formatted: Heading 3

In this paper, a Joule–Brayton based PHES system of 10 MW (nominally discharging power 10 MW, 4 h charging, and 4 h discharging) was designed and analyzed. The designed parameters of the PHES system with either argon or helium as the working gas are shown in Table 1 wherein the pressure ratio is 10 as in McTigue et al.'s study [29]. It should be noted that the heat capacity of helium is almost ten times that of argon, and thus, the mass flow rate of helium is approximately only 1/10th that of argon in a PHES system of the same power. Therefore, the pressure loss in the heat exchangers and packed-bed reservoirs would be decreased greatly on using helium instead of argon.

Table 1 Designed parameters of PHES system of 10 MW discharging power

Working gas	HP Pressure (MPa)	LP Pressure (MPa)	Average $c_{p,g}$ (J/kg/K)	Mass flow rate (kg/s)	Polytropic efficiency	ε of HXs	$\triangle p$ of HP HXs (kPa)	$\triangle p$ of LP HXs (kPa)	Cooling water temperature (K)
Argon	1.05	0.105	525	85.1	0.9	0.9	3	20	300
Helium	1.05	0.105	5193	8.6	0.9	0.9	0.3	2	300

The designed 10 MW/4 h PHES system consists of an HR and a CR with a packed bed of basalt particles. The packed-bed TES is unstable and has a larger packed bed volume, which results in a more stable output temperature but a higher cost and lower energy storage density. In consideration of the thermal front volume, the designed volumes of the HR and CR are selected to be twice the minimum design volume obtained using from the energy balance method $V = 2Q/\left(\overline{\rho_s c_s}\Delta T\right)$. The detailed parameters of the HR and CR are shown in table 2. In this design, the basalt is chosen as the hot and cold TES material, as it has a good heat capacity and thermal stability within the temperature range of −196°C–800°C. Based on the TA Q2000 DSC, the heat capacity of basalt is found to be strongly dependent on the temperature as shown in figure 5, and the linear fit equation is given in equation (23~~17~~).

$$c_p(T) = 0.23 + 0.00201 \cdot T \qquad (23\cancel{19})$$

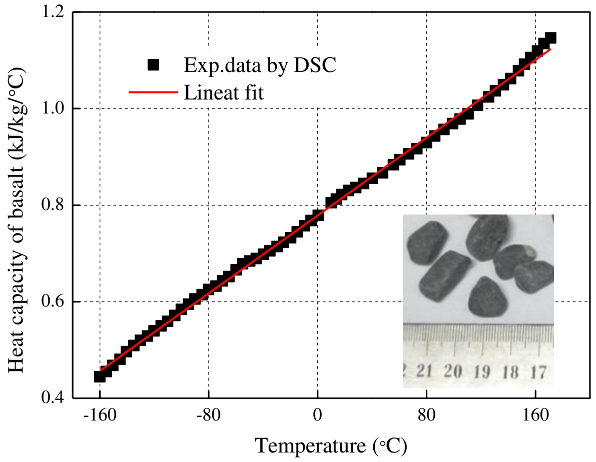

Fig.5. Dependence of heat capacity of basalt with temperature measured using DSC

Table 2 Hot and cold reservoir details for 10 MW/4 h PHES system
(the total volume is twice the minimum design volume)

Reservoir	Pressure (MPa)	Density of solid material (kg/m^3)	Porosity	Average d_p (mm)	Total Volume (m^3)	L (m)	D (m)
Heat	1.05	5175	0.35	30	460	10.96	7.31
Cold	0.105	5175	0.35	30	740	12.86	8.56

~~5.1~~3.~~5~~4.1 Heat exchangers design ~~and analysis~~

For eliminating surplus heat and stabilizing the temperature variation, two heat exchangers are required for the Joule–Brayton cycle PHES. One heat exchanger is under low pressure and the other is under medium/high pressure, and such heat exchangers are required to be compatible with a wide range of operation conditions, high efficiency and low pressure loss wherein the shell-and-tube heat exchangers are the optimal choices. According to the working conditions of the PHES system, the one shell pass, two tube pass TEMA shell-and-tube heat exchangers were designed for the hot and cold heat exchangers using the *ε-NTU* method and an empirical relation [41], wherein the heat transfer tubes have an outer diameter of 32mm and thickness of 2 mm, and the working gas passes through the shell side to minimize the pressure loss of the gas side.

Figure 6 shows the variation of the heat transfer efficiency and pressure drop of HX1 (low pressure) and HX2 (high pressure) with the tube number and tube length on using argon and helium respectively. The heat-transfer tube number ranges from 100 to 1000, and the tube length ranges from 0.5 m to 10.0 m. It can be found that an increase in the number of tubes would obviously decrease the pressure loss and improve the efficiency, and an increase in the tube length would lead to an increase in the efficiency and pressure loss. In order to obtain a high round–trip efficiency, the PHES system requires heat exchangers with a small pressure loss and high efficiency which can be obtained by using a large number of long tubes but this amount and length cannot be increased beyond a certain limit owing to the prohibitive cost.

From figure 6, it can be found that for heat exchangers of the same size, the efficiencies are similar when using argon and helium, ~~whereas~~ but the pressure drop observed when using helium is only approximately 1/10th the pressure drop observed when using argon owing to the difference in the mass flow rate. Furthermore, the pressure drop of HX1 under a low pressure is several times higher than the pressure drop of HX2 under a high pressure because of the high volume flow rate under the low pressure. From the design of the PHES system, the heat exchangers with an efficiency of 0.9, the pressure loss of HX1 of 20 kPa and pressure loss of HX2 of 3 kPa on using argon, and the heat exchangers with an efficiency of 0.9, pressure loss of HX1 of 2 kPa and pressure loss of HX2 of 0.3 kPa on using helium are achieved and such parameters are selected in the 10 MW/4 h PHES system.

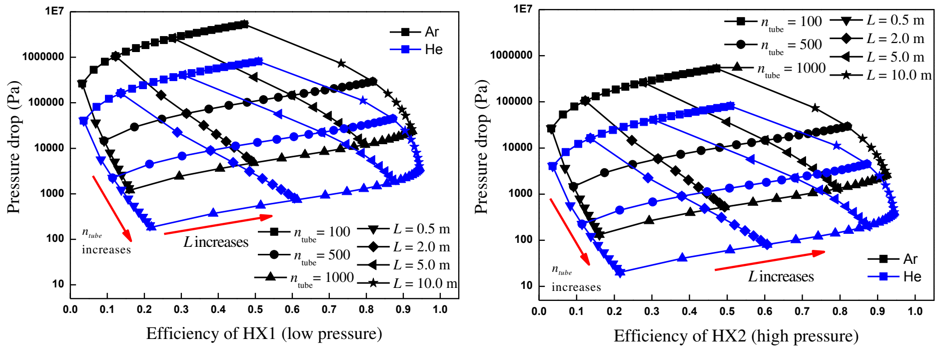

Fig.6. Efficiency versus pressure drop of the shell-and-tube heat exchangers

~~6~~4 Result and Discussion

~~6~~4.1 Cyclic behavior of PHES system

Based on the standard parameters in table 1 and 2, and the modeling method described in section 3, the working behavior of the PHES system running 100 circles was simulated using argon as the working gas; each cycle included 4 h of charging and 4 h of discharging. The axial temperature profile of the HR and CR at the end of the charging and discharging processes from the 1st circle to the 100th circle are shown in figures 7(a) and 7(b), respectively. It can be observed that, the profiles at the end of the charging and discharging process tend to coincide after several cycles. The temperature profiles in the reservoirs can be roughly divided into a stable temperature region and a thermocline region wherein the temperature gradient in the thermocline region decreases gradually with the cycling.

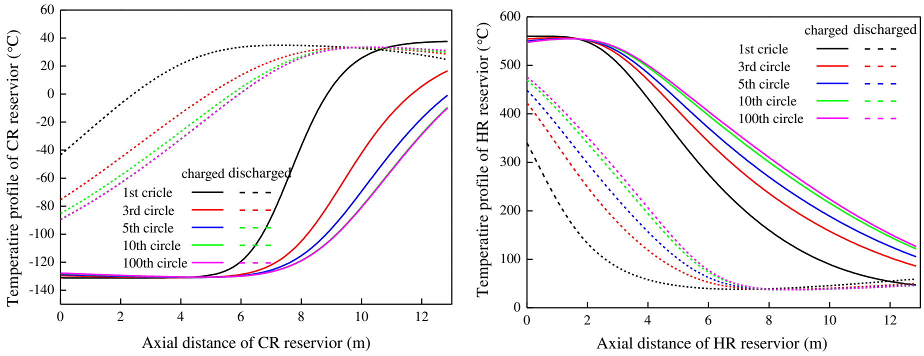

Fig.7. Cyclic behaviors of the HR and CR

In order to study the cyclic convergence of the PHES system, the factor $\Delta T_{\mathrm{Max}}(N)$ indicates the maximum temperature difference between the adjacent circles at the same axial position and is defined as shown in the equation (~~18~~22). As shown in figure 8, the factor $\Delta T_{\mathrm{Max}}(N)$ declines exponential with the circle number where argon has a higher decline rate than helium. After 40 circles, the maximum temperature difference at the same axial position between the adjacent circles is below 0.1 $^{\circ}$C for all the gases and reservoirs which is deemed cyclically stable. According to this, the following analysis is based on the data of the 40th circles which have achieved the cyclic stable state.

$$\Delta T_{\mathrm{Max}}(N) = \mathrm{Max}\left(\left|T_{\mathrm{i,\,N}} - T_{\mathrm{i,N\text{-}1}}\right|\right) \qquad N = 1,\,2,\,3\ldots. \qquad (\cancel{18}24)$$

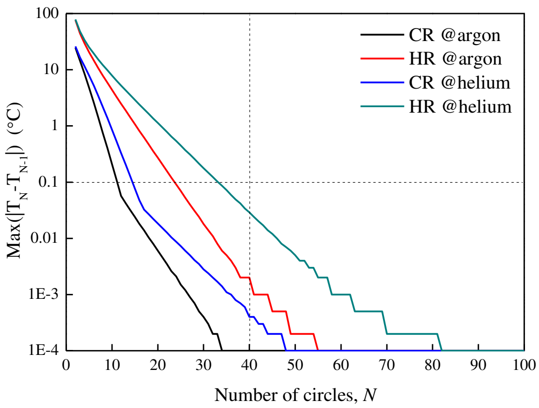

Fig.8. Maximum temperature differences between circles versus the number of circles

Under the cyclic stable state, figures 9(a) and 9(b) show the transient variation of the inflow and outflow temperatures of the HR and CR during the charging and discharging, respectively, when using argon as the working gas. This shows that the outflow temperature from the HR increases continuously after a period of stable state (approximately 1.5 h) during the charging process and decreases continuously after a period of stable state (approximately 1.5 h) during the discharging. The outflow temperature from the CR also has a similar unstable behavior but the temperature variation trend is opposite to that of the HR. Figure 9(c) shows the variation in the pressure loss of the HR and CR during the charging and discharging processes. It can be found that the pressure loss of the CR decreases linearly during the charging and increases during the discharging process, and the opposite phenomenon is observed in the case of the HR. This is because, during the charging period in the CR, the cold region grows gradually where the volume flow rate decreases owning to the high density which results in a decrease in the pressure loss, and during the discharging, the cold region retracts gradually and the pressure loss increases gradually. For similar reasons, the increase in the hot region in the HR could lead to a higher volume flow rate, hence increasing the pressure loss during the charging. The expansion ratio increases slightly during the charging and decreases during the discharging, as shown in figure 8(c), and is mainly influenced by variations in the pressure loss of the reservoirs. Figure 8(d) shows that the powers of the PHES compressor, expander and shaft are rather stable during the charging process, and during the delivery process, the compressor power increases and the expander power decreases gradually, thus leading to a decrease in shaft power. Based on the parameters listed in tables 1 and 2, the round-trip efficiency χ and the delivery working offset ratio θ using argon as the working gas is 39.3% and 71.0%, respectively, and the round-trip efficiency χ and delivery working offset ratio θ

using helium is 56.9% and 45.9%, respectively.

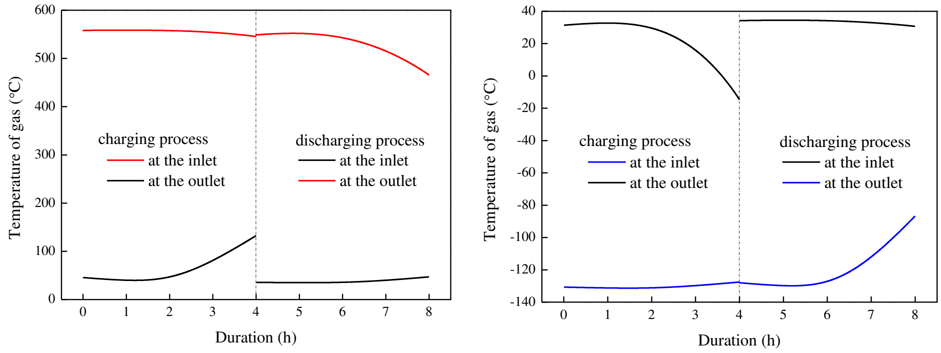

(a) inflow and outflow temperature of HP reservoir (b) inflow and outflow temperature of LP reservoir

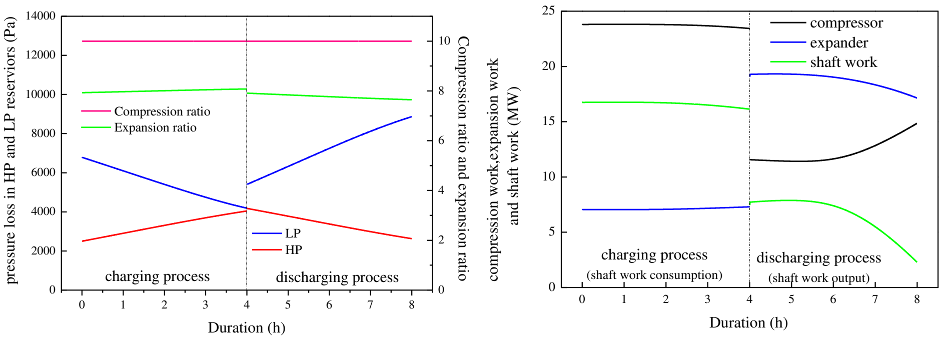

(c) pressure loss of the HP and LP reservoirs (d) transient power variation of PHES

Fig.9. Transient behaviors of the HR and CR and PHES system.

~~The influencing factors include the compression ratio in the discharging process only and that for the entire processes, the polytropic efficiency of compressors and expanders, the particle diameter of the particles in the reservoirs, the length-to-diameter ratio of the reservoirs, the efficiency and pressure loss in the heat exchangers and the discharging duration of the PHES system performance are studied using argon and helium as the working gases.~~

~~6~~4.2~~.1~~ Effect of compression ratio during charging and discharging

The influencing factors include the compression ratio in the discharging process only and that for the entire processes, the polytropic efficiency of compressors and expanders, the particle diameter of the particles in the reservoirs, the length-to-diameter ratio of the reservoirs, the efficiency and pressure loss in the heat exchangers and the discharging duration of the PHES system performance are studied using argon and helium as the working gases.

Figure 10(a) shows the influence of the compression ratio of the compressors ranging from 5 to 16 during both charging and discharging processes on the round-trip efficiency χ and the delivery working offset ratio θ wherein the other parameters are obtained from in tables 1 and 2. It can be found that the round-trip efficiency increases gradually with the compression ratio β_c from 14.3% at $\beta_c = 5$ to 49.1% at $\beta_c = 16$ for argon and from 43.0% at $\beta_c = 5$ to 63.0% at $\beta_c = 16$ for helium; the round-trip efficiency of helium is considerably higher than that of argon, with a range of 13.9% to 28.6%. This is mainly because a much smaller pressure loss occurs in the reservoirs and heat exchangers of helium than those of argon, and a greater expansion work can be obtained on using helium. From figure 10(a), it can also be observed that the delivery working offset ratio θ decreases with the compression ratio β_c, and the offset ratio θ of helium is much lower than that of argon; such a result indicates that the delivery work during the discharging using helium is more stable than that using argon. The transient charging power and delivery power profiles at the compression ratio β_c of 7, 10 and 13 on using argon are shown in figure 10(b). It can be found that both the charging power and discharging power increase with the compressor ratio and an obvious decrease in delivery power occurs during the late discharging period.

Périlhon et al. recommended that the maximum fluid temperature should not exceed 800 °C for a reasonable life of the turbomachines [464]. The maximum temperature of the gas is approximately 750 °C in the PHES system at the compression ratio β_c of 16 for both argon and helium, which is within the permitted temperature range.

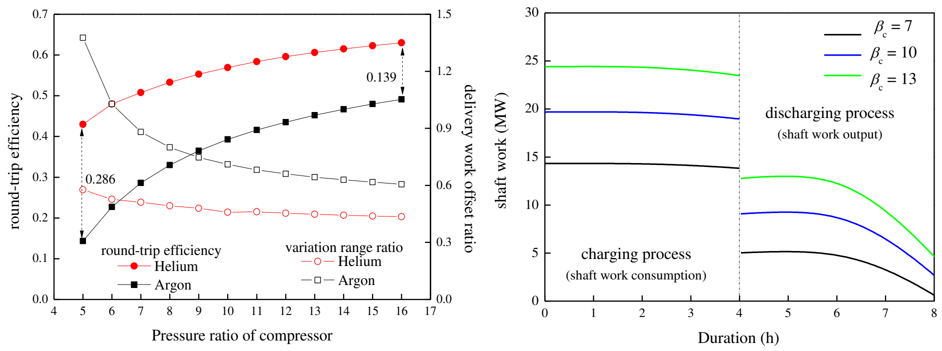

(a) (b)

Fig.10. Impact of compression ratio during both charging and discharging

~~6.2.~~4.3~~2~~ *Effect of compressor pressure ratio during discharging*

Formatted: Heading 3

Owing to the pressure loss, heat transfer loss and the irreversible loss of the compressor and expanders, setting the pressure ratio of the compressor during discharging as the same as that of during charging may not be the best choice. After the charging process, the compression ratio of the delivery process can be reset by storing some gas in the BV and recharging the system by the adjustment compressor during the idle time. At the charging compression ratio of 10 and the other parameters listed in tables 1 and 2, figure 11(a) shows the influence of the compression ratio ranging from 4 to 10 during the discharging process on the round-trip efficiency χ and the delivery working offset ratio θ. This result indicates that the round-trip efficiency χ increased first and then decreased with the discharging compress ratio and the maximum round-trip efficiency χ occurs at the discharging compress ratio of 7 for both argon and helium, the maximum round-trip efficiency χ obtained using helium is 59.0%, which is considerably higher than that obtained using argon: 41.7%. Moreover, it is also indicated from figure 11(a) that the offset ratio θ

using helium and argon increases gradually with the increase in the discharging compress ratio. As shown in figure 11(b), when the charging compression ratio $\beta_{c,chr}$ is 10, the discharging compression power and discharging expansion power at a high pressure ratio of 10 are both higher than those at a low pressure ratio of 7. The shaft power at a compression ratio of 10 is lower than that at a compression ratio of 7; this is because, the variation amplitude of the compression power is greater than that of the expansion power when the discharging compression ratio increases from 7 to 10.

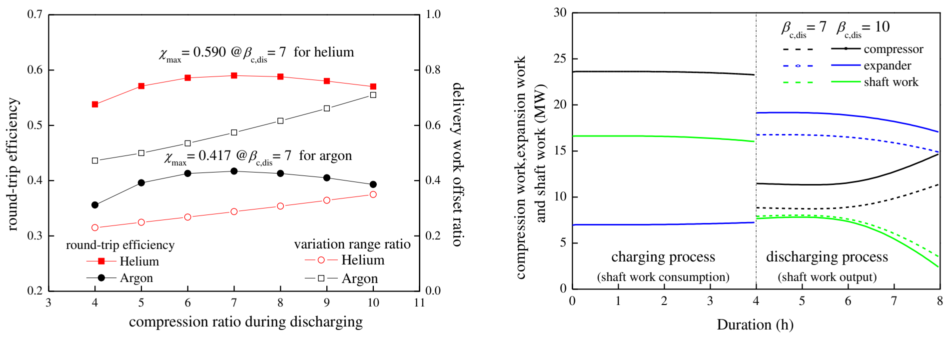

（a） （b）

Fig.11. Impact of compression ratio during discharging (at $\beta_{c,char}$ = 10)

~~6.2.3~~4.4 *Effect of polytropic efficiency of both compressors and expanders*

The plots of the round-trip efficiency χ with the polytropic efficiency of both the compressors and expanders ranging from 0.8 to 1.0 during both charging and discharging are shown in figure 12, which the use of argon and helium respectively, and the other parameters are obtained from tables 1 and 2. It can be observed that the polytropic efficiency of the compressors and expanders have an almost dominant effect on the round-trip efficiency χ, such that the round-trip efficiency increases from 16.2% at η = 0.8 to 68.3% at η = 1.0 when using argon, while the round-trip efficiency increases from 30.8% at η = 0.8 to 90.5% at η = 1.0 on using helium. The delivery working offset ratio θ in figure 11 shows that the increase in the polytropic efficiency also improves the stability of the delivery power.

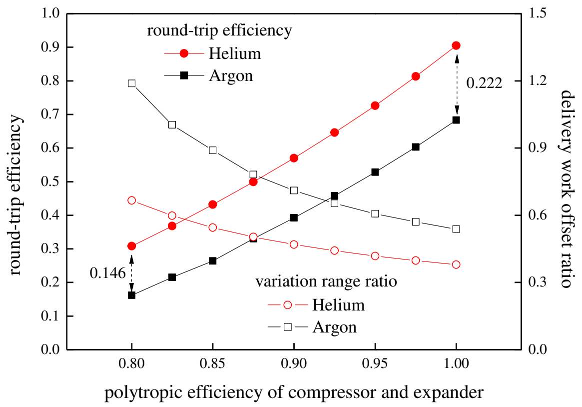

Fig.12. Impact of polytropic efficiency of compressor and expander

~~6.2.4~~4.5 Effect of TES particles diameter

Formatted: Heading 3

The diameters of the solid TES particles would affect the pressure loss and heat transfer in the packed beds and, hence, affect the PHES efficiency. Figure 13(a) shows the influence of the particle size in both the HR and CR in the range from 5mm to 70mm on the round-trip efficiency χ and the delivery working offset ratio θ. It can be observed that, the round-trip efficiency χ first increases and then gradually decreases with the particles sizes, the maximum round-trip efficiency of 40.2% occurs at $d_p = 20$ mm for argon and for helium the maximum round-trip efficiency of 58.8% is obtained at $d_p = 15$ mm, and such particle sizes always correspond to a small delivery working offset ratio θ. Such a result is mainly attributed to the joint action of the decrease in the pressure loss and increase in the heat transfer temperature difference between the gas and the TES materials as the particle size increases. Figure 13(b) shows the transient charging and delivery power in the case of particles sizes of 10 mm, 20 mm, and 40 mm using argon. It can be observed that large particles result in a relatively small charging power during the charging process; The discharging power is the lowest at d_p = 10mm during the entire discharging process which is relatively stable. However, although the discharging power at d_p = 40mm is higher than that at d_p = 20mm during the first discharging hour, it then declines fast and drops below that at d_p = 20 mm during the following discharging hours. The influence of the particle diameter mainly includes two aspects: large particles result in small pressure loss and also large thermal resistance in particles and large delivery temperature variation.

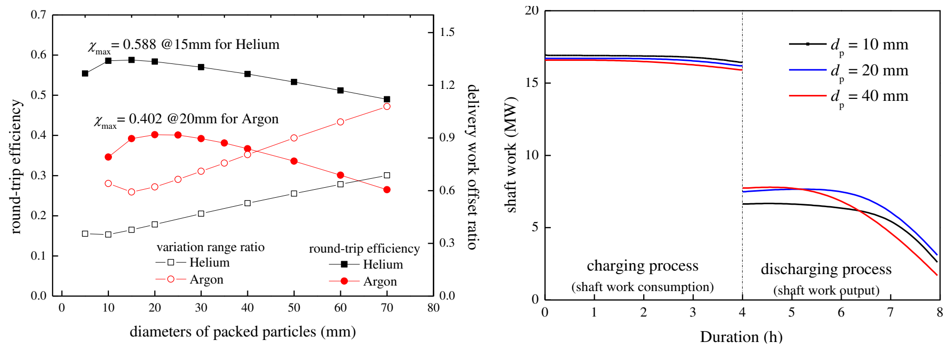

(a) (b)

Fig.13. Impact of particle diameter of compressor and expander

~~6.2.5~~4.6 *Effect of length–to–diameter ratio of reservoirs*

Formatted: Heading 3

As described in section 5, the volume of the designed HR and CR is 460 m^3 and 740 m^3, respectively, for the 10 MW/4 h PHES system. For the cylindrical reservoirs with a fixed volume, the length–to–diameter ratio *L/D* of the reservoirs is an important factor that influences the pressure loss and heat transfer of the packed beds. Figure 14(a) shows the variation in the round-trip efficiency χ and the delivery working offset ratio θ with the length–to–diameter ratio *L/D* of both the HR and CR, and the ranges of *L/D* are 0.5–3 for argon and 0.5–6 for helium. It can be observed in figure 14(a) that the influence of *L/D* is rather gentle in the case of helium whereas it is great in the case of argon. The round-trip efficiency χ increases at the beginning and decreases gradually with the increase in *L/D*, and a maximum round-trip efficiency of 41.0% and a minimum discharging power offset ratio of 72.6% occurs at *L/D* = 1 for argon; for helium the maximum round-trip efficiency is 57.0% and the minimum discharging power offset ratio of 51.8% occurs at *L/D* = 1.5. This is because a larger length–to–diameter ratio *L/D* would result in a larger pressure loss and a relatively smaller proportion of the thermocline region in the packed beds simultaneously, which is also a joint effect. Figure 14(b) shows the transient charging and discharging power under the conditions of the length–to–diameter ratio *L/D* of 0.5, 1.5, and 2.5 using argon. During the charging process, the larger length–to–diameter ratio *L/D* results in relatively higher charging power owing to the higher pressure loss; the discharging power is the lowest at *L/D* = 2.5 during the discharging process. However, the discharging power at *L/D* = 0.5 is higher than that at *L/D* = 1.5 during the discharging, and then declines fast and drops below that at *L/D* = 1.5.

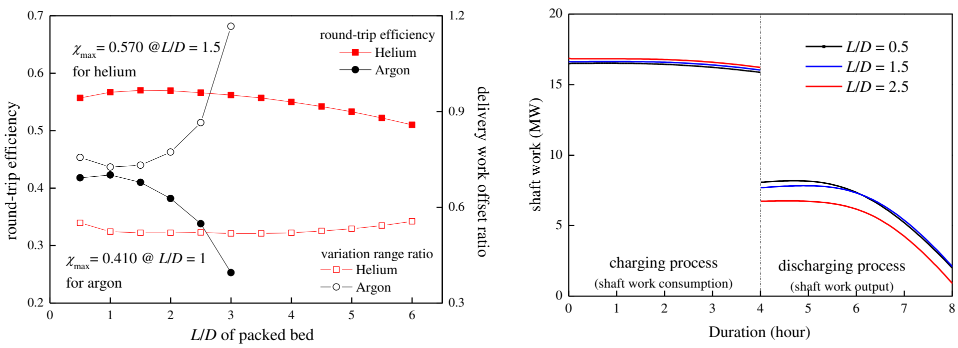

(a) (b)

Fig.14. Impact of *L/D* of packed bed reservoirs

~~6.2.6~~4.7 *Effect of efficiency and pressure drop of heat exchangers*

Formatted: Heading 3

Figure 15 shows the round-trip efficiency variation of the PHES with a 5% increase in the efficiency and pressure drop of the heat exchangers (including HX1 and HX2) based on the parameters listed in tables 1 and 2. It can be observed that the increase in the heat transfer efficiency of the heat exchangers improves the round-trip efficiency whereas the increase in the pressure loss decreases the round-trip efficiency; the effect of the heat exchangers efficiency and pressure drop on the PHES efficiency using argon is several times higher than that of helium; and the influence of the pressure loss of the low pressure heat exchanger (HX1) is more obvious than that of the high pressure heat exchanger (HX2).

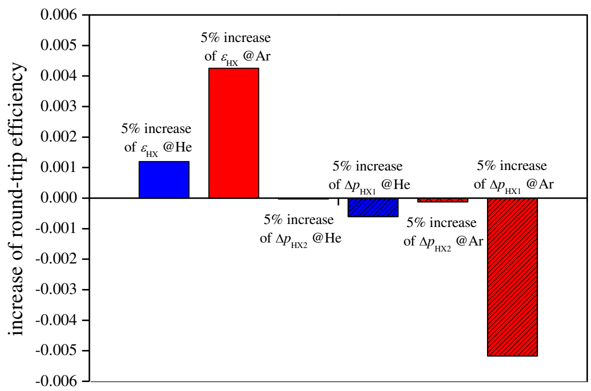

Fig.15. Impact of efficiency and pressure drop of heat exchangers

~~6.2.7~~4.8 *Effect of discharging duration*

In the above analysis, each energy storage circle comprise a charging process of 4 h and a discharging process of 4 h; however, an equal discharging and charging duration may not be optimal for such a PHES system. Figure 16(a) shows the influence of the discharging time ranging from 2 h to 5 h (one circle consists of a 4 h charging process and 2–5 h discharging process) on the round-trip efficiency χ and the delivery working offset ratio θ using argon and helium, respectively. From figure 15(a), it can be observed that the round-trip efficiency χ increases at first and then decreases with the discharging time. The best selection of the discharging duration is a few minutes shorter than the charging time such that the maximum round-trip efficiency of 40.1%

Formatted: Heading 3

occurs at the delivery duration of 3.78 h for argon, and the maximum round-trip efficiency is 57.2% at the delivery duration of 3.91 h for helium. The delivery working offset ratio θ is relatively low (<20%) for a discharging duration less than approximately 3.5 h and then increases sharply.

Figure 16(b) shows the transient shaft power during the charging and discharging with the discharging duration of 3.5 h, 4 h and 4.5 h using argon. It can be observed that for the PHES system having a 3.5 h discharging duration has the most stable delivery power, and the obvious decline of the delivery power at the later stage of the discharging process can be observed with a longer discharging duration. Figure 16(c) shows the axial temperature profile of the hot TES reservoir at the end of the charging and discharging processes for the discharging durations of 3.5 h, 4 h and 4.5 h. It also shows that more exergy with a high temperature is stored in the hot TES reservoir in the PHES system in the case of the discharging duration of 3.5 h, and a relatively stable delivery thermal energy profile can be obtained during the discharging process, but it has the drawback of relatively unstable charging power, which can be reduced through the heat exchangers.

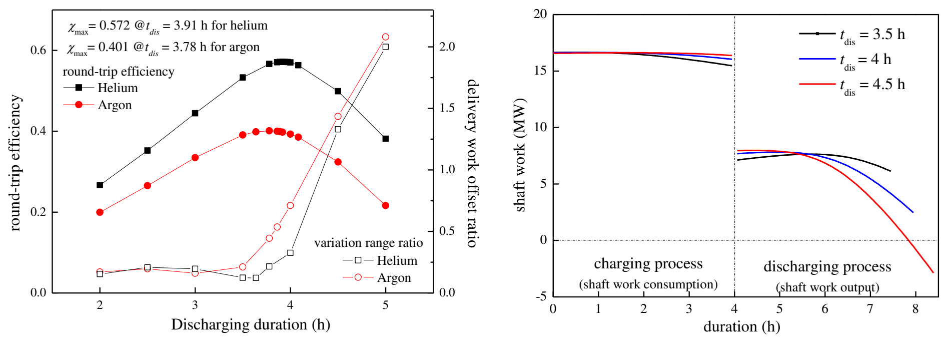

（a） （b）

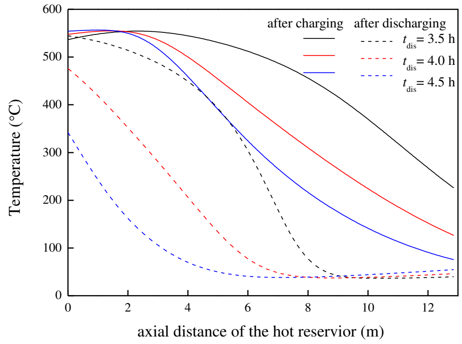

（c）

Fig.16. Impact of the discharging duration on the PHES behavior

~~7~~5 *Conclusions*

In this paper, the use of the transient analysis method on the Joule–Brayton based PHES system is proposed for the coupling dynamics, thermodynamics and heat transfer process. The cyclic transient behavior of the 10 MW/4 h Joule–Brayton PHES system is studied using argon and helium as the working gases. Based on the round-trip efficiency and the variation range ratio of the delivery power, the mechanisms influencing PHES system and components parameters on the PHES system performance are further discussed. From the result of the analysis, the following conclusions can be obtained:

1. The delivery power clearly declines during the discharging process mainly owing to the thermal energy reduction from the packed bed TES reservoirs.

2. The gas resistance loss through the TES reservoirs and heat exchangers has a great influence on the system performance. In addition, helium, with small resistance losses, has an overwhelming advantage over argon for application in the PHES. The round-trip efficiency χ of helium is 56.9%, which is much higher than 39.3%, which is obtained on using argon under the

design conditions. The PHES system using helium can also provide more stable electricity with the delivery power offset ratio of 45.9% than that using argon with a delivery power offset ratio of 71.0%.

3. The increase in the pressure ratio and isentropic efficiencies would lead to an obviously improvement in the round–trip efficiency and delivery stability. Furthermore, an appropriate discharging compression ratio that is less than the charging compression ratio will aid in improving the round–trip efficiency. For the 10 MW/4 h PHES system, the optimum round-trip efficiency is obtained at the discharging compression ratio of 7 when the charging compression ratio is 10.

4. For the TES reservoirs, there exists optimal selections of particle sizes, ratios of length –to–diameter, and discharging durations corresponding to the maximum round-trip efficiency and preferable discharging power stability; this is mainly owing to the joint effects of the pressure loss, heat transfer and thermodynamics.

Further research is required for improving the improvement of the round-trip efficiency and discharging power stability and decreasing the costs, which will be the subject of the authors' future research.

Conflict of Interest

The authors declare no conflict of interest.

Acknowledgements

The authors would like to thank the National Key R&D Plan Program (2017YFB0903605), the National Natural Science Foundation of China (NO. 51506194), the Chinese Academy of Sciences Device Research & Manufacturing Program (YJKYYQ20170005, and the Newton Advanced Fellowship of the Royal Society (NA170093).

References

[1] BP Statistical Review of World Energy; 2018.

[2] REN21, Renewables 2017 Global Status Report, REN21 Secretariat, Paris, France; 2018.

[3] Li S, Wang J, Liu Q, Li L, Hua Y, Liu W. Analysis of Status of Photovoltaic and Wind Power Abandoned in China. J Power Energy Eng 2017; 5: 91–100.

[4]Chen H, Cong TN, Yang W, Tan C, Li Y, Ding Y. Progress in electrical energy storage system: A critical review. Prog Nat Sci 2009; 19: 291–312.

[5] Luo X, Wang J, Dooner M, Clarke J. Overview of current development in electrical energy storage technologies and the application potential in power system operation. Appl Energy 2015; 137: 511–36.

[6] Walawalkar R, Apt J, Mancini R. Economics of electric energy storage for energy arbitrage and regulation in New York. Energy Policy 2007; 35: 2558–68.

[7] Dobie WC. Electrical energy storage. Power Eng J 1998; 12:177–81.

[8] Makansi J, Abboud J. Energy storage: the missing link in the electricity value chain-An ESC White Paper. Energy storage Council; 2002.

[9] Yao L, Yang B, Cui H, Zhuang J, Ye J, Xue J. Challenges and progresses of energy storage technology and its application in power systems. J Mod Power Syst Cle 2016; 4: 519–28.

[10] Aneke M, Wang M. Energy storage technologies and real life applications–A state of the art review. Appl Energy 2016; 179: 350–77.

[11] DOE Global Energy Storage Database, http://www.energystorageexchange.org/

[12] Pumped Storage in Bath County, http://www.virginiaplaces.org/

[13] Guo H, Xu Y, Chen H, Zhou X. Thermodynamic characteristics of a novel supercritical compressed air energy storage system. Energy Convers Manage 2016; 115: 167–177.

[14] Ohler C, Mercangoez M. Thermoelectric energy storage system and method for storing thermoelectric energy, EP2157317 B1, 19-Jun-2013.

[15] Hemrle J, Kaufmann L, Mercangoez M. Thermoelectric energy storage system having two thermal baths and method for storing thermoelectric energy, WO2010118915; 2009.

[16] Morandin M, Maréchal F, Mercangöz M, Buchter F. Conceptual design of a thermo–electrical energy storage system based on heat integration of thermodynamic cycles–Part A: Methodology and base case. Energy 2012; 45: 375–85.

[17] Morandin M, Maréchal F, Mercangöz M, Buchter F. Conceptual design of a thermo–electrical energy storage system based on heat integration of thermodynamic cycles–Part B: Alternative system configurations. Energy 2012; 45: 386–96.

[18] Kim YM, Shin D G, Lee S Y, Favrat D. Isothermal transcritical CO2 cycles with TES (thermal energy storage) for electricity storage. Energy 2013; 49: 484–501.

[19] Abarr M, Geels B, Hertzberg J, Montoya LD. Pumped thermal energy storage and bottoming system part A: Concept and model. Energy 2017; 120: 320–31.

[20] Abarr M, Hertzberg J, Montoya LD. Pumped Thermal Energy Storage and Bottoming System Part B: Sensitivity analysis and baseline performance. Energy 2017; 119: 601–11.

[21] Wang G, Zhang X. Thermodynamic analysis of a novel pumped thermal energy storage system utilizing ambient thermal energy and LNG cold energy. Energy Convers Manage 2017, 148: 1248–64.

[22] Steinmann WD. The CHEST (Compressed Heat Energy STorage) concept for facility scale

thermo mechanical energy storage. Energy 2014; 69: 543–52.

[23] Jockenhöfer H, Steinmann WD, Bauer D. Detailed numerical investigation of a pumped thermal energy storage with low temperature heat integration. Energy 2018; 145: 665–76.

[24] Frate GF, Antonelli M, Desideri U. A novel Pumped Thermal Electricity Storage (PTES) system with thermal integration. Appl Therm Eng 2017; 121: 1051–58.

[25] Desrues T, Ruer J, Marty P, Fourmigu´e J, A thermal energy storage process for large scale electric applications. Appl Therm Eng 2010; 30:425–432.

[26] Ni F, Caram HS. Analysis of pumped heat electricity storage process using exponential matrix solutions. Appl Therm Eng 2015; 84: 34–44.

[27] Howes J. Concept and development of a pumped heat electricity storage device. Proc IEEE 2012; 100: 493–503.

[28] White A, Parks G, Markides CN. Thermodynamic analysis of pumped thermal electricity storage. Appl Therm Eng 2013; 53:291–8.

[29] McTigue JD, White AJ, Markides CN. Parametric studies and optimization of pumped thermal electricity storage. Appl Energy 2015; 137:800–11.

[30] Benato A. Performance and cost evaluation of an innovative Pumped Thermal Electricity Storage power system. Energy 2017, 138: 419–36.

[31] Benato A, Stoppato A. Heat transfer fluid and material selection for an innovative Pumped Thermal Electricity Storage system. Energy 2018; 147: 155–68.

[32] Gil A, Medrano M, Martorell I, Lázaro A, Dolado P, Zalba B et al. State of the art on high temperature thermal energy storage for power generation. Part 1 –Concepts, materials and modellization. Renew. Sustain. Energy Rev 2009; 14: 31–55.

[33] Dixon SL, Hall C. Fluid mechanics and thermodynamics of turbomachinery. 6th ed. USA: Butterworth-Heinemann, Elsevier Science Boston; 2010.

[34] Ergun S, Fluid flow through packed columns, Chem Eng Prog 1952; 48:89–94.

[35] Chandra P, Willits DH. Pressure drop and heat transfer characteristics of air rock bed thermal storage system. Sol. Energy 1981; 27:547–53.

[36] Liu J, Wang L, Yang L, Yue L, Chai L, Sheng Y et al. Experimental study on heat storage and transfer characteristics of supercritical air in a rock bed. Int J Heat Mass Transfer 2014; 77:883–90.

[37] Xu B, Li P, Chan C. Extending the validity of lumped capacitance method for large Biot number in thermal storage application. Sol Energy 2012; 86: 1709–24.

[38] Bruggeman DAG. Calculation of various physical constants in heterogeneous substances. Ann Phys 1935; 24:636–9.

[39] Abyzov AM, Goryunov AV, Shakhov FM. Effective thermal conductivity of disperse materials. I. Compliance of common models with experimental data. Int J Heat Mass Transfer 2013; 67: 752–67.

[40] Robertson EC, Hemingway BS. Estimating heat capacity and heat content of rocks. US Geological Surve; 1995.

[41] Shah RK, Sekulic DP. Fundamentals of heat exchanger design. John Wiley & Sons; 2003.

[42] Li W, Wang X, Zhang X, Zhang X, Zhu Y, Chen H. Experimental and Numerical Investigations of Closed Radial Inflow Turbine With Labyrinth Seals. J Eng Gas Turbines Power 2018; 140: 102502.

[43]The 10MW compressed air energy storage is under integrated test,

http://www.escn.com.cn/news/show-377349.html.
[~~42~~44] Meier A, Winkler C, Wuillemin D. Experiment for modelling high temperature rock bed storage. Sol Energy Mater 1991; 24: 255–64.
[45~~3~~] Hänchen M, Brückner S, Steinfeld A. High–temperature thermal storage using a packed bed of rocks–heat transfer analysis and experimental validation. Appl Therm Eng 2011; 31: 1798–806.
[46~~4~~] Périlhon C, Lacour S, Podevin P, Descombes G. Thermal electricity storage by a thermodynamic process: study of temperature impact on the machines. Energy Procedia 2013, 36: 923–38.

Nomenclature

Abbreviations

BOT	Bottoming system
BV	Buffer vessel
CAES	Compressed air energy storage
CHEST	Compressed heat energy storage
CR	Cold Reservoir
DSC	differential scanning calorimetry
EES	Electrical energy storage
HP	High pressure
HR	Hot reservoir
HX	Heat exchanger
LNG	Liquefied natural gas
LP	Low pressure
NIST	National Institute of Standards and Technology
ORC	Organic Rankine cycle
PHS	Pumped hydro storage
PHES	Pumped heat electricity storage
PTES	Pumped thermal electricity storage
TEES	Thermo-electrical energy storage
TEMA	Tubular Exchanger Manufacturers Association
TES	Thermal energy storage

Symbols

Bi	Biot number
C	Specific heat capacity, J K^{-1} kg^{-1}
d	Ddiameter of particles, m
D	Diameter of packed bed reservoir, m
e	Specific energy, J kg^{-1}
G	Mass flow rate, kg s^{-1}
h	Volumetric heat transfer coefficient, W m^{-3} K^{-1}

i	Number i	771
I	Moment of inertia, kg m^2	
K	Thermal conductivity, W m^{-1} K^{-1}	
L	Length scale of packed bed, m	
m	Mass of gas, kg	
n	Number	
N	Number of circles	
P	Power, W	
Q	Volume flow rate, m^3 s^{-1}	
Re	Reynolds number	
t	Time, s	
T	Temperature, K	
β	Compression/expansion ratio of compressor/expander	
γ	Adiabatic exponent of gas	
ε	Efficiency of heat exchanger	
η	Polytropic efficiency of compressor/expander	
θ	Offset ratio of delivery power	
κ	Parameter, $(\gamma-1)/\gamma$	
μ	Dynamic viscosity, Pa s	
ρ	Density, kg m^{-3}	
Φ	Porosity of packed bed	
X	Round-trip efficiency	
ω	Angular velocity, rad s^{-1}	
Subscript		
0	Point 0	
1	Point 1	
c	Compressor	
chr	Charge	
des	Design	
dis	Discharge	
e	Expander	
eff	Effective	
g	Gas	
HP	High pressure	
HX1	Heat exchanger 1	
HX2	Heat exchanger 2	
i	Number i	
in	At the inlet	
LP	Low pressure	
p	Particle	
s	Solid	
w	Water	

Cyclic transient behavior of the Joule–Brayton based pumped heat electricity storage: Modeling and analysis

Liang Wang[1, 2], Xipeng Lin[1], Lei Chai[3], Long Peng[1], Dong Yu[1], Haisheng Chen[1, 2]

(1Institute of Engineering Thermophysics, Chinese Academy of Sciences, Beijing 100190, People's Republic of China; 2University of Chinese Academy of Sciences, Beijing 100049, People's Republic of China；3RCUK National Centre for Sustainable Energy Use in Food Chain (CSEF), Brunel University London, Uxbridge, Middlesex UB8 3PH, United Kingdom)

*Corresponding author. Tel.: +86 10 82543148, E-mail: chen_hs@iet.cn

Abstract

Pumped heat electricity storage (PHES) has the advantages of a high energy density and high efficiency and is especially suitable for large-scale energy storage. The performance of PHES has attracted much attention which has been studied mostly based on steady thermodynamics, whereas the transient characteristic of the real energy storage process of PHES cannot be presented. In this paper, a transient analysis method for the PHES system coupling dynamics, heat transfer, and thermodynamics is proposed. Judging with the round trip efficiency and the stability of delivery power, the energy storage behavior of a 10 MW/4 h PHES system is studied with argon and helium as the working gas. The influencing factors such as the pressure ratio, polytropic efficiency, particle diameters, structure of thermal energy storage reservoirs are also analyzed. The results obtained indicate that, mainly owing to a small resistance loss, helium with a round-trip efficiency of 56.9% has an overwhelming advantage over argon with an efficiency of 39.3%. Furthermore,

the increases in the pressure ratio and isentropic efficiencies improve the energy storage performance considerably. There also exit optimal values of the delivery compression ratio, particle sizes, length-to-diameter ratios of the reservoirs, and discharging durations corresponding to the maximum round-trip efficiency and preferable discharging power stability. The above can provide a basis for the optimal design and operation of the Joule–Brayton based PHES.

Key words: pumped heat electricity storage, pumped thermal electricity storage, Brayton, thermal energy storage, heat storage, energy storage

1 Introduction

The increase in energy consumption and the demand for decrease in carbon emission have result in great changes in the global energy structure owing to which the proportion of renewable energy usage has increased and that of fossil energy has gradually decreased [1]. From 2007 to 2017, the total renewable power capacity of non-hydropower renewables increased more than six-fold (that of solar energy and wind energy increased 48-fold and six-fold respectively) [1, 2]. In particular in 2017, renewable power accounted for 70% of net additions to the global power generation capacity and 26.5% of the global electricity production [1, 2]. However, the majority of renewable energy resources have inherent intermittency and instability characteristics, which results in the carryover of oscillation and unreliability to the power network. For example, 6% photovoltaic power and 12% wind power was wasted in China in 2017 [3]. Electrical energy Storage (EES) that converts electrical energy into another form of energy for storage and converts it back to electrical energy when required, is considered as one of the most promising solutions for increasing the penetration depth of renewable energy resources [4, 5]. Moreover, EES is an essential link in the energy supply chain, which provides services such as load leveling, peaking shaving, power quality improvement, and frequency regulation for the traditional power grid, thus improving the security and utilization rate of the power grid [6-8].

Nowadays, there exist various energy storage technologies and different criteria for their classification. Based on the form of energy storage in the system, the energy storage technologies can be mainly categorized into five classes: chemical (hydrogen and synthetic natural gas), electrical (capacitors and superconducting magnetic), electrochemical (classic batteries and flow batteries), mechanical (flywheels, adiabatic compressed air, pumped heat electrical storage, pumped hydro and cryogenic energy storage) and thermal (sensible heat, latent heat and thermochemical heat) [4, 5]. Each EES technology has a suitable range of applications (e.g. batteries, compressed air energy storage (CAES), and pumped hydro storage are suitable candidates for peak shaving; flywheels, super-capacitors and superconducting magnetic energy storage are suitable candidates for frequency regulation) depending on its advantages, drawbacks, and scales [4, 9].

Among the available storage technologies, only pumped hydro storage (PHS) and CAES are mature large-scale stand-alone electricity storage technologies that can be used to store power greater than 100 MW under commercial operation [4, 5, 10]. PHS is the most mature EES technology having a high capacity, long storage period, high efficiency and relatively low cost per unit of energy. To date, there are more than 300 facilities with a total power of over 170 GW in operation, which accounts for approximately 96% of the global energy storage capacity [4, 11]. The Bath County Pumped Storage Station in the USA is the largest PHS power station in the world which has a generation capacity of 3 GW and a storage capacity of 11 h [12]. CAES is another mature technology that is typically used for large scale energy storage. The operational CAES units in the world are 290 MW/2 h CAES in Huntorf, Germany with an underground storage cavern of approximately 310,000 m^3 and 110 MW/26 h CAES in McIntosh, Alabama, USA, with a cavern of approximately 500,000 m^3 [4, 5, 13]. The main barriers for PHS and CAES plants are similar, in that their construction requires appropriate geographical conditions for the huge volume of storage.

A category of novel energy storage technologies "pumped heat electricity storage (PHES)" was proposed, which is also called "pumped thermal electricity storage (PTES)" and "thermo-electrical energy storage (TEES)". During the charging process of the energy storage, heat is pumped from cold reservoirs (CRs) to hot reservoirs (HRs) via a heat pump circle and then stored; during the discharging process electricity is generated by the stored thermal energy through the heat-work conversion circle. Owning to the advantages of its high energy density and high efficiency, PHES has captured the attention of researchers as a promising technology for large-scale energy storage in recent years [14-31]. The categories of the PHES systems is mainly based on two types of reversible heat-work conversion circles thus far: The Joule–Brayton cycles [25-31] and the Rankine cycles [14-24].

The Rankine-cycle-based PHES system was first proposed by the ABB Company by the name of TEES [14, 15]. It mainly includes the transcritical CO_2 Rankine cycle, organic Rankine cycles (ORCs), and subcritical stream Rankine cycle. Morandin et al. studied a TEES system based on a transcritical CO_2 Rankine cycle with hot-water thermal storage and ice-cold storage, and then optimized the system with an achieved round-trip efficiency of 60% on using the pinch analysis approach [16, 17]. Kim et al. then presented an isothermal TEES system based on the transcritical CO_2 Rankine cycle wherein water was sprayed to cool/heat transcritical CO_2 directly, and it was found that the expansion work and efficiency were improved via the isothermal expansion owing to the high efficient heat transfer with the thermal storage tanks [18]. Abarr et al. proposed the use of a PTES and bottoming system based on the transcritical ammonia cycle connected to a natural-gas peak plant and the obtained result indicates that the stand-alone energy storage efficiencies is between 51%-66% with a stand-alone bottoming efficiency of 24% [19, 20]. Wang and Zhang proposed and analyzed a PHES based on the transcritical CO_2 heat pump cycle during charging and the cascaded system of the transcritical CO_2 Rankine cycle and the subcritical NH3 Rankine cycle utilizing liquid natural gas cold energy with a round-trip efficiency of up to 139% [21]. Steinmann developed the compressed heat energy storage (CHEST) concept based on stream Rankine cycles combined with sensible and latent heat storage with an estimated round-trip efficiency of 70% based on the isentropic efficiencies of 0.9 [22]. A PHES based on the ORC system with the integration of low-temperature heat was also studied. Jockenhöfer et al. found that the ORC-CHEST system could provide 1.25 times the net power with a heat resource temperature of 100°C and a maximum exergetic efficiency of 0.59 [23]. Frate et al. studied a PHES system comprising of a vapor-compression heat pump integrated with a low-grade heat source for charging and an ORC system for discharging and found that the achievable round-trip efficiency was 130% on using R1233zd at the heat source temperature of 110 °C and the isentropic efficiency was 0.8 [24].

Using a single-phase gas as the working fluid, the Joule–Brayton-cycle based PHES generally consists of cold (low-pressure) thermal energy storage (TES) reservoirs, hot (high-pressure) TES reservoirs, and compressor–turbine-pairs, wherein the CRs and HRs are generally comprise packed-bed solid thermal energy storage owning to its wide temperature range, high efficiency, and small pressure loss. Desrues et al. presented a PHES system based on the Joule–Brayton cycle consisting of two TES reservoirs connected by two compressor-turbine-pairs and two heat exchangers comprising argon as the working gas and obtained an optimized round-trip efficiency of 66.7% based on the turbo machines' polytrophic efficiency of 0.9 [25]. Ni and Caram analyzed the influence of gas and pressure ratios etc. through a simulation and found the efficiency of the turbomachinery to be the factor limiting the round-trip efficiency [26]. Howes from the company Isentropic introduced three prototype of PTES and proposed a 2 MW PTES system with heat and cold thermal storage temperatures of 500 °C and -160 °C having a round-trip efficiency of up to 72% [27]. White et al. found that the round-trip efficiency and energy storage density increase with the temperature ratio between the hot and cold TES [28]. McTigue et al. presented a PTES system based on the Joule–Brayton cycle with a buffer vessel and performed a theoretical analysis on the PTES system coupled with a packed bed model of the HRs and CRs [29]. Benato presented a Joule–Brayton PHES system with an electric heater settled after the compressor in order to maintain the hot–tank temperature during charging, and the performance and cost evaluation of such a system with different TES materials and different working gases was analyzed [30,31].

There are mainly three categories of TES technologies: sensible heat storage, latent heat storage, and chemical heat storage [32]. Among the TES technologies, packed bed sensible TES has been identified as the most suitable technology for the PHES system owing to its advantages of low cost, small pressure loss, wide applicable temperature range, and large heat transfer surface area that results in a small temperature difference, etc. [30].

The performance of a PHES comprising heat and cold packed–bed reservoirs of different materials was analyzed in terms of the round-trip efficiency [25, 29, 30], energy density [30, 31], and costs [30, 31]. However, there still exist defects in the published studies: (1) such a PHES comprising heat and cold packed-bed reservoirs have strong unsteady characteristics whereas the majority of the analyses on the PHES were performed using the stable thermodynamics method, (2) it is not based on continuous cycles, and the initial state of each cycle is strong related to the state at the end of last cycle for the continuous cycles, (3) it neglects the coupling effect of dynamics, heat transfer and thermodynamics, (4) it involves the oversimplification of heat exchangers, and (5) argon or air is used as the working fluid.

In this context, we make the first attempt to investigate the cyclic transient behavior of the Joule–Brayton PHES system. Specifically, on a 10 MW/4 h PHES system, a transient analysis method for the coupling of the dynamics, heat transfer and thermodynamics of the PHES system with the components including the compressor, expander, TES reservoirs and heat exchangers is proposed and solved numerically for multiple continuous cycles. The research presents a more realistic behavior that is close to the real cyclic operations of the Joule–Brayton PHES, wherein the working performance including both the round-trip efficiency and power attenuation during discharging can obtained. Helium is studied as a monoatomic molecular gas with a high energy density that can be used as the working gas. This paper is thus focused on the influencing mechanism of the parameters of the PHES system and the key components that are presented in figure 1.

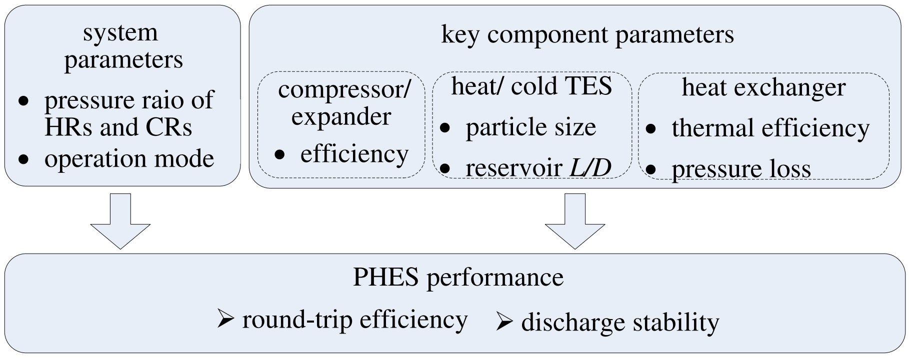

Fig.1. Parameters influencing on PHES performance

In the following, section 2 presents a detailed description of the Joule–Brayton based PHES system, section 3 describes the coupling analysis method of the PHES system and the components, and introduces the parameters design of the 10 MW/4 h PHES system, section 4 presents the results and findings, and the last section concludes the paper.

2 Description of Joule–Brayton based PHES system

Based on the PHES system proposed by White et al. [28], and McTigue et al. [29], the Joule–Brayton PHES discussed in this paper, as shown in figure 2, mainly consists of a cold (low–pressure) TES reservoir, a hot (high–pressure) TES reservoir, two compressor–turbine–pairs(one for charging and the other for discharging) and two heat exchangers. The heat exchangers are required to remove surplus heat from the PHES system and stabilize the temperature variation in the packed–bed reservoirs during the charging process. A buffer vessel is also required to store/release gas in order to stabilize the system pressure during charging/discharging to balance the gas mass changes in the two reservoirs. During the charging and discharging processes, approximately 0.36% of the total flow rate of the gas is required to be exported to the buffer vessel through position 1 in figure 2 to maintain the system under a constant pressure. Furthermore, the same amount of gas returns the system through position 2 during the discharging process. Moreover, a different pressure ratio of the compressor and expander during the charging and discharging processes can be obtained by adjusting the buffer vessel, valves, and a pressure adjustment compressor coordinately during the idle period.

The working principal of the Joule–Brayton based PHES system is that during the charging process, the working gas driven by the compressor (for charging) goes through the HR, heat exchanger 2 (HX2), the expander (for charging), the CR and heat exchanger 1 (HX1) in the indicated direction of charging. During the charging process, the system operates as a heat pump wherein the heat is extracted from the CR to the HR while consuming electricity, and cold and heat thermal energy are stored in the CR and HR respectively. During discharging, the system operates as a heat engine with the working gas flowing along the indicated direction of discharge, which is opposite to direction of charging, when the heat returns from the HR to the CR in order to generate electricity.

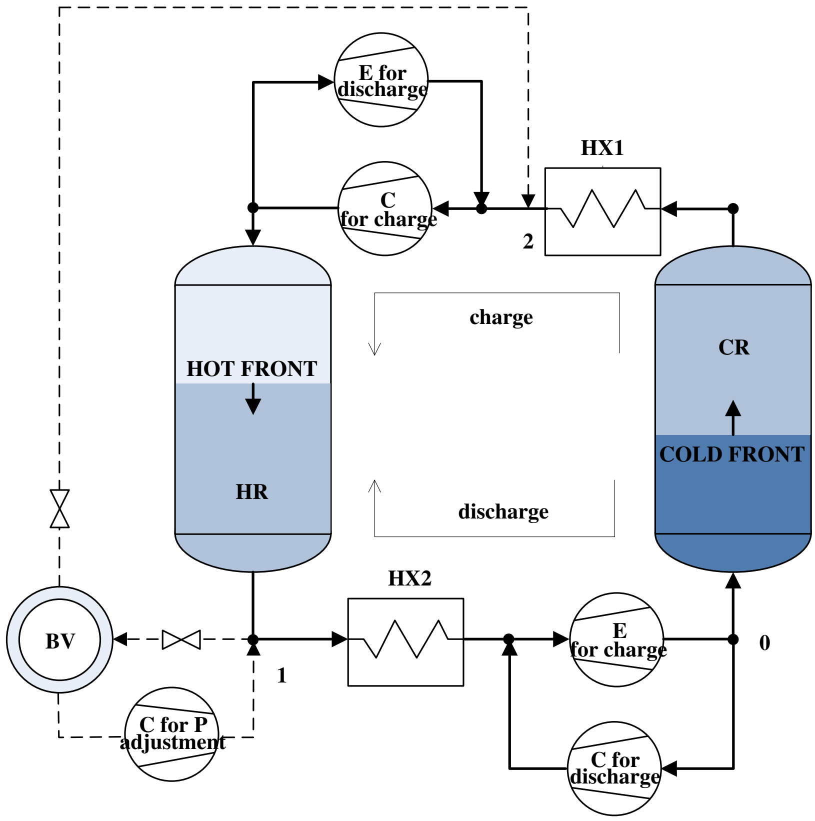

Fig.2. Layout of the PHES system. BV = buffer vessel; C = compressor; E = expander; HX = heat exchanger; CR = cold reservoir; HR = hot reservoir.

3 Methodology: coupling analysis of dynamics, transient heat transfer, and thermodynamics

Dynamics: In the PHES system, the compressor is the driving component of the gas flow, whereas the expander, the cold and hot storage reservoirs and the heat exchangers are the components that consume the mechanical energy of the gas during both the processes of charging and discharging. During the working process, the temperature profiles and thermophysical properties of the gas in the CR and HR are changing with time, thus resulting in a change in the pressure loss of the packed bed and leading to a pressure variation of the entire system. The pressure at point 1 during charging and at point 2 during discharging are maintained constant by the buffer vessel as shown in figure 3. *Heat transfer:* the transient temperature at the outflow of the CR and HR solved using the unsteady mass and energy conservation equations of the packed bed. *Thermodynamics:* For a fixed compression ratio of the compressor, the expansion ratio of the expander changes with time owing to the variation in the components' pressure loss. Along with the transient variation of the temperatures at the inlets and pressure ratios, the power and outflow temperatures of the compressor and the expander changes are time-varying. *Thermal properties:* The thermal properties of a gas, such as its density, thermal conductivity, and viscosity, have a great influence on the system performance. Moreover, the properties of the gas are obtained from the National Institute of Standards and Technology (NIST) database and updated in real-time during the solution procedure. Therefore, a coupling analysis including dynamics, transient heat transfer, thermodynamics and thermal properties is performed to obtain the transient behavior of the PHES system as shown in figure 3.

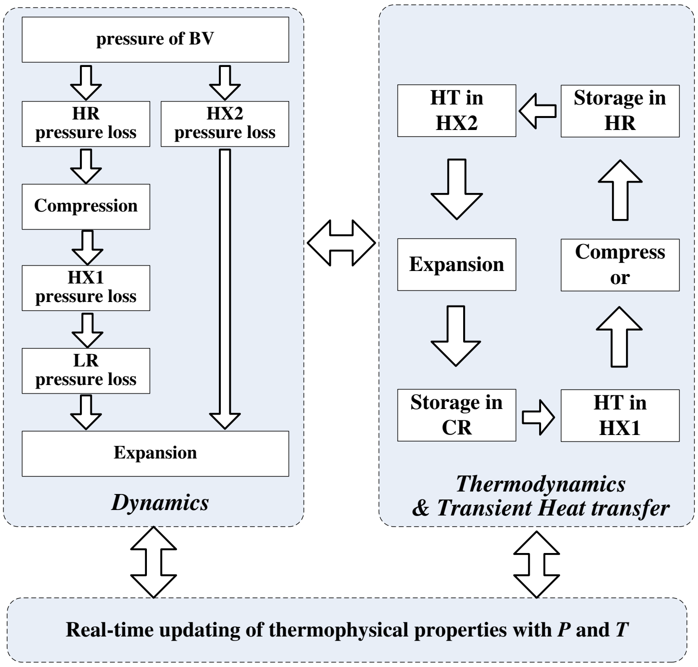

Fig.3. Coupling analysis of PHES during charging process

3.1 Dynamic conservation equation of PHES system

In the typically closed PHES system, the compressor provides the driving force of the expander and the gas flow in the components including the HR and CR and heat exchangers during both the charging and discharging processes. For the PHES system shown in figure 2, if we suppose that the total pressure at position 0 is P_0 during the charging and $p_0^{'}$ during the discharging respectively, we obtain:

$$\left(p_0 - \Delta p_{\mathrm{LP}} - \Delta p_{\mathrm{HX1}}\right)\beta_{\mathrm{c}} - \Delta p_{\mathrm{HP}} - \Delta p_{\mathrm{HX2}} - p_0\beta_{\mathrm{e}} = 0 \tag{1}$$

during the charging process and

$$p_0^{'}\beta_c^{'} - \Delta p_{\mathrm{HX2}}^{'} - \Delta p_{\mathrm{HP}}^{'} - \left(p_0^{'} + \Delta p_{\mathrm{LP}}^{'} + \Delta p_{\mathrm{HX1}}^{'}\right)\beta_e^{'} = 0 \tag{2}$$

during the discharging process, wherein the superscript ‘denotes the discharging process. Δp indicates the total pressure loss at each component, and β_{c} and β_{e} are the compression ratio and expansion ratio respectively.

3.2 Thermodynamics of PHES system

3.2.1 Compressor and expander

Taking into account the irreversibility loss of turbomachines, the polytropic process of compression and expansion occurs with the polytropic efficiencies η_{c} and η_{e} respectively. For the compressor

$$T_{\mathrm{c,out}}/T_{\mathrm{c,in}} = \beta_{\mathrm{c}}^{\kappa/\eta_{\mathrm{c}}} \tag{3}$$

For the expander

$$T_{\mathrm{e,out}}/T_{\mathrm{e,in}} = \beta_{\mathrm{e}}^{-\kappa\eta_{\mathrm{e}}} \tag{4}$$

where the parameter κ is defined as $\kappa = (\gamma-1)/\gamma$ and γ is the specific heat ratio ($c_{\mathrm{p}}/c_{\mathrm{v}}$) of the gas [25, 33].

During the charging and discharging process, temperatures and densities of the HR and CR

outflow gas transiently vary leading to the variation of volume flow rates and rotation rates in the compressor and the expander. The unsteady variation of the turbo-machines shaft power P(t) owing to the inertia of rotors can be calculated by:

$$P\left(t\right)=-I\cdot\omega\left(t\right)\frac{\mathrm{d}\omega\left(t\right)}{\mathrm{d}t} \tag{5}$$

Where I is the moment of inertia of rotor and ϖ(t) is the angular velocity. The angular velocity is proportional to the volume flow rate Q(t) and inversely proportional to the gas density at the constant mass flow rate.

$$\omega(t)=\frac{\omega_{\mathrm{des}}}{Q_{\mathrm{des}}}Q(t)=\frac{\omega_{\mathrm{des}}\rho_{\mathrm{des}}}{\rho(t)} \tag{6}$$

Where ϖ_{des} and Q_{des} are the angular velocity and the volume flow rate under the design condition, respectively.

3.2.2 Packed bed heat/cold thermal energy storage reservoirs

The domains of the hot and cold thermal energy storage reservoirs are considered as cylindrical tanks, which include the packed bed of the TES particles and the heat transfer gas flowing through the void space. On assuming that the flow pattern is a 1D Newtonian plug flow, neglecting the temperature gradient in the radial direction and neglecting the heat loss through the well-insulated wall, the governing energy conservation equations of the unsteady two-phase model of such packed beds is given as follows.

For the fluid phase,

$$\varphi\frac{\partial\rho_g}{\partial t}+\frac{\partial G}{\partial x}=0 \tag{7}$$

$$\frac{\partial T_{\mathrm{g}}}{\partial t}+\frac{G}{\rho_{\mathrm{g}}\varphi}\frac{\partial T_{\mathrm{g}}}{\partial x}=\frac{h_{\mathrm{v}}}{\rho_{\mathrm{g}}c_{\mathrm{p,g}}\varphi}\left(T_{\mathrm{s}}-T_{\mathrm{g}}\right) \tag{8}$$

For the solid phase,

$$\frac{\partial T_{\mathrm{s}}}{\partial t}=\frac{h_{\mathrm{v,eff}}}{\rho_{\mathrm{s}}c_{\mathrm{s}}(1-\varphi)}\left(T_{\mathrm{g}}-T_{\mathrm{s}}\right)+\frac{k_{\mathrm{s,eff}}}{\rho_{\mathrm{s}}c_{\mathrm{s}}(1-\varphi)}\frac{\partial^2 T}{\partial x^2} \tag{9}$$

where $h_{\mathrm{v,eff}}$ is the effective volumetric heat transfer coefficient on considering the internal heat conduction resistance in a solid (for a Biot number smaller than 100) having the relationship with the volumetric heat transfer coefficient $h_{\mathrm{v}} = h_{\mathrm{p}}6(1\text{-}\varphi)/d$. The volumetric heat transfer coefficient of Chandra's equation is used which fits well with the experimental results under both low and high pressures [35, 36]

$$h_{\mathrm{v,eff}}=\begin{cases} h_{\mathrm{v}} & \text{for } Bi\le 0.1 \\ \dfrac{1}{\dfrac{1}{h_{\mathrm{v}}}+\dfrac{d_{\mathrm{p}}^2}{60k_s\left(1-\varphi\right)}} & \text{for } 0.1< Bi\le 100 \end{cases} \tag{10}$$

$$h_{\mathrm{v}}=1.45\frac{Re^{0.7}k_{\mathrm{g}}}{d^2} \tag{11}$$

where the characteristic length for the Biot number is $d_{\mathrm{p}}/6$ [37].

$$Bi=\frac{h_{\mathrm{p}}d_{\mathrm{p}}}{6k_s} \tag{12}$$

$k_{\mathrm{s,eff}}$ is the effective thermal conductivity for the non-contiguous spherical particles in a dispersion medium given by [38, 39]:

$$\frac{k_{\mathrm{s}}-k_{\mathrm{s,eff}}}{k_{\mathrm{s}}-k_{\mathrm{g}}}\left(\frac{k_{\mathrm{s,eff}}}{k_{\mathrm{g}}}\right)^{-\frac{1}{3}}=\varphi \tag{13}$$

which is solved by performing iteration.

The dramatic temperature changes dramatically in the packed beds would lead to a change in the volume flow rate and thermoproperty of the gas in the packed bed. In this paper, the packed bed is divided into n sections along the axis, and the pressure drop across the packed bed and each section are given by the Ergun equation shown as below [34].

$$\Delta p\left(i\right)=\frac{\Delta L\cdot G^{2}}{\rho(i)\cdot d}\left(1.75\frac{1-\varphi}{\varphi^{3}}+150\frac{1-\varphi}{\varphi^{3}}\frac{\mu(i)}{Gd}\right) \tag{14}$$

$$\Delta p=\sum_{i=1}^{n}\Delta p(i) \tag{15}$$

where Δp and $\Delta p(i)$ are the pressure drop across the packed bed and the pressure drop across the i_{th} section, respectively, and ΔL ($\Delta L = L/n$) is the length of each section.

3.2.3 Heat exchanger

In the PHES system, the heat exchangers play important roles including removing the surplus heat and stabilizing the temperature fluctuations from the HR and CR during the charging process. Water from the cooling towers is usually selected as an efficient cooling media for heat exchangers having a temperature approximately about 2–5° C higher than the ambient temperature. As the heat capacity of the cooling water is greater than that of the gas and on ignoring the influence of the heat exchanger heat capacity, the outflow temperature from the heat exchanger can be obtained as follows.

$$T_{\mathrm{g,o}}\left(t\right)=T_{\mathrm{g,i}}\left(t\right)-\varepsilon\frac{\dot{m}_{\mathrm{g}}c_{\mathrm{p,g}}}{\dot{m}_{\mathrm{w}}c_{\mathrm{p,w}}}(T_{\mathrm{g,i}}\left(t\right)-T_{\mathrm{w,i}}) \tag{16}$$

where $\dot{m}$ and c_{p} are the mass flow rate and heat capacity, and ε is the heat exchanger effectiveness.

3.3 Systemic analyses of PHES system

For the PHES system, the transient specific energy performed during charging and delivered during discharging, with considering the unsteadiness of the compressor and expander, can be obtained using equation (17) and equation (18), respectively.

$$e_{\mathrm{chr}}(t)=e_{\mathrm{c,chr}}(t)-e_{\mathrm{e,chr}}(t)+\frac{1}{\dot{m}c_{\mathrm{p}}}\left(P_{\mathrm{e}}(t)+P_{\mathrm{c}}(t)\right) \tag{17}$$

$$e_{\mathrm{dis}}(t)=e_{\mathrm{e,dis}}(t)-e_{\mathrm{c,dis}}(t)-\frac{1}{\dot{m}c_{\mathrm{p}}}\left(P_{\mathrm{e}}(t)+P_{\mathrm{c}}(t)\right) \tag{18}$$

As shown in equation (5), the moment of inertia of the compressor and the expander are needed for calculating P(t), whereas there is no available compressor and expander for the 10MW PTES system. In this study, referring to the compressor and the expander in the 10MW Advanced compressed air energy storage, the moment of inertia of compressor and the expander rotor is taken 1800 kgm^2 at the rated speed of 1500 rpm [42, 43]. Under the situations in this study, the maximum absolute value of angular acceleration of the expander rotor and the compressor rotor is 0.0063 rad/s^2 and 0.0026 rad/s^2 respectively, and the corresponding P_{e}(t) and P_{c}(t) is -3.47 kW and 0.36 kW, which are less than ±0.04% of the transient shaft power and can be neglected.

By bringing equation (3), (4) into equation (15), (16), and neglecting the unsteady variation of the turbine machines, the transient specific energy can be calculated as below:

For the charging process,

$$e_{\mathrm{chr}}(t)=T_{\mathrm{c,in}}(t)\cdot\left(r_{\mathrm{c}}(t)^{\kappa/\eta_{\mathrm{c}}}-1\right)-T_{\mathrm{e,in}}(t)\cdot\left(1-r_{\mathrm{e}}(t)^{-\kappa\eta_{\mathrm{e}}}\right) \tag{19}$$

For the discharging process,

$$e_{\mathrm{dis}}(t)=T'_{\mathrm{e,in}}(t)\cdot\left(1-r'_{\mathrm{e}}(t)^{-\kappa\eta_{\mathrm{e}}}\right)-T'_{\mathrm{c,in}}(t)\cdot\left(r'_{\mathrm{c}}(t)^{\kappa/\eta_{\mathrm{c}}}-1\right) \tag{20}$$

Where e_{chr} and e_{dis} are specific energy (J/kg) of shaft work during charging and discharging, $T_{\mathrm{c,in}}$ and $T_{\mathrm{e,in}}$ are the inflow temperatures (K) of the compressor and the expander during charging, and the superscript ‘denotes the discharging process.

On assuming no mechanical loss, the round-trip coefficient of the PHES system is obtained on using the quotient of the net delivered shaft work during the discharging process and the consumed shaft work during the charging process, as shown in equation (21)

$$\chi = \frac{\text{net work output}}{\text{net work input}} = \frac{\int_{\text{dis}} \dot{m}_{\text{dis}} c_{\text{p}} e_{\text{dis}}\left(t\right)\text{d}t}{\int_{\text{chr}} \dot{m}_{\text{chr}} c_{\text{p}} e_{\text{chr}}\left(t\right)\text{d}t} \tag{21}$$

where $\dot{m}$ is the mass flow rate though the compressors and expanders.

The stability of the delivery power is another important factor affecting for the energy storage system. In this paper, the offset ratio of the delivery power is increased to evaluate the stability which is defined as the ratio of the offset range of the delivery power to the maximum value during the delivery period, as presented in equation (22).

$$\theta = \frac{\text{Max}\left(e_{\text{dis}}(t)\right) - \text{Min}\left(e_{\text{dis}}(t)\right)}{\text{Max}\left(e_{\text{dis}}(t)\right)} \tag{22}$$

For the PHES system, a smaller offset ratio indicates a more stable delivery power during the discharging process.

In order to validate the transient equation of the packed beds, the numerical simulations of the TES process of the crushed steatite (magnesium silicate rock) packed beds are performed by solving equations (7)–(13) with the parameters used in reference [44] and [45]. The temperature dependence of the heat capacity of the crushed steatite ($Mg_3Si_4O_{10}(OH)_2$) is taken in to consideration in the simulation [40]. The temperature profiles along the axial distance of the packed beds of the simulated and experimental results are shown in figures 4 (a) and 4(b); it can be observed that an obvious thermocline occurs during the charging process and the simulated profiles fit well with the experimental results which proves the accuracy of the simulation method [42, 43].

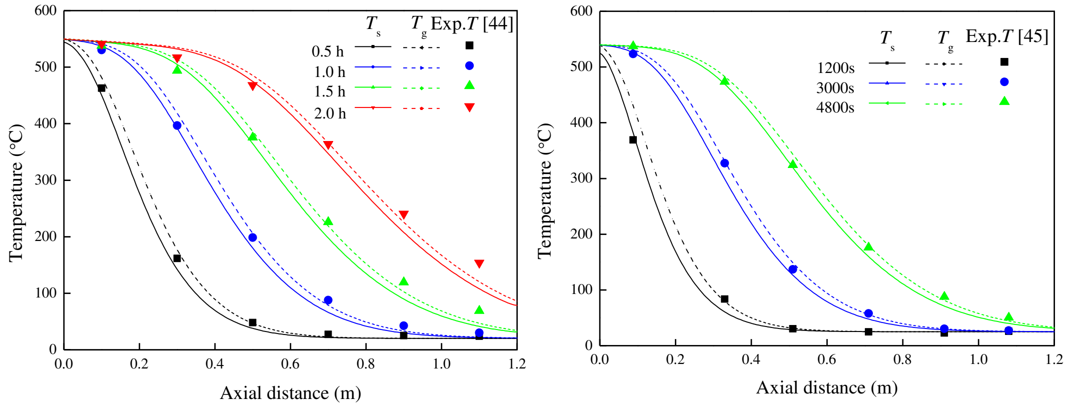

(a) with Meier et al.'s study [44] (b)with Hänchen et al.'s study [45]

Fig.4. Comparison between the simulation and experimental results of the temperature profiles in the packed beds

3.4 Parameters design of the 10 MW/4 h PHES system

In this paper, a Joule–Brayton based PHES system of 10 MW (nominally discharging power 10 MW, 4 h charging, and 4 h discharging) was designed and analyzed. The designed parameters of the PHES system with either argon or helium as the working gas are shown in Table 1 wherein the pressure ratio is 10 as in McTigue et al.'s study [29]. It should be noted that the heat capacity of helium is almost ten times that of argon, and thus, the mass flow rate of helium is approximately only 1/10th that of argon in a PHES system of the same power. Therefore, the pressure loss in the heat exchangers and packed-bed reservoirs would be decreased greatly on using helium instead of argon.

Table 1 Designed parameters of PHES system of 10 MW discharging power

Working gas	HP Pressure (MPa)	LP Pressure (MPa)	Average $c_{p,g}$ (J/kg/K)	Mass flow rate (kg/s)	Polytropic efficiency	ε of HXs	Δp of HP HXs (kPa)	Δp of LP HXs (kPa)	Cooling water temperature (K)
Argon	1.05	0.105	525	85.1	0.9	0.9	3	20	300
Helium	1.05	0.105	5193	8.6	0.9	0.9	0.3	2	300

The designed 10 MW/4 h PHES system consists of an HR and a CR with a packed bed of basalt particles. The packed-bed TES is unstable and has a larger packed bed volume, which results in a more stable output temperature but a higher cost and lower energy storage density. In consideration of the thermal front volume, the designed volumes of the HR and CR are selected to be twice the minimum design volume obtained using from the energy balance method $V = 2Q/\left(\overline{\rho_s c_s}\Delta T\right)$. The detailed parameters of the HR and CR are shown in table 2. In this design, the basalt is chosen as the hot and cold TES material, as it has a good heat capacity and thermal stability within the temperature range of -196° C–800° C. Based on the TA Q2000 DSC, the heat capacity of basalt is found to be strongly dependent on the temperature as shown in figure 5, and the linear fit equation is given in equation (23).

$$c_p(T) = 0.23 + 0.00201 \cdot T \tag{23}$$

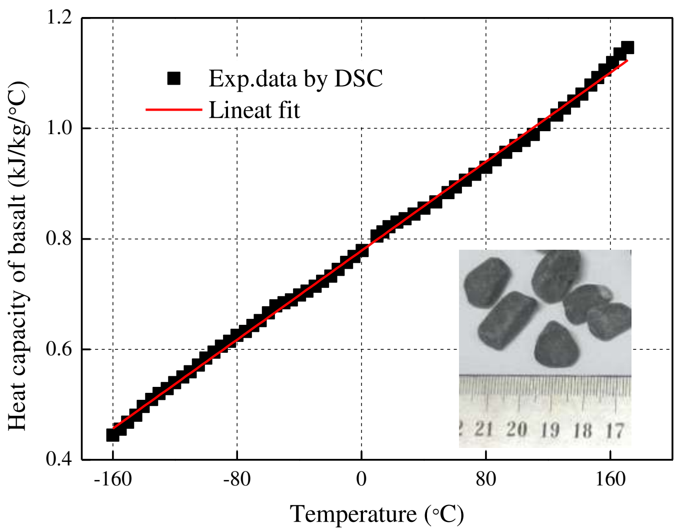

Fig.5. Dependence of heat capacity of basalt with temperature measured using DSC

Table 2 Hot and cold reservoir details for 10 MW/4 h PHES system
(the total volume is twice the minimum design volume)

Reservoir	Pressure (MPa)	Density of solid material (kg/m^3)	Porosity	Average d_p (mm)	Total Volume (m^3)	L (m)	D (m)

Heat	1.05	5175	0.35	30	460	10.96	7.31
Cold	0.105	5175	0.35	30	740	12.86	8.56

3.4.1 Heat exchangers design

For eliminating surplus heat and stabilizing the temperature variation, two heat exchangers are required for the Joule–Brayton cycle PHES. One heat exchanger is under low pressure and the other is under medium/high pressure, and such heat exchangers are required to be compatible with a wide range of operation conditions, high efficiency and low pressure loss wherein the shell-and-tube heat exchangers are the optimal choices. According to the working conditions of the PHES system, the one shell pass, two tube pass TEMA shell-and-tube heat exchangers were designed for the hot and cold heat exchangers using the *ε-NTU* method and an empirical relation [41], wherein the heat transfer tubes have an outer diameter of 32mm and thickness of 2 mm, and the working gas passes through the shell side to minimize the pressure loss of the gas side.

Figure 6 shows the variation of the heat transfer efficiency and pressure drop of HX1 (low pressure) and HX2 (high pressure) with the tube number and tube length on using argon and helium respectively. The heat-transfer tube number ranges from 100 to 1000, and the tube length ranges from 0.5 m to 10.0 m. It can be found that an increase in the number of tubes would obviously decrease the pressure loss and improve the efficiency, and an increase in the tube length would lead to an increase in the efficiency and pressure loss. In order to obtain a high round–trip efficiency, the PHES system requires heat exchangers with a small pressure loss and high efficiency which can be obtained by using a large number of long tubes but this amount and length cannot be increased beyond a certain limit owing to the prohibitive cost.

From figure 6, it can be found that for heat exchangers of the same size, the efficiencies are similar when using argon and helium, but the pressure drop observed when using helium is only approximately 1/10th the pressure drop observed when using argon owing to the difference in the mass flow rate. Furthermore, the pressure drop of HX1 under a low pressure is several times higher than the pressure drop of HX2 under a high pressure because of the high volume flow rate under the low pressure. From the design of the PHES system, the heat exchangers with an efficiency of 0.9, the pressure loss of HX1 of 20 kPa and pressure loss of HX2 of 3 kPa on using argon, and the heat exchangers with an efficiency of 0.9, pressure loss of HX1 of 2 kPa and pressure loss of HX2 of 0.3 kPa on using helium are achieved and such parameters are selected in the 10 MW/4 h PHES system.

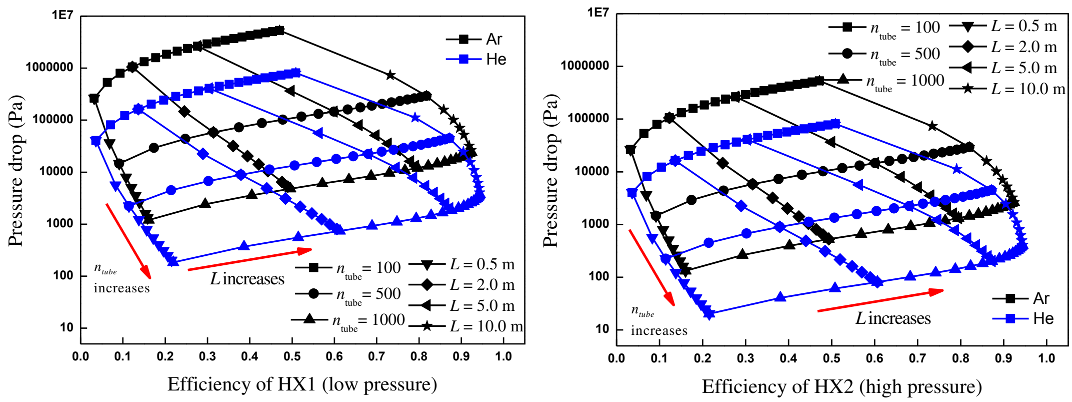

Fig.6. Efficiency versus pressure drop of the shell-and-tube heat exchangers

4 Result and Discussion

4.1 Cyclic behavior of PHES system

Based on the standard parameters in table 1 and 2, and the modeling method described in section 3, the working behavior of the PHES system running 100 circles was simulated using argon as the working gas; each cycle included 4 h of charging and 4 h of discharging. The axial temperature profile of the HR and CR at the end of the charging and discharging processes from the 1st circle to the 100th circle are shown in figures 7(a) and 7(b), respectively. It can be observed that, the profiles at the end of the charging and discharging process tend to coincide after several cycles. The temperature profiles in the reservoirs can be roughly divided into a stable temperature region and a thermocline region wherein the temperature gradient in the thermocline region decreases gradually with the cycling.

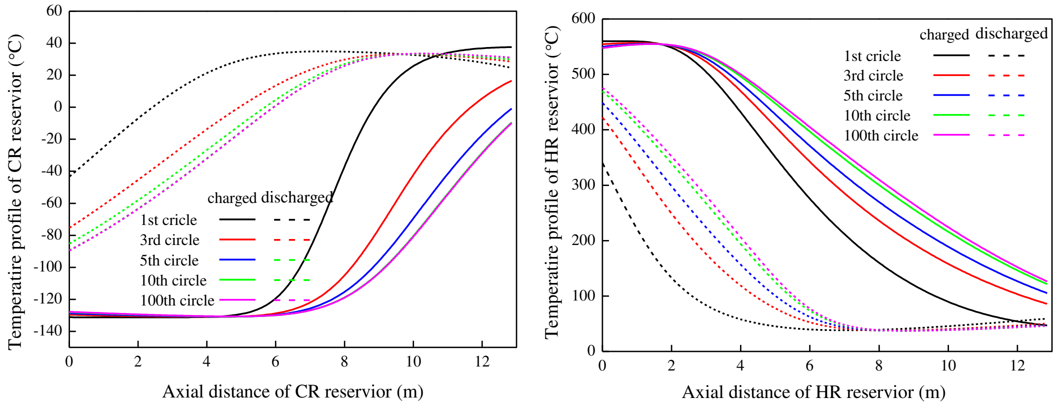

Fig.7. Cyclic behaviors of the HR and CR

In order to study the cyclic convergence of the PHES system, the factor $\Delta T_{\mathrm{Max}}(N)$ indicates the maximum temperature difference between the adjacent circles at the same axial position and is defined as shown in the equation (22). As shown in figure 8, the factor $\Delta T_{\mathrm{Max}}(N)$ declines exponential with the circle number where argon has a higher decline rate than helium. After 40 circles, the maximum temperature difference at the same axial position between the adjacent circles is below 0.1 °C for all the gases and reservoirs which is deemed cyclically stable. According to this, the following analysis is based on the data of the 40th circles which have achieved the cyclic stable state.

$$\Delta T_{\mathrm{Max}}(N) = \mathrm{Max}\left(\left|T_{i,N} - T_{i}\right|\right) \qquad N=1, 2, 3\ldots \tag{24}$$

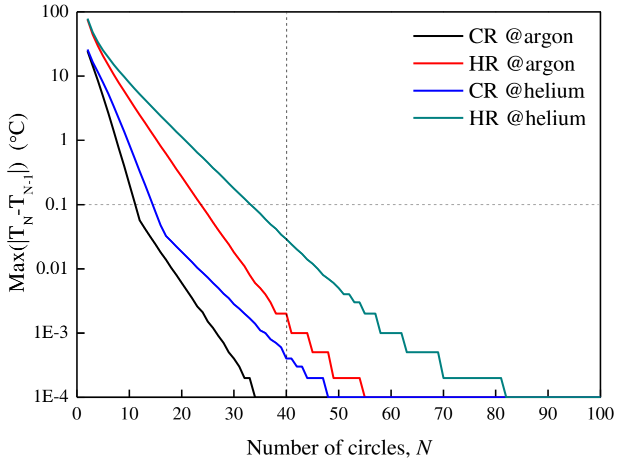

Fig.8. Maximum temperature differences between circles versus the number of circles

Under the cyclic stable state, figures 9(a) and 9(b) show the transient variation of the inflow and outflow temperatures of the HR and CR during the charging and discharging, respectively, when using argon as the working gas. This shows that the outflow temperature from the HR increases continuously after a period of stable state (approximately 1.5 h) during the charging process and decreases continuously after a period of stable state (approximately 1.5 h) during the discharging. The outflow temperature from the CR also has a similar unstable behavior but the temperature variation trend is opposite to that of the HR. Figure 9(c) shows the variation in the pressure loss of the HR and CR during the charging and discharging processes. It can be found that the pressure loss of the CR decreases linearly during the charging and increases during the discharging process, and the opposite phenomenon is observed in the case of the HR. This is because, during the charging period in the CR, the cold region grows gradually where the volume flow rate decreases owning to the high density which results in a decrease in the pressure loss, and during the discharging, the cold region retracts gradually and the pressure loss increases gradually. For similar reasons, the increase in the hot region in the HR could lead to a higher volume flow rate, hence increasing the pressure loss during the charging. The expansion ratio increases slightly during the charging and decreases during the discharging, as shown in figure 8(c), and is mainly influenced by variations in the pressure loss of the reservoirs. Figure 8(d) shows that the powers of the PHES compressor, expander and shaft are rather stable during the charging process, and during the delivery process, the compressor power increases and the expander power decreases gradually, thus leading to a decrease in shaft power. Based on the parameters listed in tables 1 and 2, the round-trip efficiency χ and the delivery working offset ratio θ using argon as the working gas is 39.3% and 71.0%, respectively, and the round-trip efficiency χ and delivery working offset ratio θ using helium is 56.9% and 45.9%, respectively.

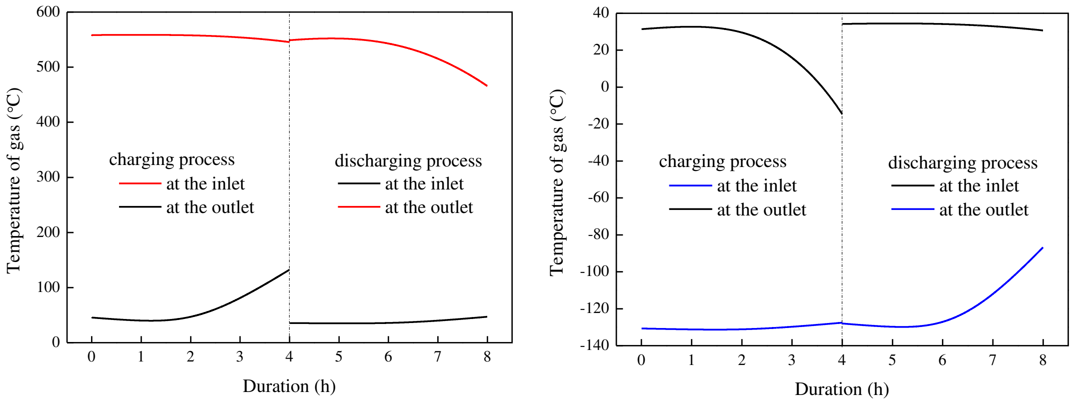

(a) inflow and outflow temperature of HP reservoir (b) inflow and outflow temperature of LP reservoir

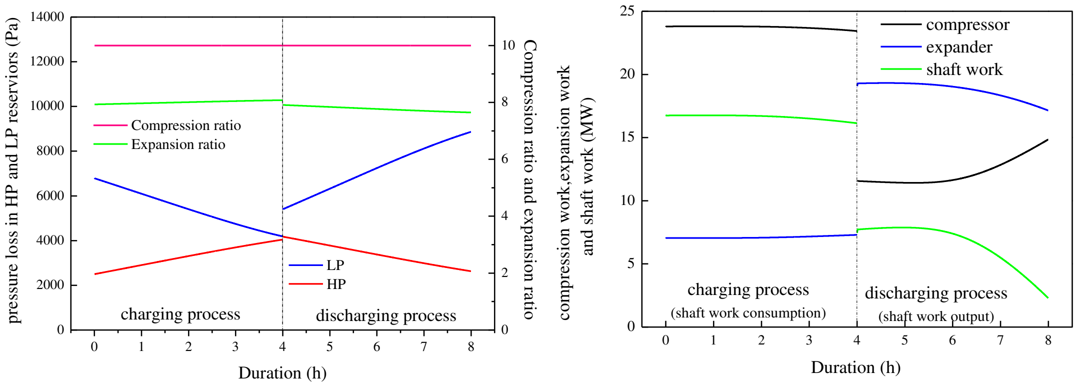

(c) pressure loss of the HP and LP reservoirs (d) transient power variation of PHES

Fig.9. Transient behaviors of the HR and CR and PHES system.

4.2 Effect of compression ratio during charging and discharging

The influencing factors include the compression ratio in the discharging process only and that for the entire processes, the polytropic efficiency of compressors and expanders, the particle diameter of the particles in the reservoirs, the length-to-diameter ratio of the reservoirs, the efficiency and pressure loss in the heat exchangers and the discharging duration of the PHES system performance are studied using argon and helium as the working gases.

Figure 10(a) shows the influence of the compression ratio of the compressors ranging from 5 to 16 during both charging and discharging processes on the round-trip efficiency χ and the delivery working offset ratio θ wherein the other parameters are obtained from in tables 1 and 2. It can be found that the round-trip efficiency increases gradually with the compression ratio β_c from 14.3% at $\beta_c = 5$ to 49.1% at $\beta_c = 16$ for argon and from 43.0% at $\beta_c = 5$ to 63.0% at $\beta_c = 16$ for helium; the round-trip efficiency of helium is considerably higher than that of argon, with a range of 13.9% to 28.6%. This is mainly because a much smaller pressure loss occurs in the reservoirs and heat exchangers of helium than those of argon, and a greater expansion work can be obtained on using helium. From figure 10(a), it can also be observed that the delivery working offset ratio θ decreases with the compression ratio β_c, and the offset ratio θ of helium is much lower than that of argon; such a result indicates that the delivery work during the discharging using helium is more stable than that using argon. The transient charging power and delivery power profiles at the compression ratio β_c of 7, 10 and 13 on using argon are shown in figure 10(b). It can be found that both the charging power and discharging power increase with the compressor ratio and an obvious decrease in delivery power occurs during the late discharging period.

Périlhon et al. recommended that the maximum fluid temperature should not exceed 800 °C for a reasonable life of the turbomachines [46]. The maximum temperature of the gas is approximately 750 °C in the PHES system at the compression ratio β_c of 16 for both argon and helium, which is within the permitted temperature range.

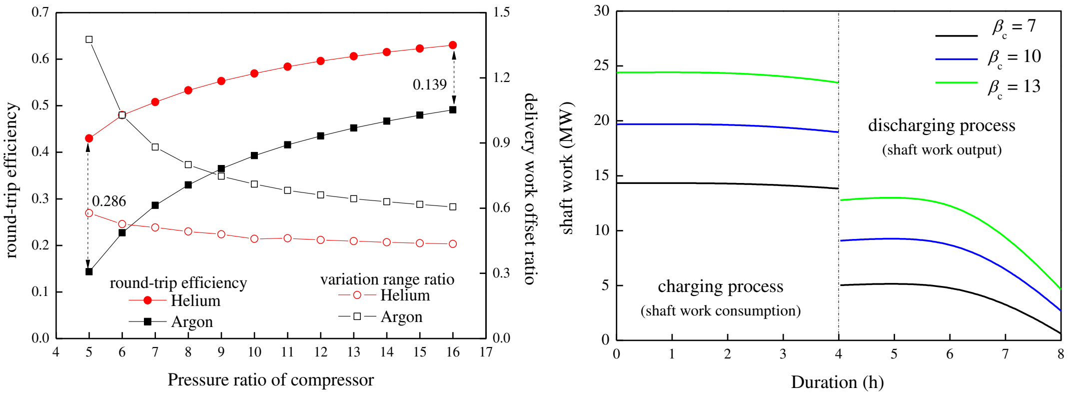

(a) (b)

Fig.10. Impact of compression ratio during both charging and discharging

4.3 Effect of compressor pressure ratio during discharging

Owing to the pressure loss, heat transfer loss and the irreversible loss of the compressor and expanders, setting the pressure ratio of the compressor during discharging as the same as that of during charging may not be the best choice. After the charging process, the compression ratio of the delivery process can be reset by storing some gas in the BV and recharging the system by the adjustment compressor during the idle time. At the charging compression ratio of 10 and the other parameters listed in tables 1 and 2, figure 11(a) shows the influence of the compression ratio ranging from 4 to 10 during the discharging process on the round-trip efficiency χ and the delivery working offset ratio θ. This result indicates that the round-trip efficiency χ increased first and then decreased with the discharging compress ratio and the maximum round-trip efficiency χ occurs at the discharging compress ratio of 7 for both argon and helium, the maximum round-trip efficiency χ obtained using helium is 59.0%, which is considerably higher than that obtained using argon: 41.7%. Moreover, it is also indicated from figure 11(a) that the offset ratio θ using helium and argon increases gradually with the increase in the discharging compress ratio. As shown in figure 11(b), when the charging compression ratio $\beta_{c,chr}$ is 10, the discharging compression power and discharging expansion power at a high pressure ratio of 10 are both higher than those at a low pressure ratio of 7. The shaft power at a compression ratio of 10 is lower than that at a compression ratio of 7; this is because, the variation amplitude of the compression power is greater than that of the expansion power when the discharging compression ratio increases from 7 to 10.

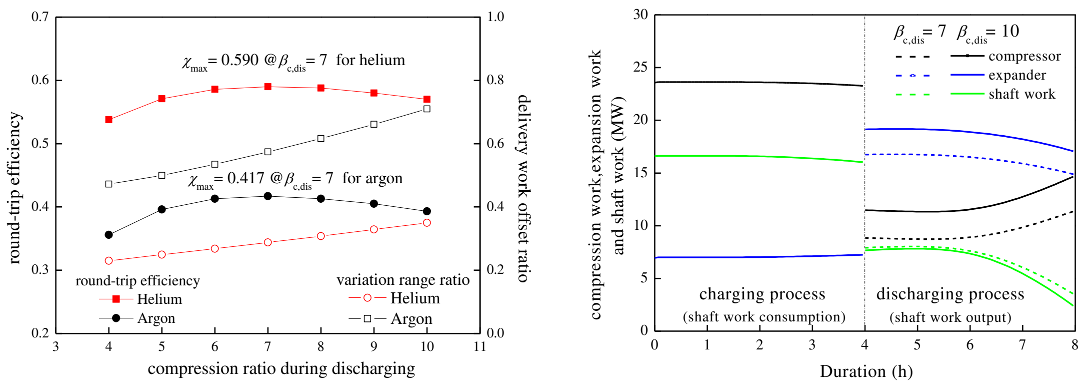

（a） （b）

Fig.11. Impact of compression ratio during discharging (at $\beta_{c,char} = 10$)

4.4 Effect of polytropic efficiency of both compressors and expanders

The plots of the round-trip efficiency χ with the polytropic efficiency of both the compressors and expanders ranging from 0.8 to 1.0 during both charging and discharging are shown in figure 12, which the use of argon and helium respectively, and the other parameters are obtained from tables 1 and 2. It can be observed that the polytropic efficiency of the compressors and expanders have an almost dominant effect on the round-trip efficiency χ, such that the round-trip efficiency increases from 16.2% at η = 0.8 to 68.3% at η = 1.0 when using argon, while the round-trip efficiency increases from 30.8% at η = 0.8 to 90.5% at η = 1.0 on using helium. The delivery working offset ratio θ in figure 11 shows that the increase in the polytropic efficiency also improves the stability of the delivery power.

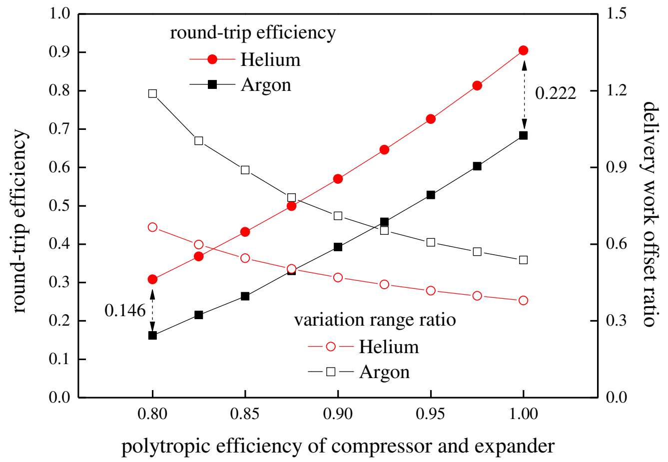

Fig.12. Impact of polytropic efficiency of compressor and expander

4.5 Effect of TES particles diameter

The diameters of the solid TES particles would affect the pressure loss and heat transfer in the packed beds and, hence, affect the PHES efficiency. Figure 13(a) shows the influence of the particle size in both the HR and CR in the range from 5mm to 70mm on the round-trip efficiency χ and the delivery working offset ratio θ. It can be observed that, the round-trip efficiency χ first increases and then gradually decreases with the particles sizes, the maximum round-trip efficiency of 40.2% occurs at d_p = 20 mm for argon and for helium the maximum round-trip efficiency of 58.8% is obtained at d_p = 15 mm, and such particle sizes always correspond to a small delivery working offset ratio θ. Such a result is mainly attributed to the joint action of the decrease in the pressure loss and increase in the heat transfer temperature difference between the gas and the TES materials as the particle size increases. Figure 13(b) shows the transient charging and delivery power in the case of particles sizes of 10 mm, 20 mm, and 40 mm using argon. It can be observed that large particles result in a relatively small charging power during the charging process; The discharging power is the lowest at d_p = 10mm during the entire discharging process which is relatively stable. However, although the discharging power at d_p = 40mm is higher than that at d_p = 20mm during the first discharging hour, it then declines fast and drops below that at d_p = 20 mm during the following discharging hours. The influence of the particle diameter mainly includes two aspects: large particles result in small pressure loss and also large thermal resistance in particles and large delivery temperature variation.

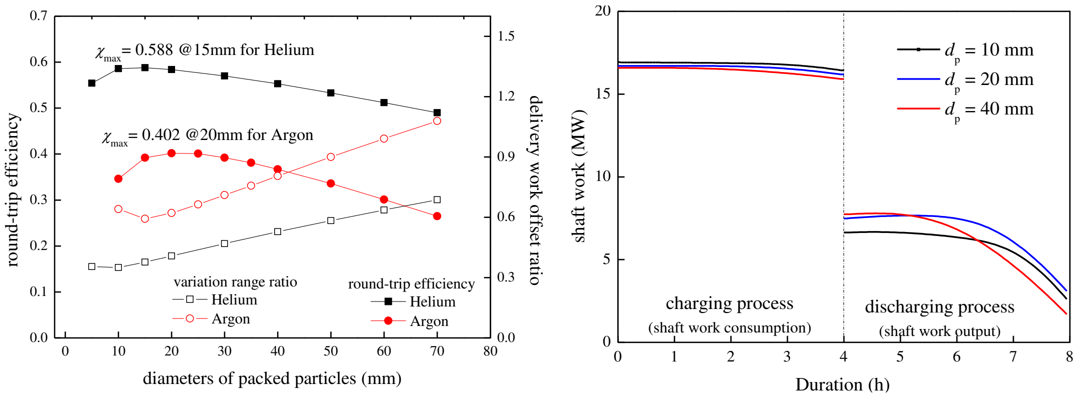

(a) (b)

Fig.13. Impact of particle diameter of compressor and expander

4.6 Effect of length–to–diameter ratio of reservoirs

As described in section 5, the volume of the designed HR and CR is 460 m^3 and 740 m^3, respectively, for the 10 MW/4 h PHES system. For the cylindrical reservoirs with a fixed volume, the length–to–diameter ratio *L/D* of the reservoirs is an important factor that influences the pressure loss and heat transfer of the packed beds. Figure 14(a) shows the variation in the round-trip efficiency χ and the delivery working offset ratio θ with the length–to–diameter ratio *L/D* of both the HR and CR, and the ranges of *L/D* are 0.5–3 for argon and 0.5–6 for helium. It can be observed in figure 14(a) that the influence of *L/D* is rather gentle in the case of helium whereas it is great in the case of argon. The round-trip efficiency χ increases at the beginning and decreases gradually with the increase in *L/D*, and a maximum round-trip efficiency of 41.0% and a minimum discharging power offset ratio of 72.6% occurs at *L/D* = 1 for argon; for helium the maximum round-trip efficiency is 57.0% and the minimum discharging power offset ratio of 51.8% occurs at *L/D* = 1.5. This is because a larger length–to–diameter ratio *L/D* would result in a larger pressure loss and a relatively smaller proportion of the thermocline region in the packed beds simultaneously, which is also a joint effect. Figure 14(b) shows the transient charging and discharging power under the conditions of the length–to–diameter ratio *L/D* of 0.5, 1.5, and 2.5 using argon. During the charging process, the larger length–to–diameter ratio *L/D* results in relatively higher charging power owing to the higher pressure loss; the discharging power is the lowest at *L/D* = 2.5 during the discharging process. However, the discharging power at *L/D* = 0.5 is higher than that at *L/D* = 1.5 during the discharging, and then declines fast and drops below that at *L/D* = 1.5.

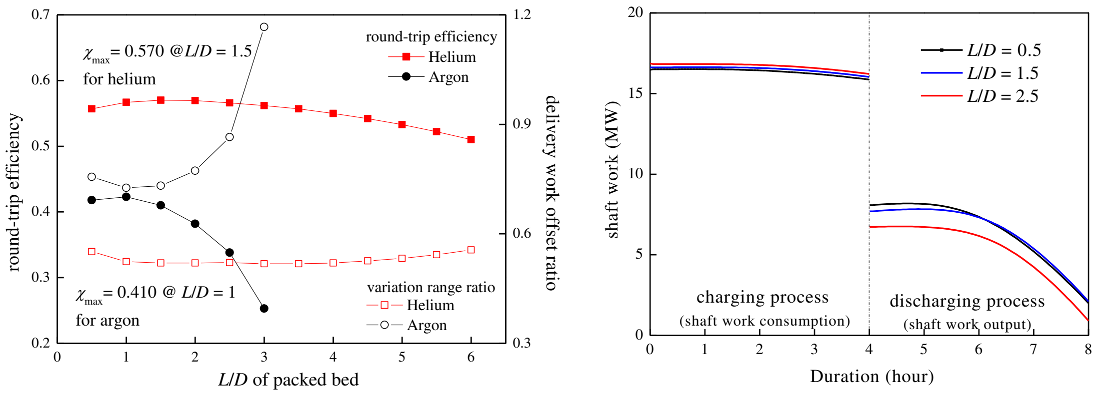

(a) (b)

Fig.14. Impact of *L/D* of packed bed reservoirs

4.7 Effect of efficiency and pressure drop of heat exchangers

Figure 15 shows the round-trip efficiency variation of the PHES with a 5% increase in the efficiency and pressure drop of the heat exchangers (including HX1 and HX2) based on the parameters listed in tables 1 and 2. It can be observed that the increase in the heat transfer efficiency of the heat exchangers improves the round-trip efficiency whereas the increase in the pressure loss decreases the round-trip efficiency; the effect of the heat exchangers efficiency and pressure drop on the PHES efficiency using argon is several times higher than that of helium; and the influence of the pressure loss of the low pressure heat exchanger (HX1) is more obvious than that of the high pressure heat exchanger (HX2).

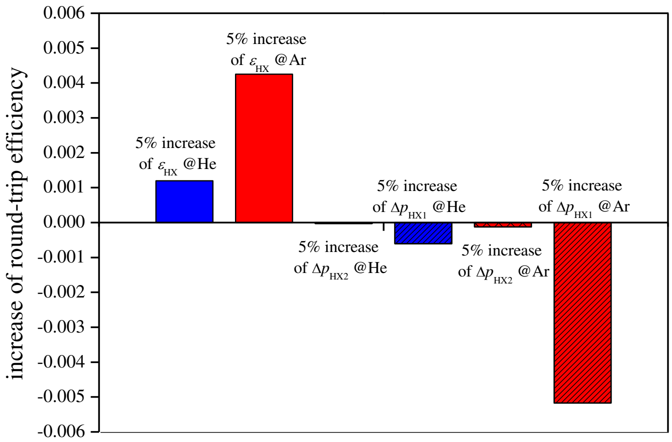

Fig.15. Impact of efficiency and pressure drop of heat exchangers

4.8 Effect of discharging duration

In the above analysis, each energy storage circle comprise a charging process of 4 h and a discharging process of 4 h; however, an equal discharging and charging duration may not be optimal for such a PHES system. Figure 16(a) shows the influence of the discharging time ranging from 2 h to 5 h (one circle consists of a 4 h charging process and 2–5 h discharging process) on the round-trip efficiency χ and the delivery working offset ratio θ using argon and helium, respectively. From figure 15(a), it can be observed that the round-trip efficiency χ increases at first and then decreases with the discharging time. The best selection of the discharging duration is a few minutes shorter than the charging time such that the maximum round-trip efficiency of 40.1% occurs at the delivery duration of 3.78 h for argon, and the maximum round-trip efficiency is 57.2% at the delivery duration of 3.91 h for helium. The delivery working offset ratio θ is relatively low (<20%) for a discharging duration less than approximately 3.5 h and then increases sharply.

Figure 16(b) shows the transient shaft power during the charging and discharging with the discharging duration of 3.5 h, 4 h and 4.5 h using argon. It can be observed that for the PHES system having a 3.5 h discharging duration has the most stable delivery power, and the obvious decline of the delivery power at the later stage of the discharging process can be observed with a longer discharging duration. Figure 16(c) shows the axial temperature profile of the hot TES reservoir at the end of the charging and discharging processes for the discharging durations of 3.5 h, 4 h and 4.5 h. It also shows that more exergy with a high temperature is stored in the hot TES reservoir in the PHES system in the case of the discharging duration of 3.5 h, and a relatively stable delivery thermal energy profile can be obtained during the discharging process, but it has the drawback of relatively unstable charging power, which can be reduced through the heat exchangers.

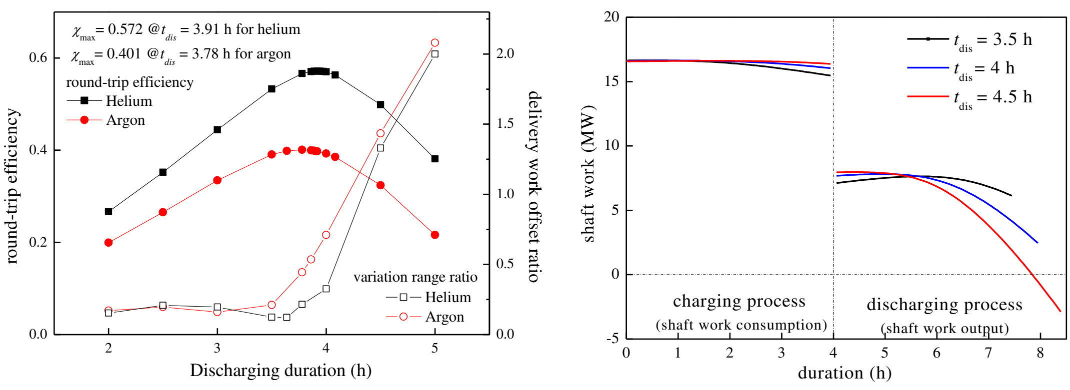

（a）　　　　　　　　　　　　（b）

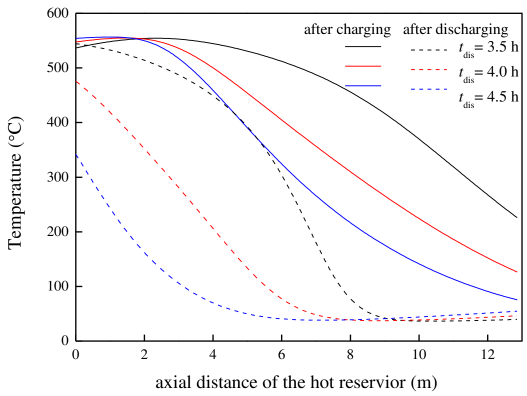

（c）

Fig.16. Impact of the discharging duration on the PHES behavior

5 Conclusions

In this paper, the use of the transient analysis method on the Joule–Brayton based PHES system is proposed for the coupling dynamics, thermodynamics and heat transfer process. The cyclic transient behavior of the 10 MW/4 h Joule–Brayton PHES system is studied using argon and helium as the working gases. Based on the round-trip efficiency and the variation range ratio of the delivery power, the mechanisms influencing PHES system and components parameters on the PHES system performance are further discussed. From the result of the analysis, the following conclusions can be obtained:

1. The delivery power clearly declines during the discharging process mainly owing to the thermal energy reduction from the packed bed TES reservoirs.

2. The gas resistance loss through the TES reservoirs and heat exchangers has a great influence on the system performance. In addition, helium, with small resistance losses, has an overwhelming advantage over argon for application in the PHES. The round-trip efficiency χ of helium is 56.9%, which is much higher than 39.3%, which is obtained on using argon under the

design conditions. The PHES system using helium can also provide more stable electricity with the delivery power offset ratio of 45.9% than that using argon with a delivery power offset ratio of 71.0%.

3. The increase in the pressure ratio and isentropic efficiencies would lead to an obviously improvement in the round–trip efficiency and delivery stability. Furthermore, an appropriate discharging compression ratio that is less than the charging compression ratio will aid in improving the round–trip efficiency. For the 10 MW/4 h PHES system, the optimum round-trip efficiency is obtained at the discharging compression ratio of 7 when the charging compression ratio is 10.

4. For the TES reservoirs, there exists optimal selections of particle sizes, ratios of length –to–diameter, and discharging durations corresponding to the maximum round-trip efficiency and preferable discharging power stability; this is mainly owing to the joint effects of the pressure loss, heat transfer and thermodynamics.

Further research is required for improving the improvement of the round-trip efficiency and discharging power stability and decreasing the costs, which will be the subject of the authors' future research.

Conflict of Interest

The authors declare no conflict of interest.

Acknowledgements

The authors would like to thank the National Key R&D Plan Program (2017YFB0903605), the National Natural Science Foundation of China (NO. 51506194), the Chinese Academy of Sciences Device Research & Manufacturing Program (YJKYYQ20170005, and the Newton Advanced Fellowship of the Royal Society (NA170093).

References

[1] BP Statistical Review of World Energy; 2018.

[2] REN21, Renewables 2017 Global Status Report, REN21 Secretariat, Paris, France; 2018.

[3] Li S, Wang J, Liu Q, Li L, Hua Y, Liu W. Analysis of Status of Photovoltaic and Wind Power Abandoned in China. J Power Energy Eng 2017; 5: 91–100.

[4]Chen H, Cong TN, Yang W, Tan C, Li Y, Ding Y. Progress in electrical energy storage system: A critical review. Prog Nat Sci 2009; 19: 291–312.

[5] Luo X, Wang J, Dooner M, Clarke J. Overview of current development in electrical energy storage technologies and the application potential in power system operation. Appl Energy 2015; 137: 511–36.

[6] Walawalkar R, Apt J, Mancini R. Economics of electric energy storage for energy arbitrage and regulation in New York. Energy Policy 2007; 35: 2558–68.

[7] Dobie WC. Electrical energy storage. Power Eng J 1998; 12:177–81.

[8] Makansi J, Abboud J. Energy storage: the missing link in the electricity value chain-An ESC White Paper. Energy storage Council; 2002.

[9] Yao L, Yang B, Cui H, Zhuang J, Ye J, Xue J. Challenges and progresses of energy storage technology and its application in power systems. J Mod Power Syst Cle 2016; 4: 519–28.

[10] Aneke M, Wang M. Energy storage technologies and real life applications–A state of the art review. Appl Energy 2016; 179: 350–77.

[11] DOE Global Energy Storage Database, http://www.energystorageexchange.org/

[12] Pumped Storage in Bath County, http://www.virginiaplaces.org/

[13] Guo H, Xu Y, Chen H, Zhou X. Thermodynamic characteristics of a novel supercritical compressed air energy storage system. Energy Convers Manage 2016; 115: 167–177.

[14] Ohler C, Mercangoez M. Thermoelectric energy storage system and method for storing thermoelectric energy, EP2157317 B1, 19-Jun-2013.

[15] Hemrle J, Kaufmann L, Mercangoez M. Thermoelectric energy storage system having two thermal baths and method for storing thermoelectric energy, WO2010118915; 2009.

[16] Morandin M, Maréchal F, Mercangöz M, Buchter F. Conceptual design of a thermo–electrical energy storage system based on heat integration of thermodynamic cycles–Part A: Methodology and base case. Energy 2012; 45: 375–85.

[17] Morandin M, Maréchal F, Mercangöz M, Buchter F. Conceptual design of a thermo–electrical energy storage system based on heat integration of thermodynamic cycles–Part B: Alternative system configurations. Energy 2012; 45: 386–96.

[18] Kim YM, Shin D G, Lee S Y, Favrat D. Isothermal transcritical CO2 cycles with TES (thermal energy storage) for electricity storage. Energy 2013; 49: 484–501.

[19] Abarr M, Geels B, Hertzberg J, Montoya LD. Pumped thermal energy storage and bottoming system part A: Concept and model. Energy 2017; 120: 320–31.

[20] Abarr M, Hertzberg J, Montoya LD. Pumped Thermal Energy Storage and Bottoming System Part B: Sensitivity analysis and baseline performance. Energy 2017; 119: 601–11.

[21] Wang G, Zhang X. Thermodynamic analysis of a novel pumped thermal energy storage system utilizing ambient thermal energy and LNG cold energy. Energy Convers Manage 2017, 148: 1248–64.

[22] Steinmann WD. The CHEST (Compressed Heat Energy STorage) concept for facility scale

thermo mechanical energy storage. Energy 2014; 69: 543–52.

[23] Jockenhöfer H, Steinmann WD, Bauer D. Detailed numerical investigation of a pumped thermal energy storage with low temperature heat integration. Energy 2018; 145: 665–76.

[24] Frate GF, Antonelli M, Desideri U. A novel Pumped Thermal Electricity Storage (PTES) system with thermal integration. Appl Therm Eng 2017; 121: 1051–58.

[25] Desrues T, Ruer J, Marty P, Fourmigu´e J, A thermal energy storage process for large scale electric applications. Appl Therm Eng 2010; 30:425–432.

[26] Ni F, Caram HS. Analysis of pumped heat electricity storage process using exponential matrix solutions. Appl Therm Eng 2015; 84: 34–44.

[27] Howes J. Concept and development of a pumped heat electricity storage device. Proc IEEE 2012; 100: 493–503.

[28] White A, Parks G, Markides CN. Thermodynamic analysis of pumped thermal electricity storage. Appl Therm Eng 2013; 53:291–8.

[29] McTigue JD, White AJ, Markides CN. Parametric studies and optimization of pumped thermal electricity storage. Appl Energy 2015; 137:800–11.

[30] Benato A. Performance and cost evaluation of an innovative Pumped Thermal Electricity Storage power system. Energy 2017, 138: 419–36.

[31] Benato A, Stoppato A. Heat transfer fluid and material selection for an innovative Pumped Thermal Electricity Storage system. Energy 2018; 147: 155–68.

[32] Gil A, Medrano M, Martorell I, Lázaro A, Dolado P, Zalba B et al. State of the art on high temperature thermal energy storage for power generation. Part 1 –Concepts, materials and modellization. Renew. Sustain. Energy Rev 2009; 14: 31–55.

[33] Dixon SL, Hall C. Fluid mechanics and thermodynamics of turbomachinery. 6th ed. USA: Butterworth-Heinemann, Elsevier Science Boston; 2010.

[34] Ergun S, Fluid flow through packed columns, Chem Eng Prog 1952; 48:89–94.

[35] Chandra P, Willits DH. Pressure drop and heat transfer characteristics of air rock bed thermal storage system. Sol. Energy 1981; 27:547–53.

[36] Liu J, Wang L, Yang L, Yue L, Chai L, Sheng Y et al. Experimental study on heat storage and transfer characteristics of supercritical air in a rock bed. Int J Heat Mass Transfer 2014; 77:883–90.

[37] Xu B, Li P, Chan C. Extending the validity of lumped capacitance method for large Biot number in thermal storage application. Sol Energy 2012; 86: 1709–24.

[38] Bruggeman DAG. Calculation of various physical constants in heterogeneous substances. Ann Phys 1935; 24:636–9.

[39] Abyzov AM, Goryunov AV, Shakhov FM. Effective thermal conductivity of disperse materials. I. Compliance of common models with experimental data. Int J Heat Mass Transfer 2013; 67: 752–67.

[40] Robertson EC, Hemingway BS. Estimating heat capacity and heat content of rocks. US Geological Surve; 1995.

[41] Shah RK, Sekulic DP. Fundamentals of heat exchanger design. John Wiley & Sons; 2003.

[42] Li W, Wang X, Zhang X, Zhang X, Zhu Y, Chen H. Experimental and Numerical Investigations of Closed Radial Inflow Turbine With Labyrinth Seals. J Eng Gas Turbines Power 2018; 140: 102502.

[43]The 10MW compressed air energy storage is under integrated test,

http://www.escn.com.cn/news/show-377349.html.[44] Meier A, Winkler C, Wuillemin D. Experiment for modelling high temperature rock bed storage. Sol Energy Mater 1991; 24: 255–64.
[45] Hänchen M, Brückner S, Steinfeld A. High–temperature thermal storage using a packed bed of rocks–heat transfer analysis and experimental validation. Appl Therm Eng 2011; 31: 1798–806.
[46] Périlhon C, Lacour S, Podevin P, Descombes G. Thermal electricity storage by a thermodynamic process: study of temperature impact on the machines. Energy Procedia 2013, 36: 923–38.

Nomenclature

Abbreviations

BOT	Bottoming system
BV	Buffer vessel
CAES	Compressed air energy storage
CHEST	Compressed heat energy storage
CR	Cold Reservoir
DSC	differential scanning calorimetry
EES	Electrical energy storage
HP	High pressure
HR	Hot reservoir
HX	Heat exchanger
LNG	Liquefied natural gas
LP	Low pressure
NIST	National Institute of Standards and Technology
ORC	Organic Rankine cycle
PHS	Pumped hydro storage
PHES	Pumped heat electricity storage
PTES	Pumped thermal electricity storage
TEES	Thermo-electrical energy storage
TEMA	Tubular Exchanger Manufacturers Association
TES	Thermal energy storage

Symbols

Bi	Biot number
C	Specific heat capacity, J K^{-1} kg^{-1}
d	Ddiameter of particles, m
D	Diameter of packed bed reservoir, m
e	Specific energy, J kg^{-1}
G	Mass flow rate, kg s^{-1}
h	Volumetric heat transfer coefficient, W m^{-3} K^{-1}
i	Number i

I	Moment of inertia, kg m^2
K	Thermal conductivity, W m^{-1} K^{-1}
L	Length scale of packed bed, m
m	Mass of gas, kg
n	Number
N	Number of circles
P	Power, W
Q	Volume flow rate, m^3 s^{-1}
Re	Reynolds number
t	Time, s
T	Temperature, K
β	Compression/expansion ratio of compressor/expander
γ	Adiabatic exponent of gas
ε	Efficiency of heat exchanger
η	Polytropic efficiency of compressor/expander
θ	Offset ratio of delivery power
κ	Parameter, $(\gamma-1)/\gamma$
μ	Dynamic viscosity, Pa s
ρ	Density, kg m^{-3}
Φ	Porosity of packed bed
X	Round-trip efficiency
ω	Angular velocity, rad s^{-1}
Subscript	
0	Point 0
1	Point 1
c	Compressor
chr	Charge
des	Design
dis	Discharge
e	Expander
eff	Effective
g	Gas
HP	High pressure
HX1	Heat exchanger 1
HX2	Heat exchanger 2
i	Number i
in	At the inlet
LP	Low pressure
p	Particle
s	Solid
w	Water

Figure 1
Click here to download high resolution image

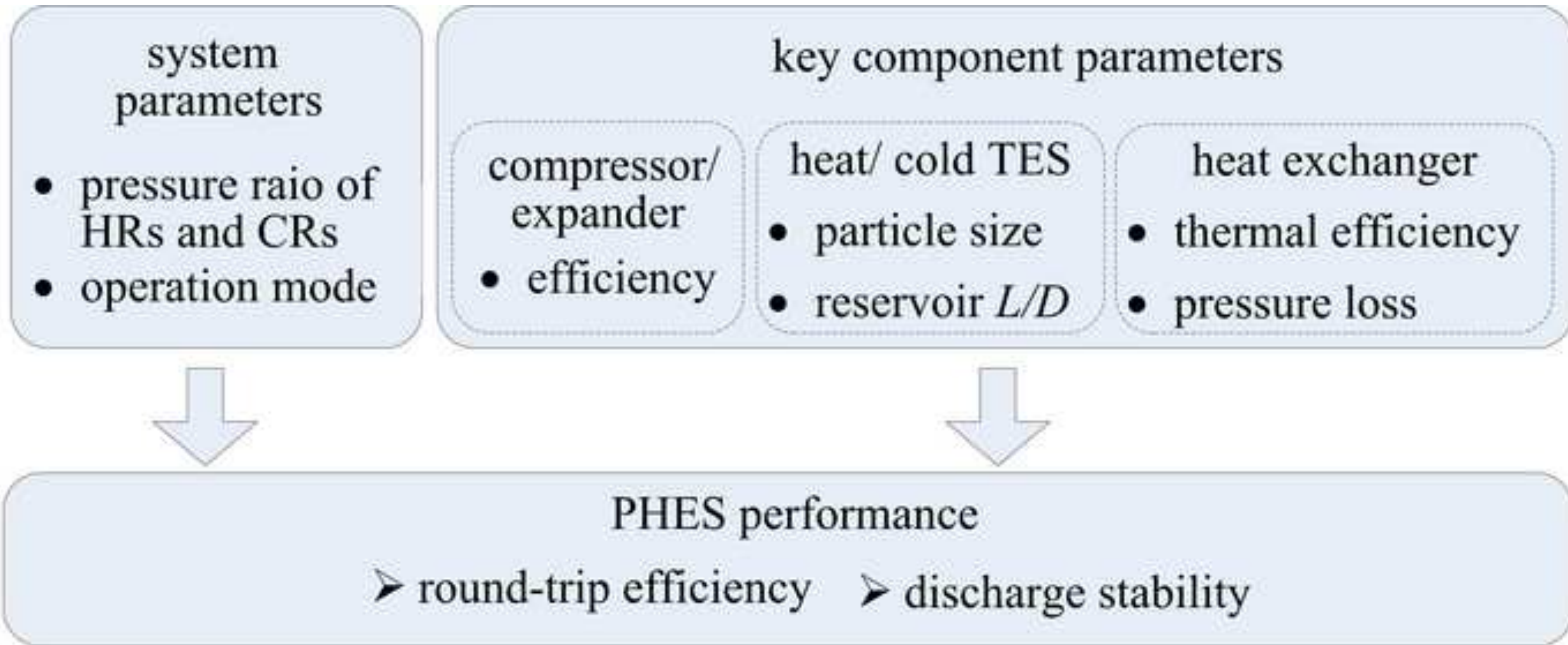

Figure 2
Click here to download high resolution image

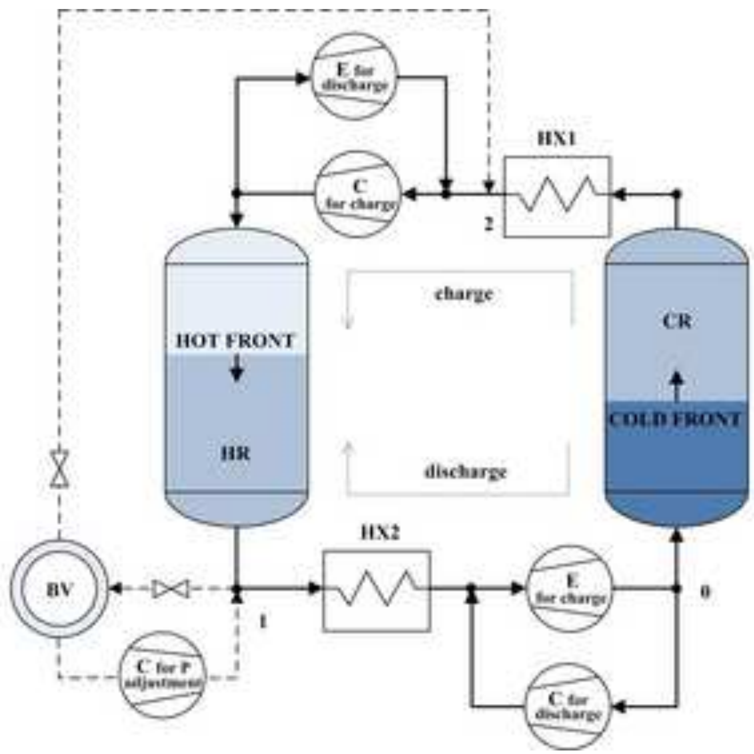

Figure 3
Click here to download high resolution image

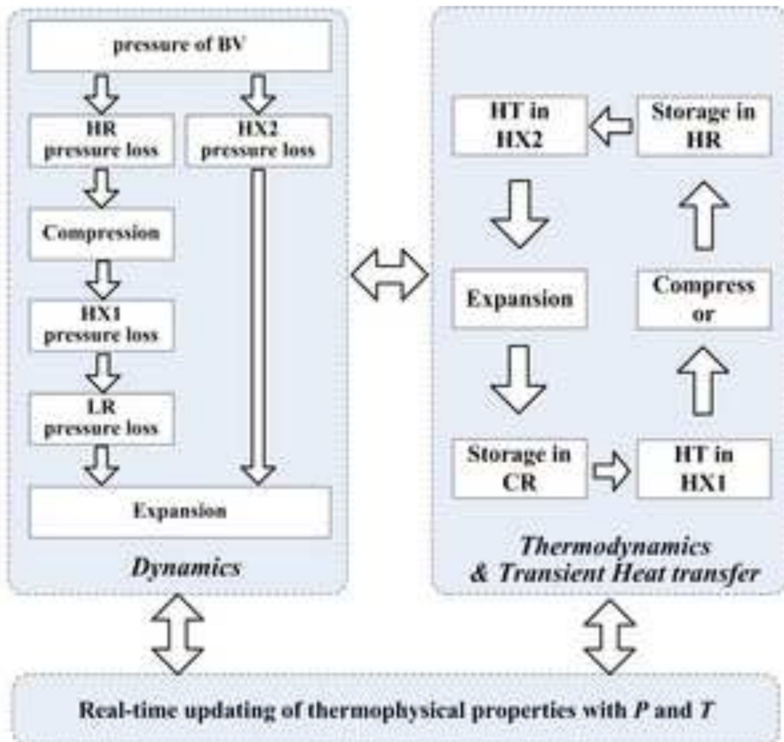

Figure 4a

Click here to download high resolution image

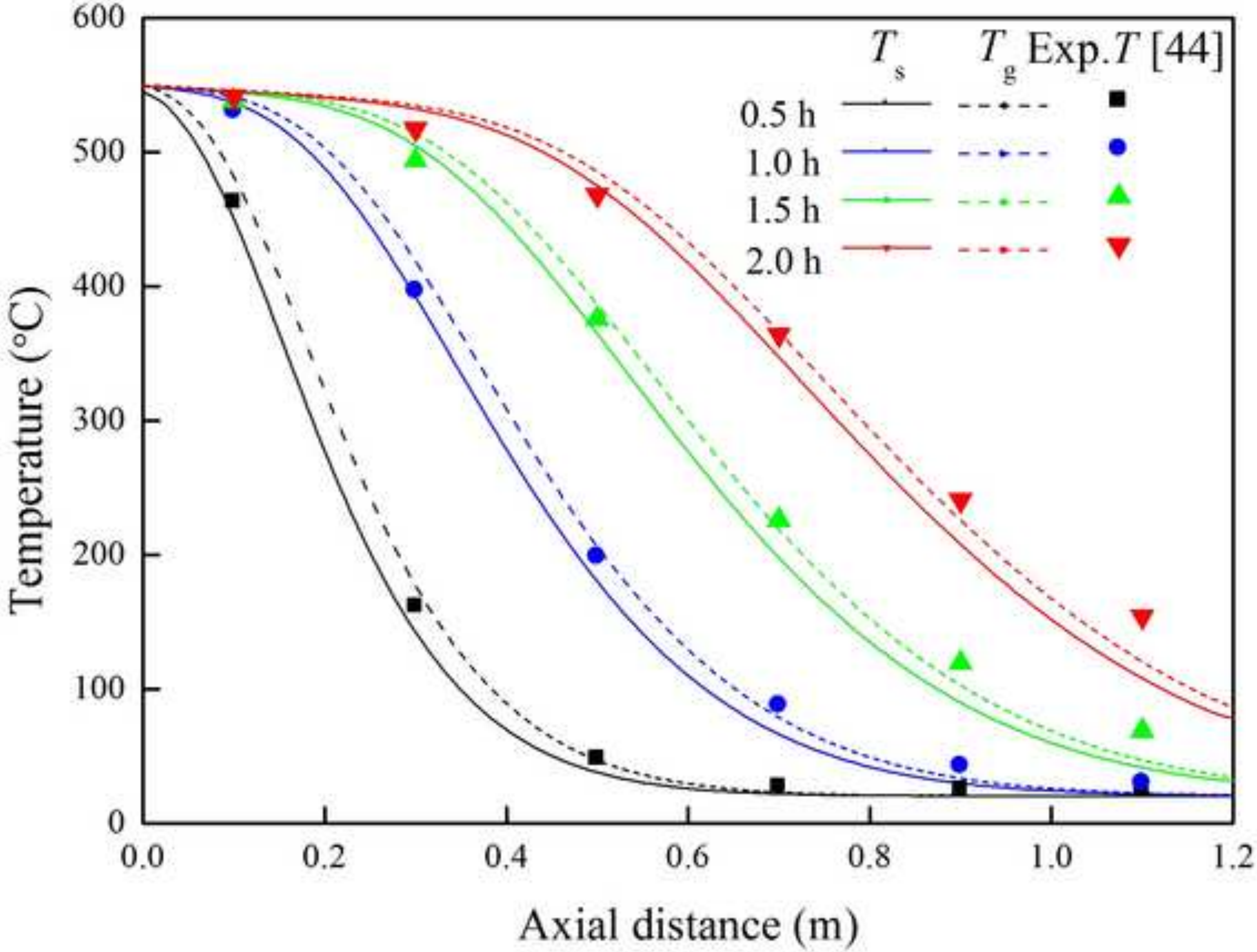

Figure 4b

Click here to download high resolution image

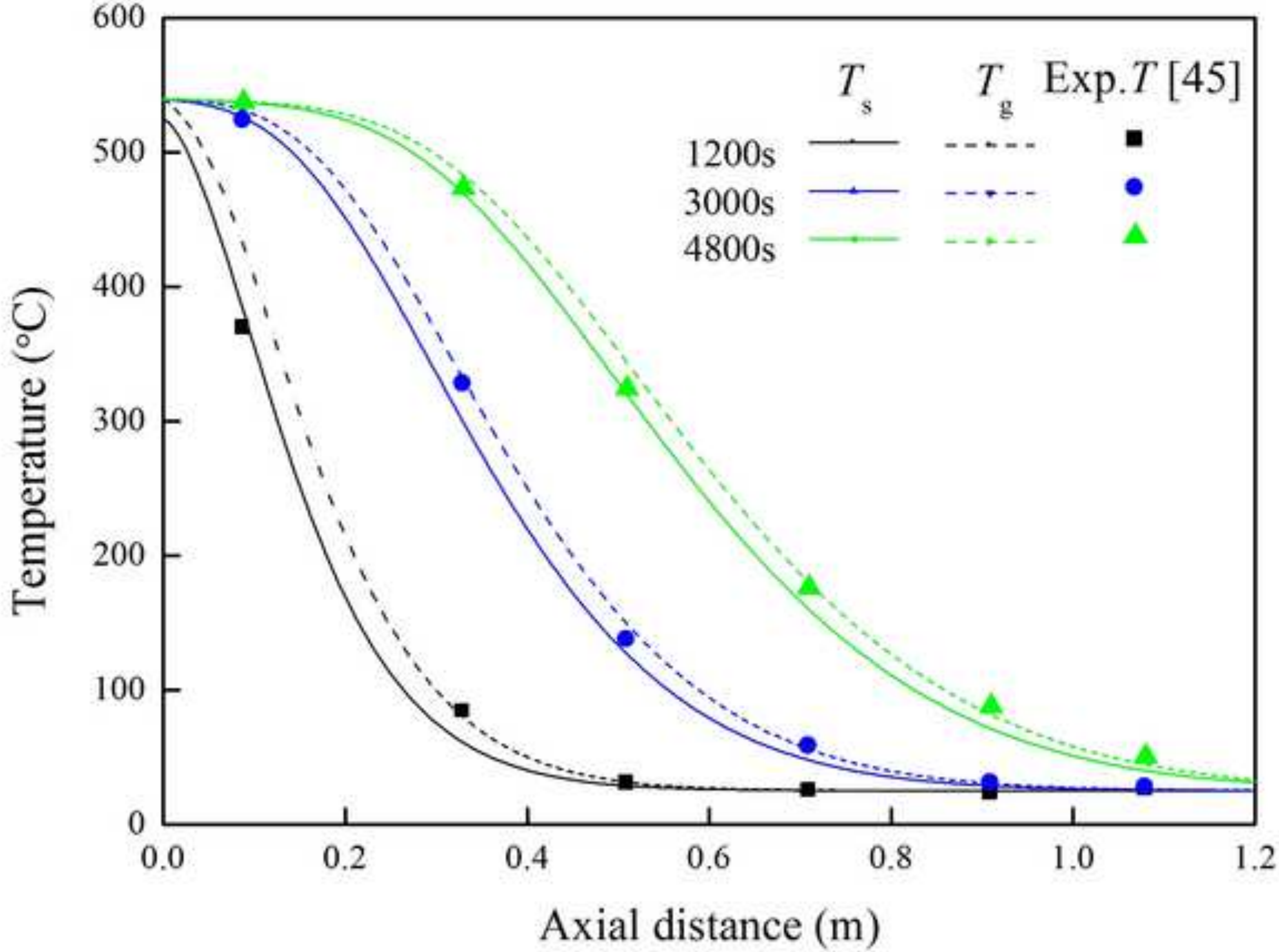

Figure 5
Click here to download high resolution image

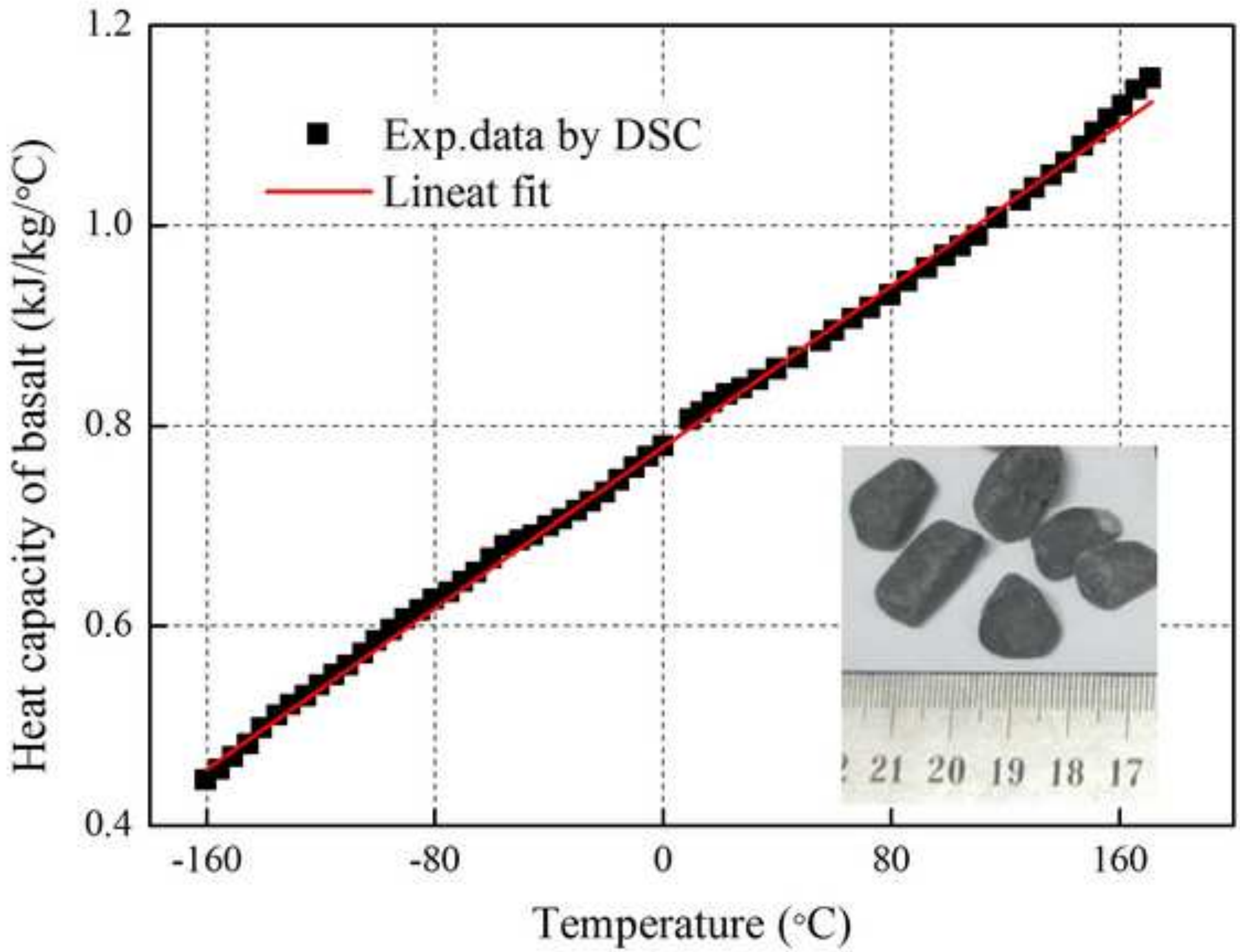

Figure 6a
Click here to download high resolution image

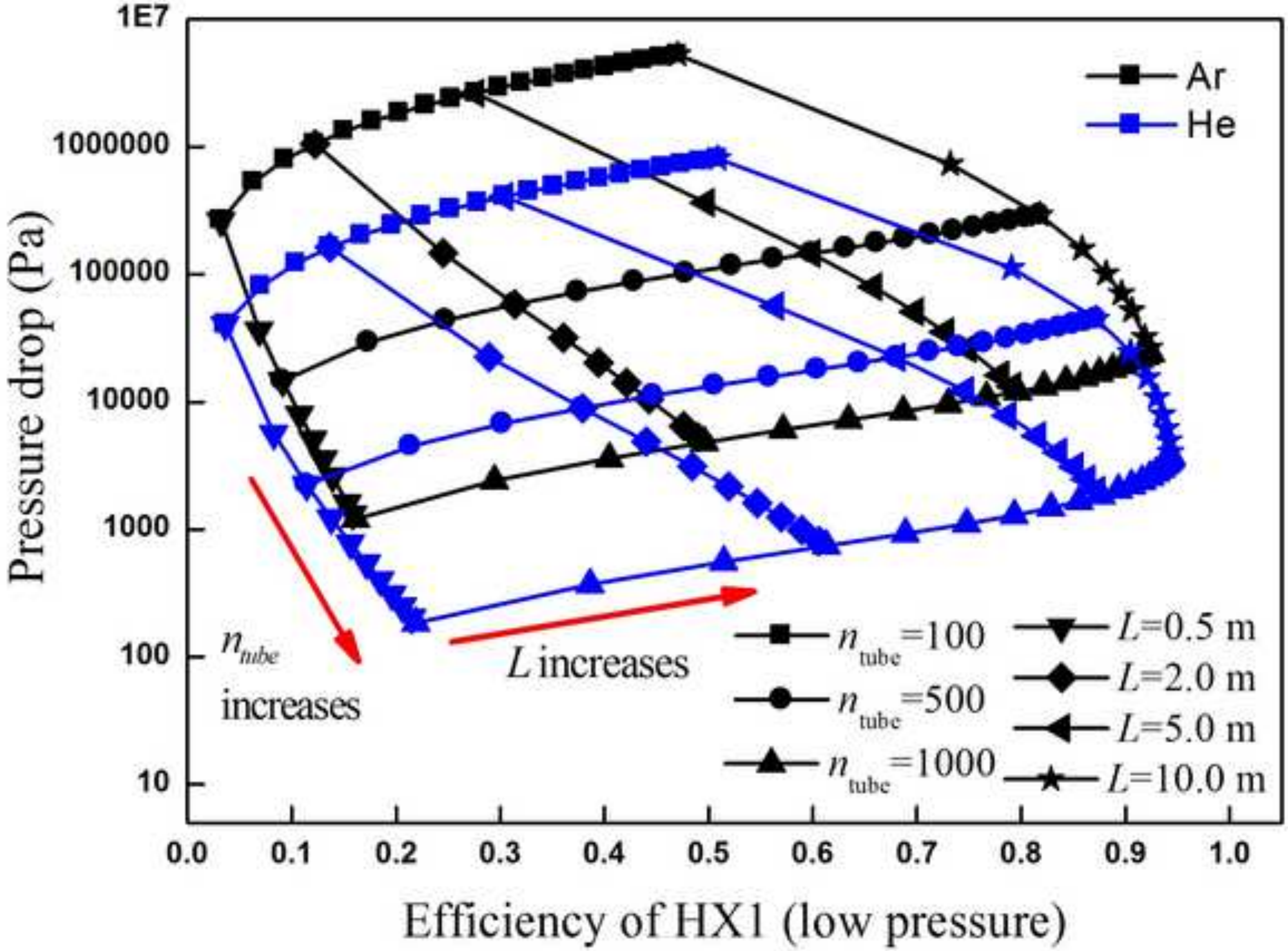

Figure 6b
Click here to download high resolution image

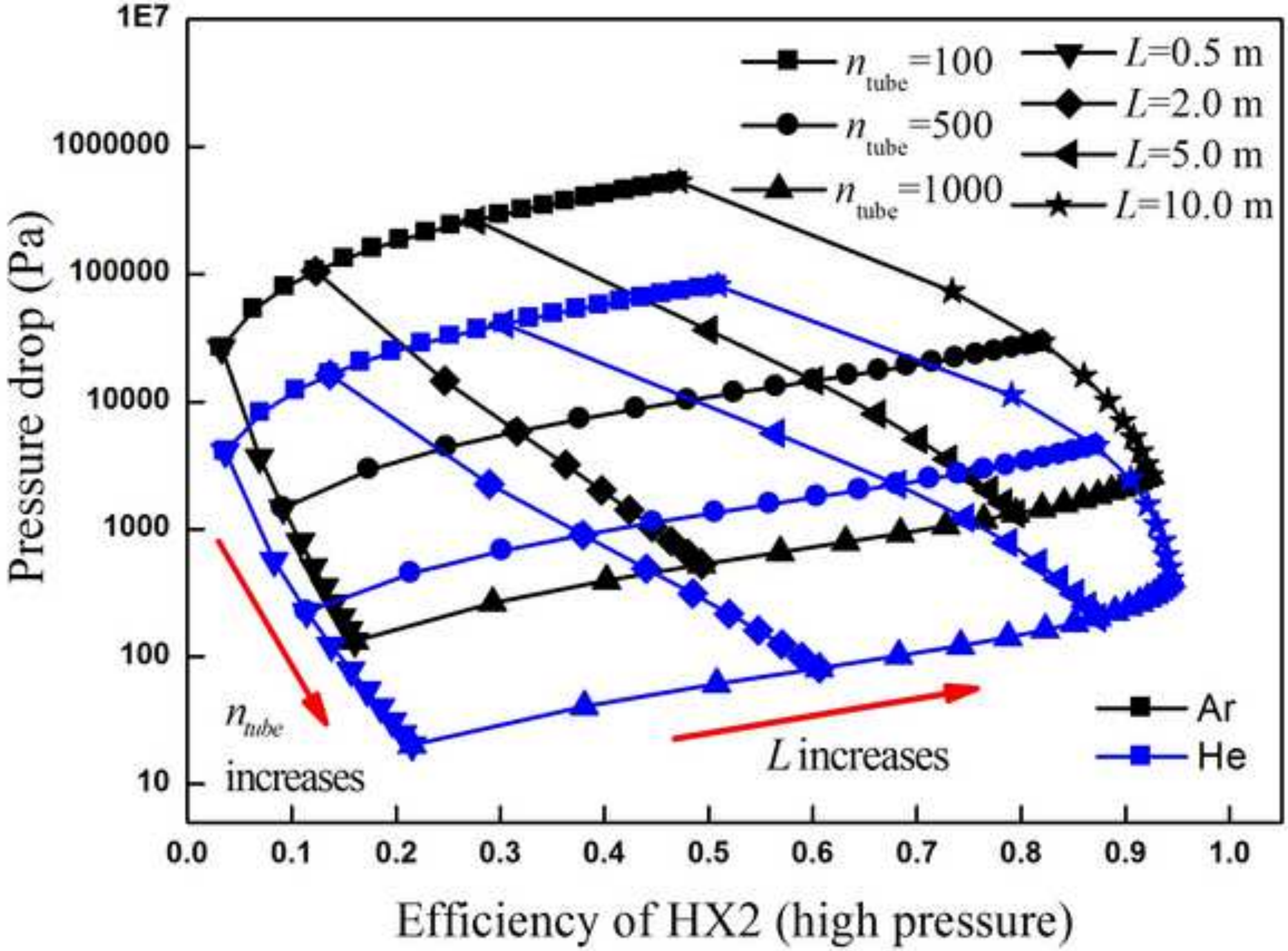

Figure 7a
Click here to download high resolution image

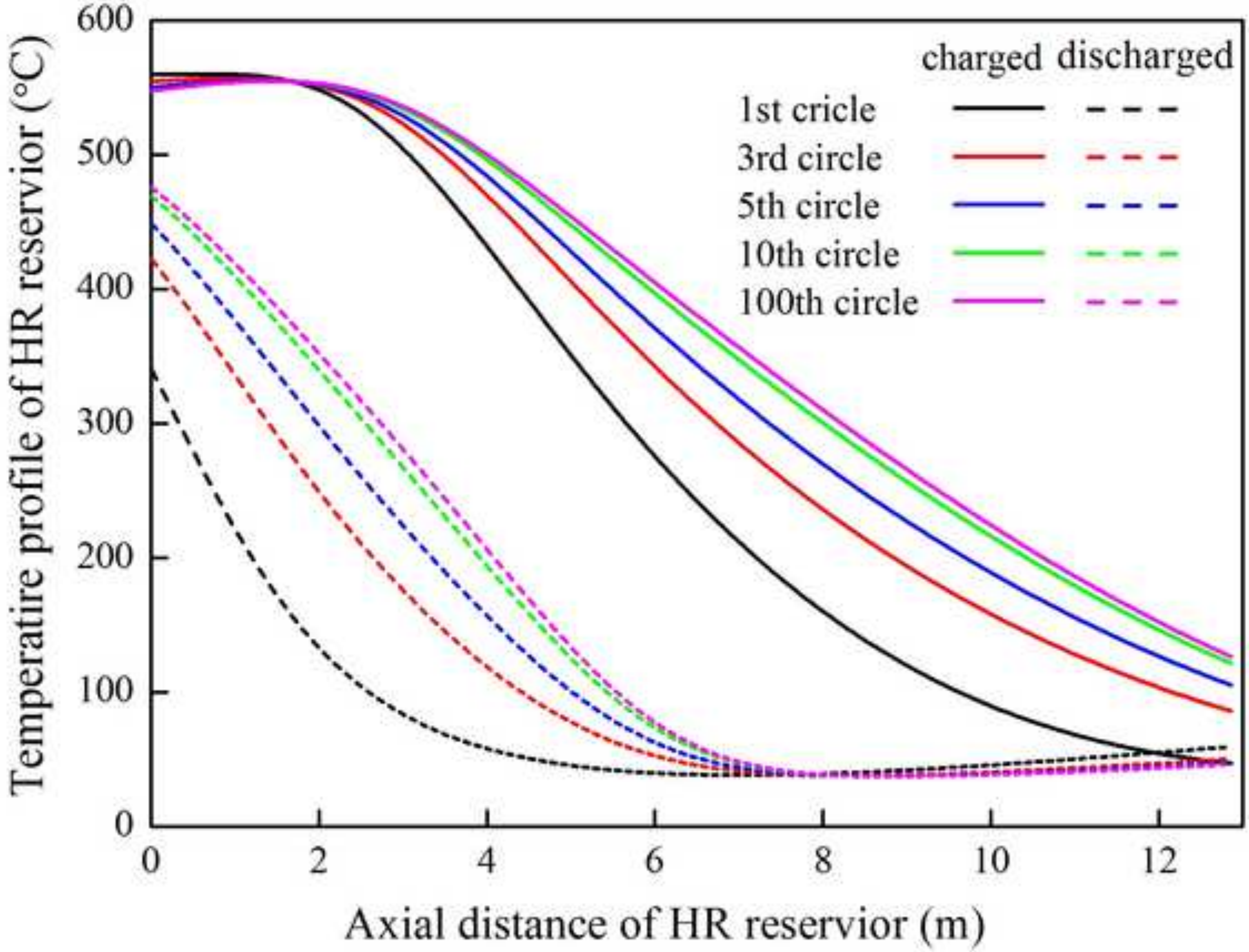

Figure 7b
Click here to download high resolution image

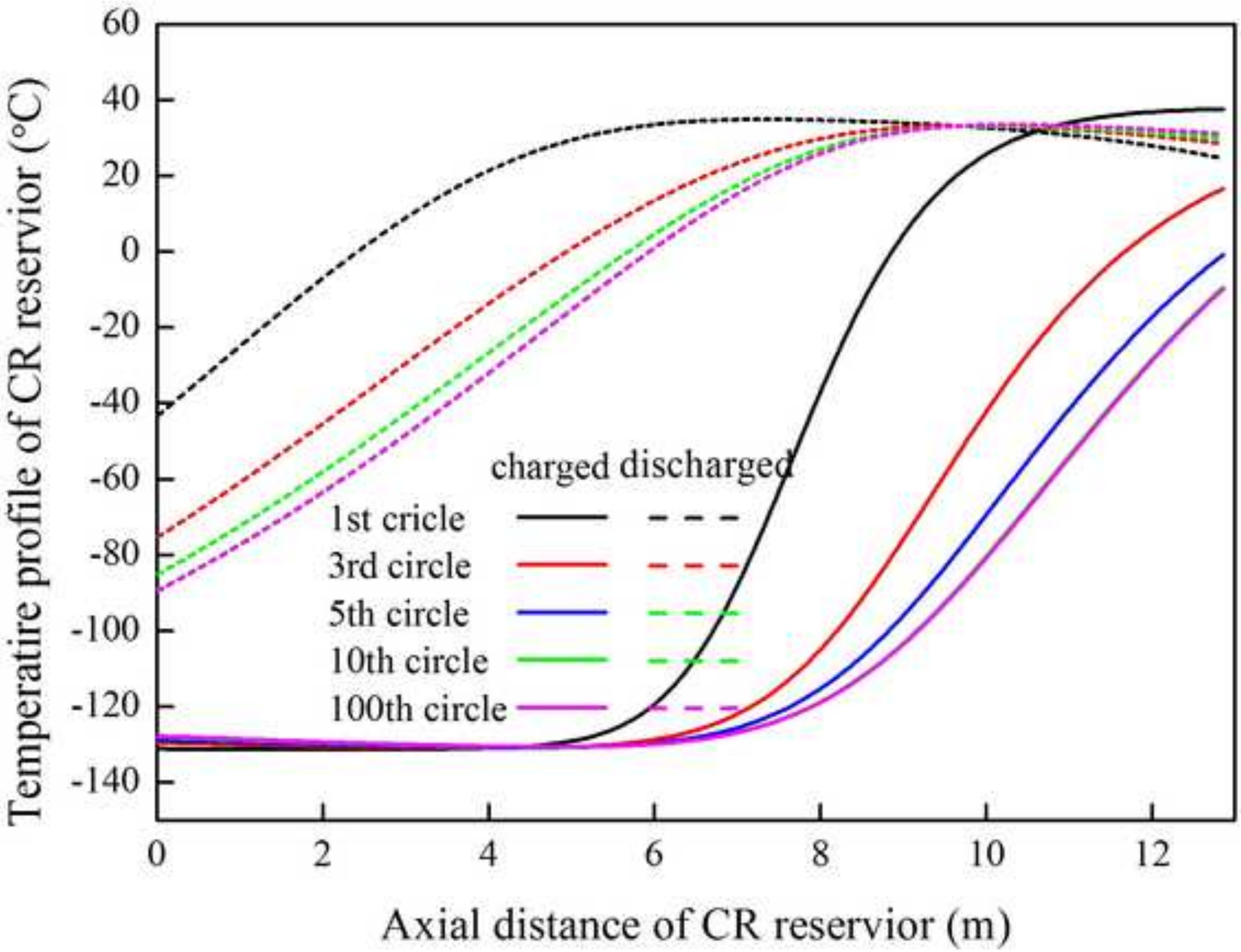

Figure 8
Click here to download high resolution image

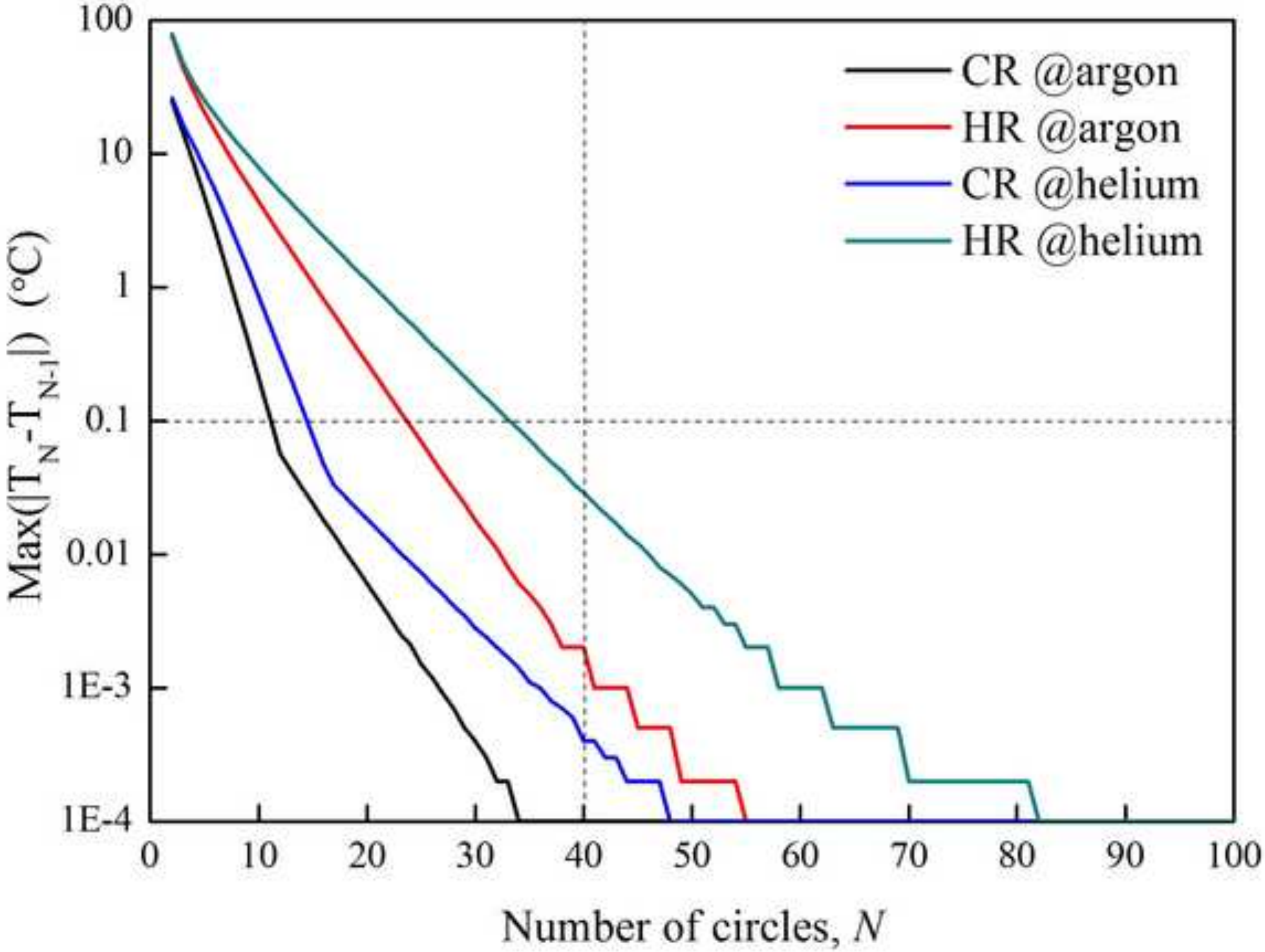

Figure 9a
Click here to download high resolution image

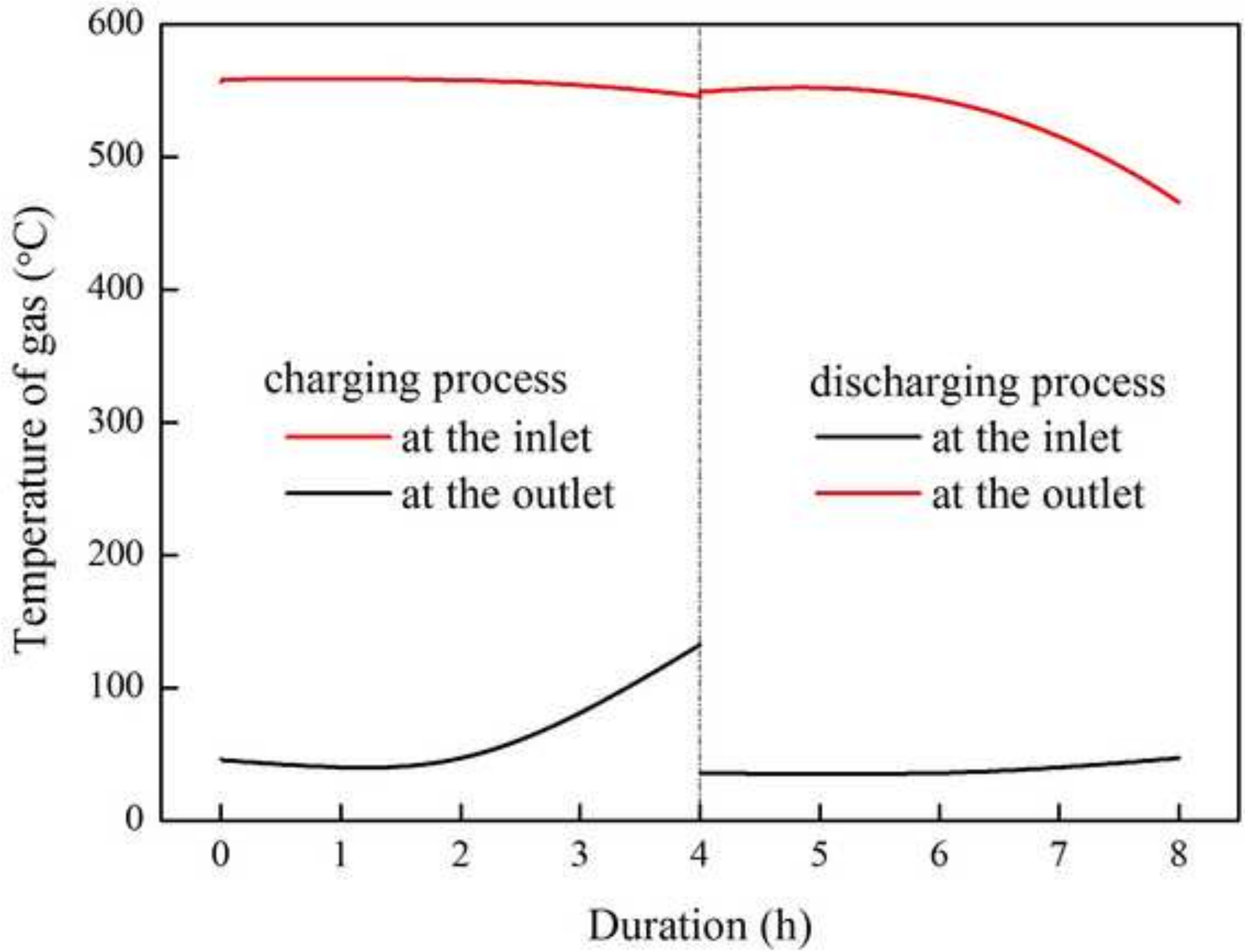

Figure 9b

Click here to download high resolution image

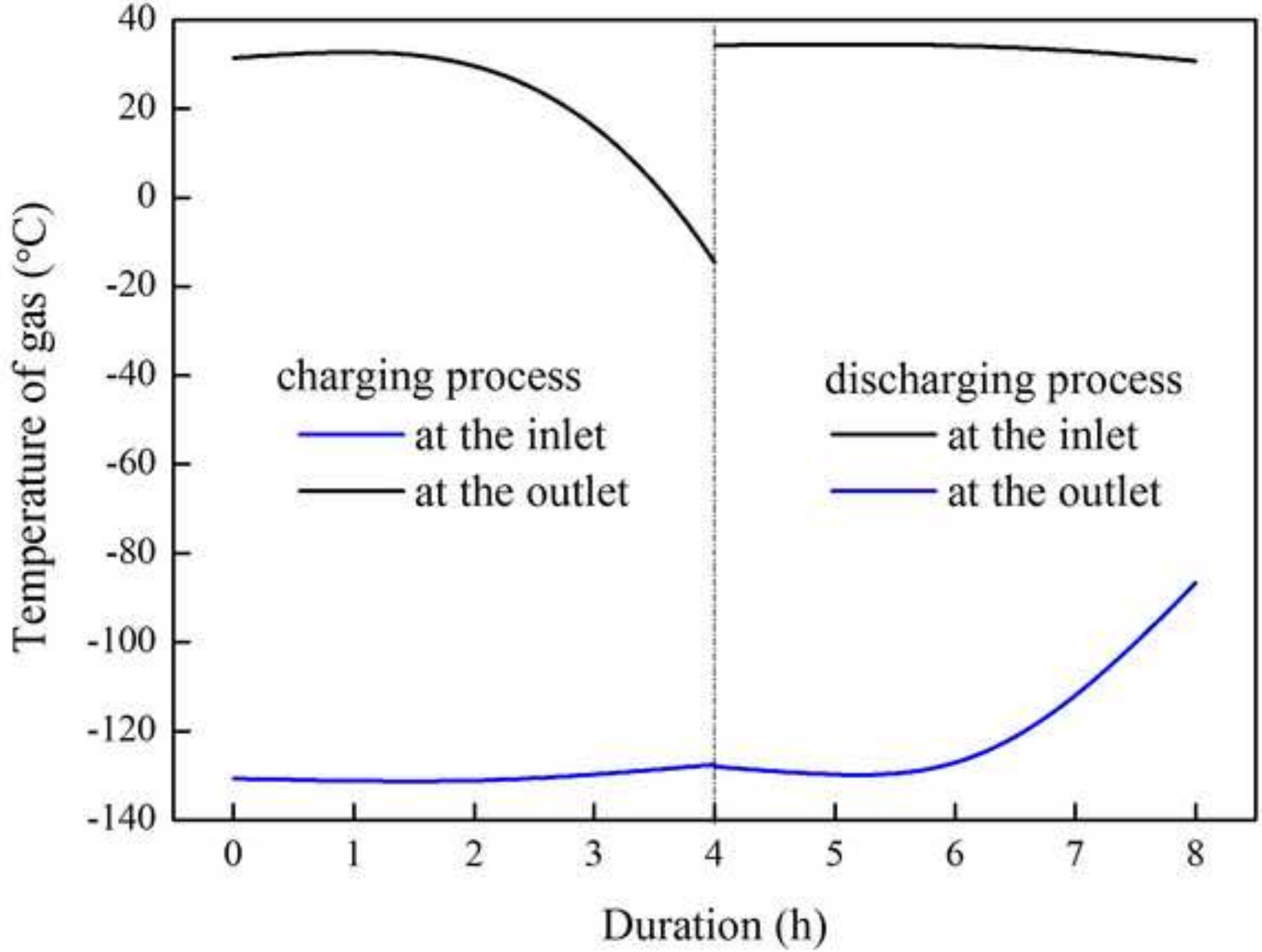

Figure 9c
Click here to download high resolution image

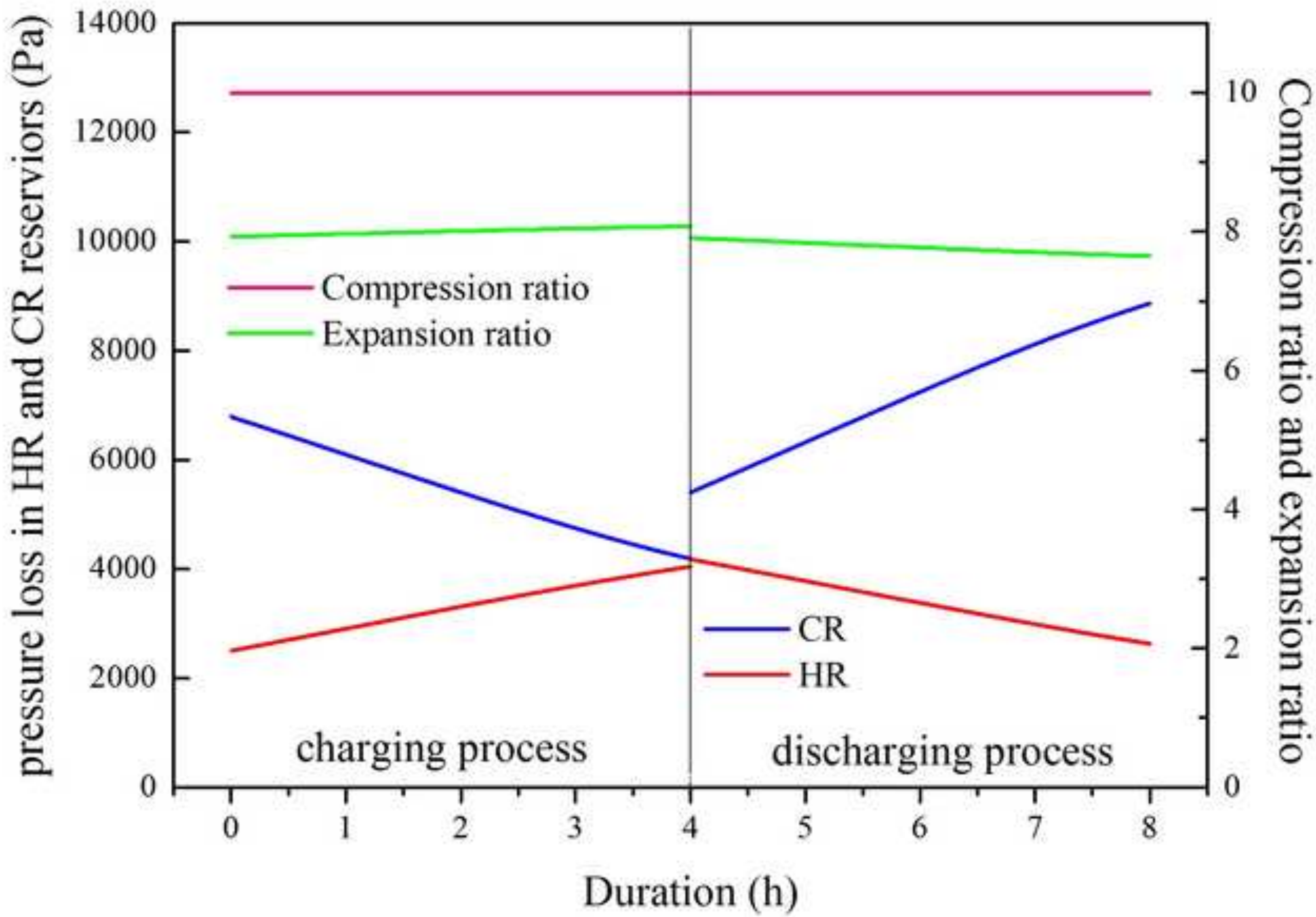

Figure 9d
Click here to download high resolution image

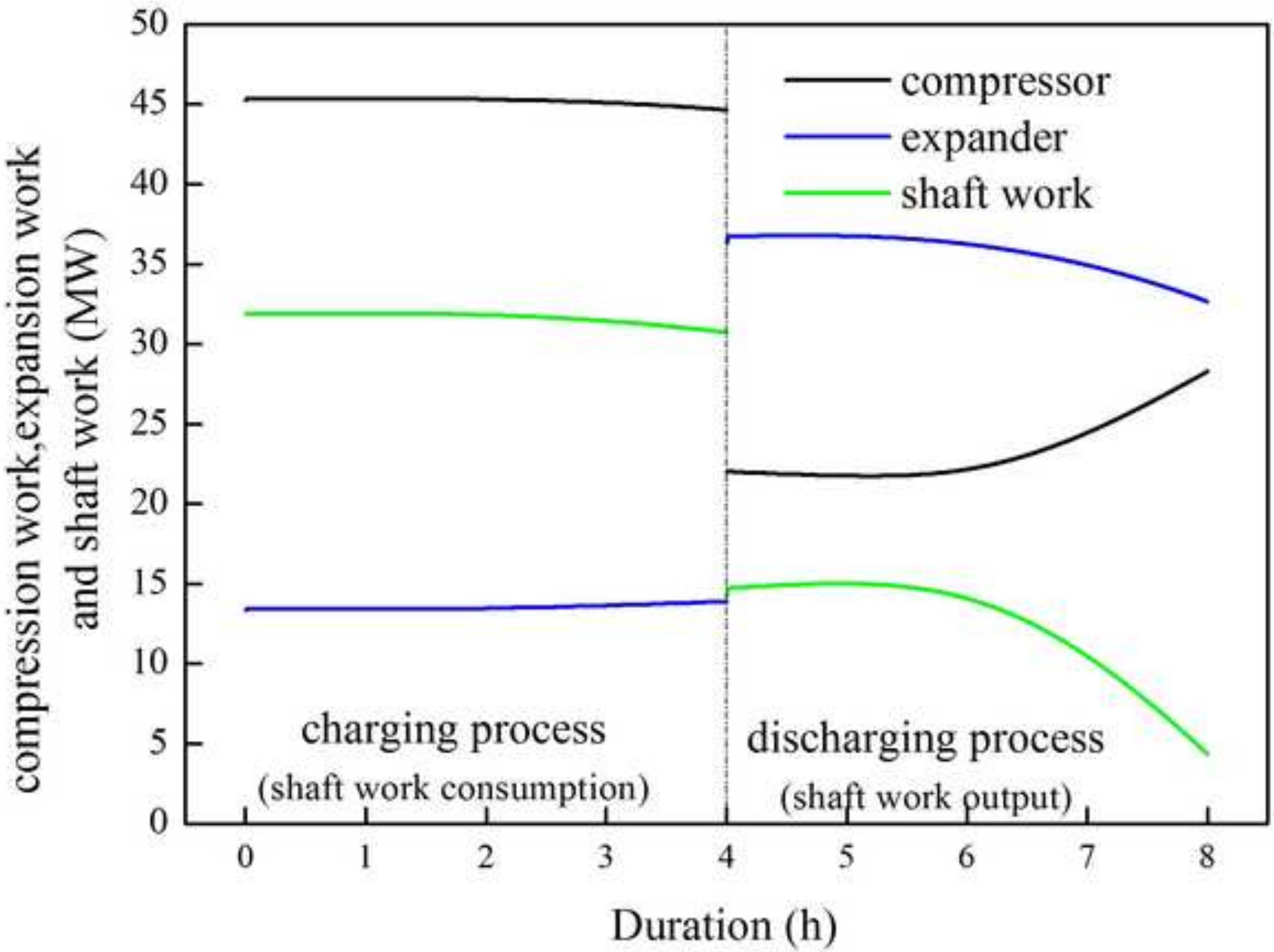

Figure 10a

Click here to download high resolution image

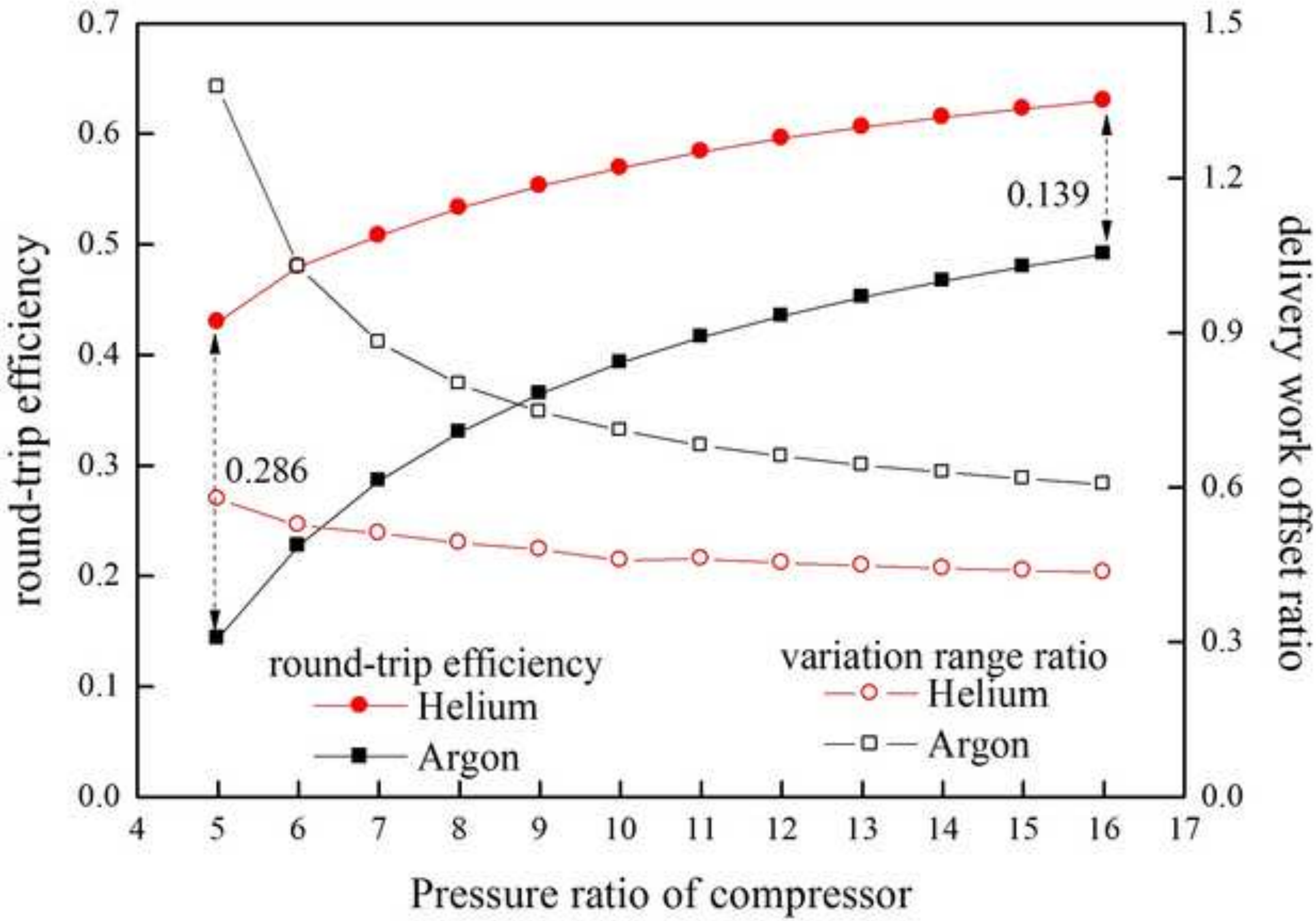

Figure 10b
Click here to download high resolution image

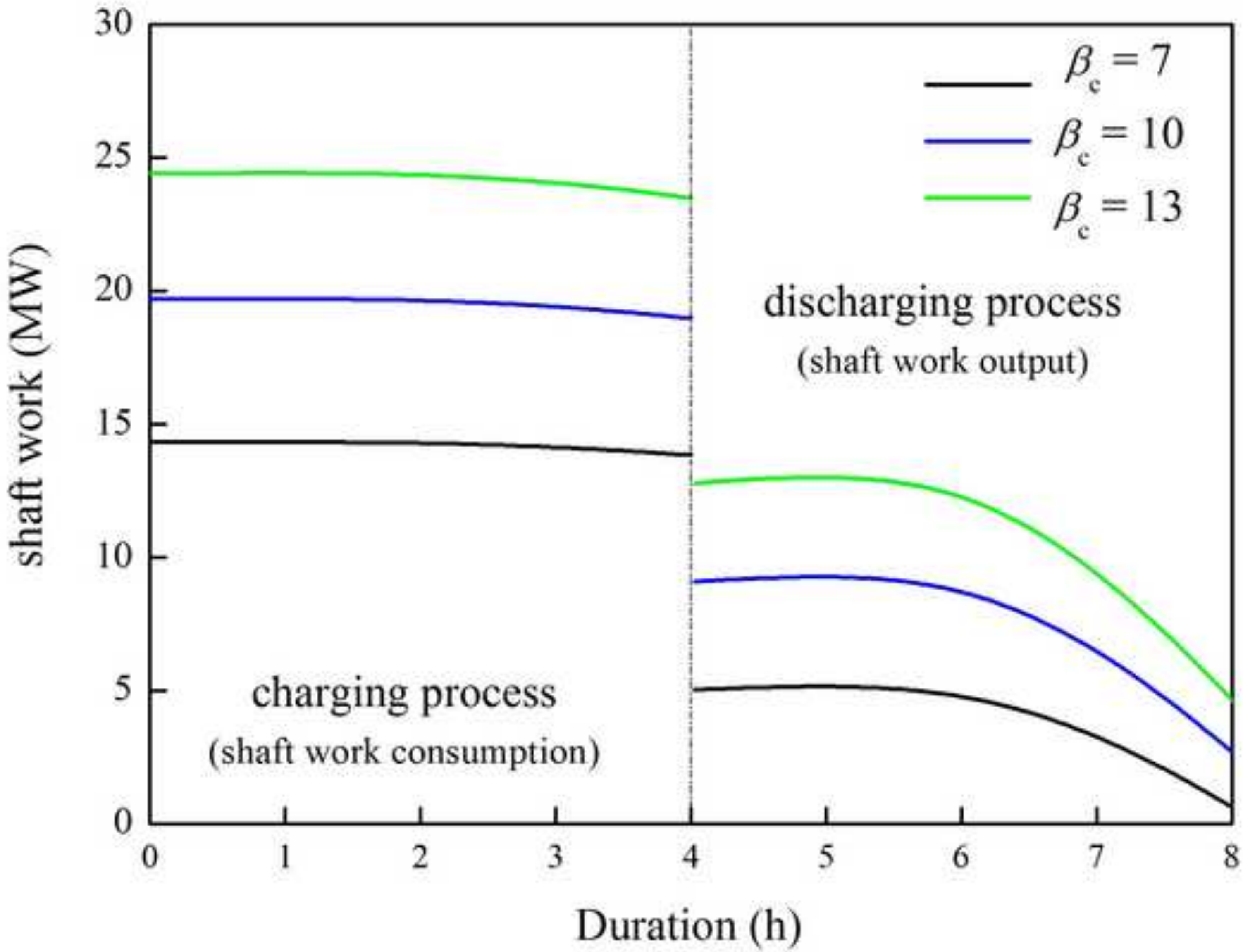

Figure 11a
Click here to download high resolution image

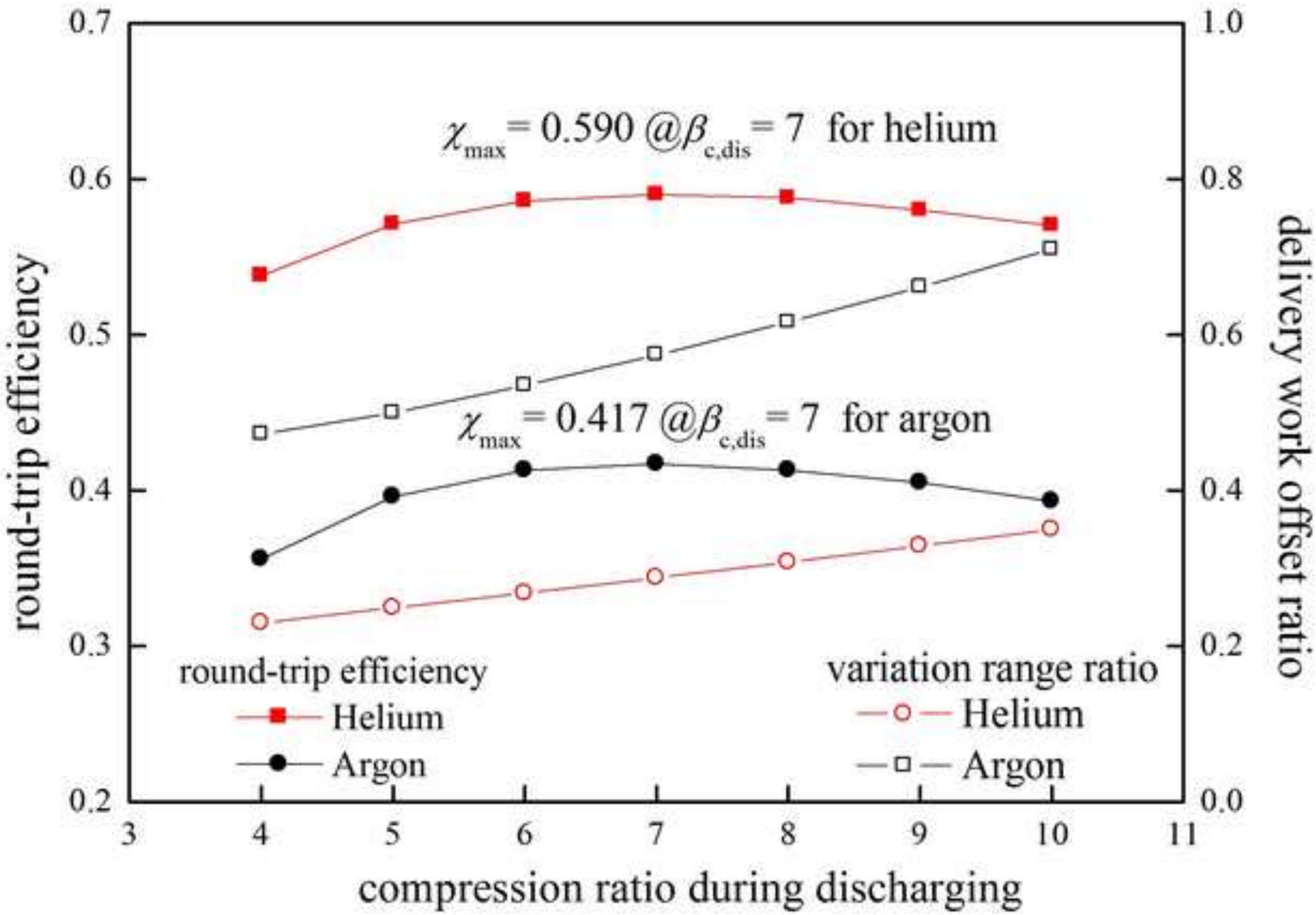

Figure 11b
Click here to download high resolution image

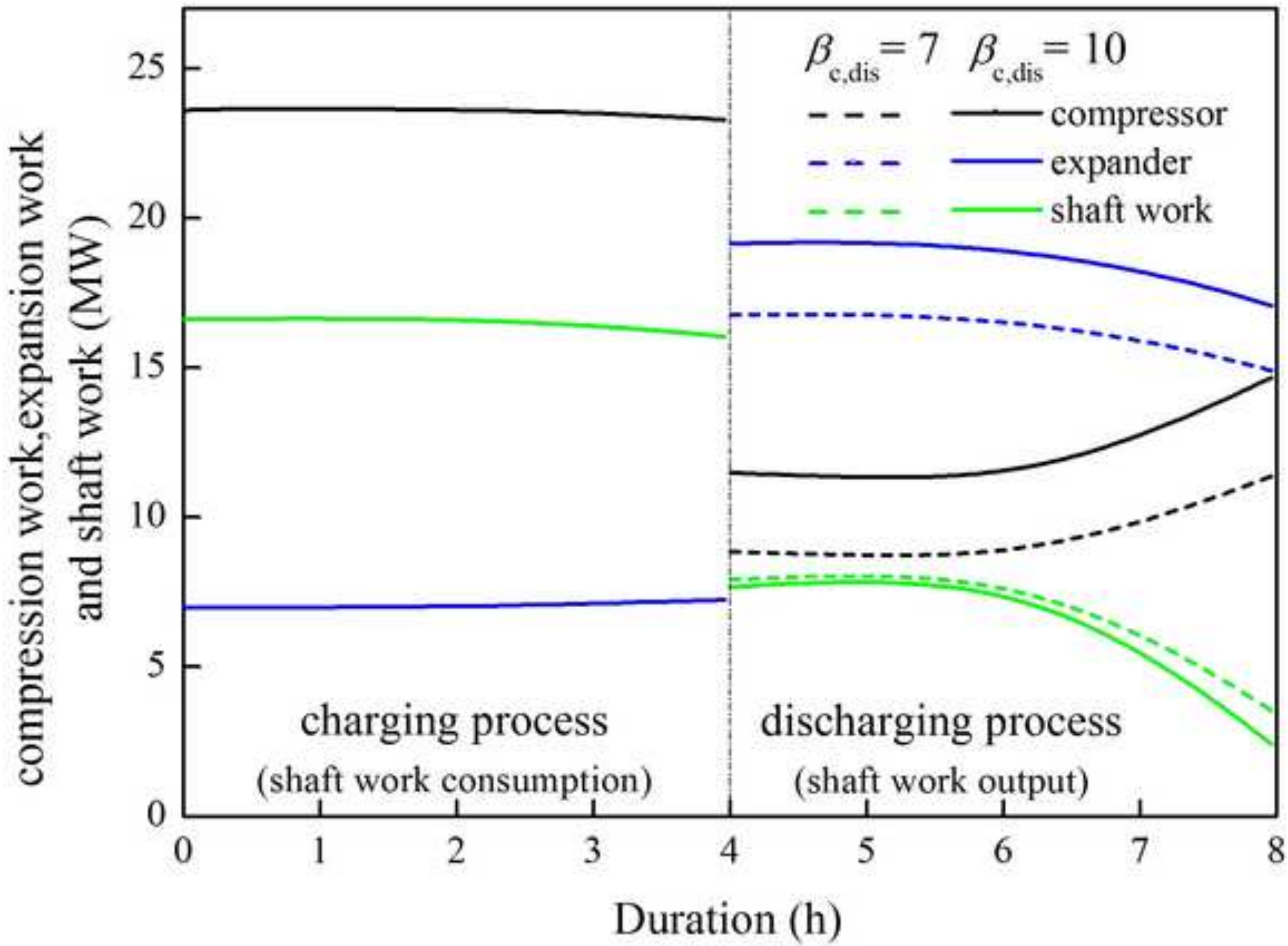

Figure 12
Click here to download high resolution image

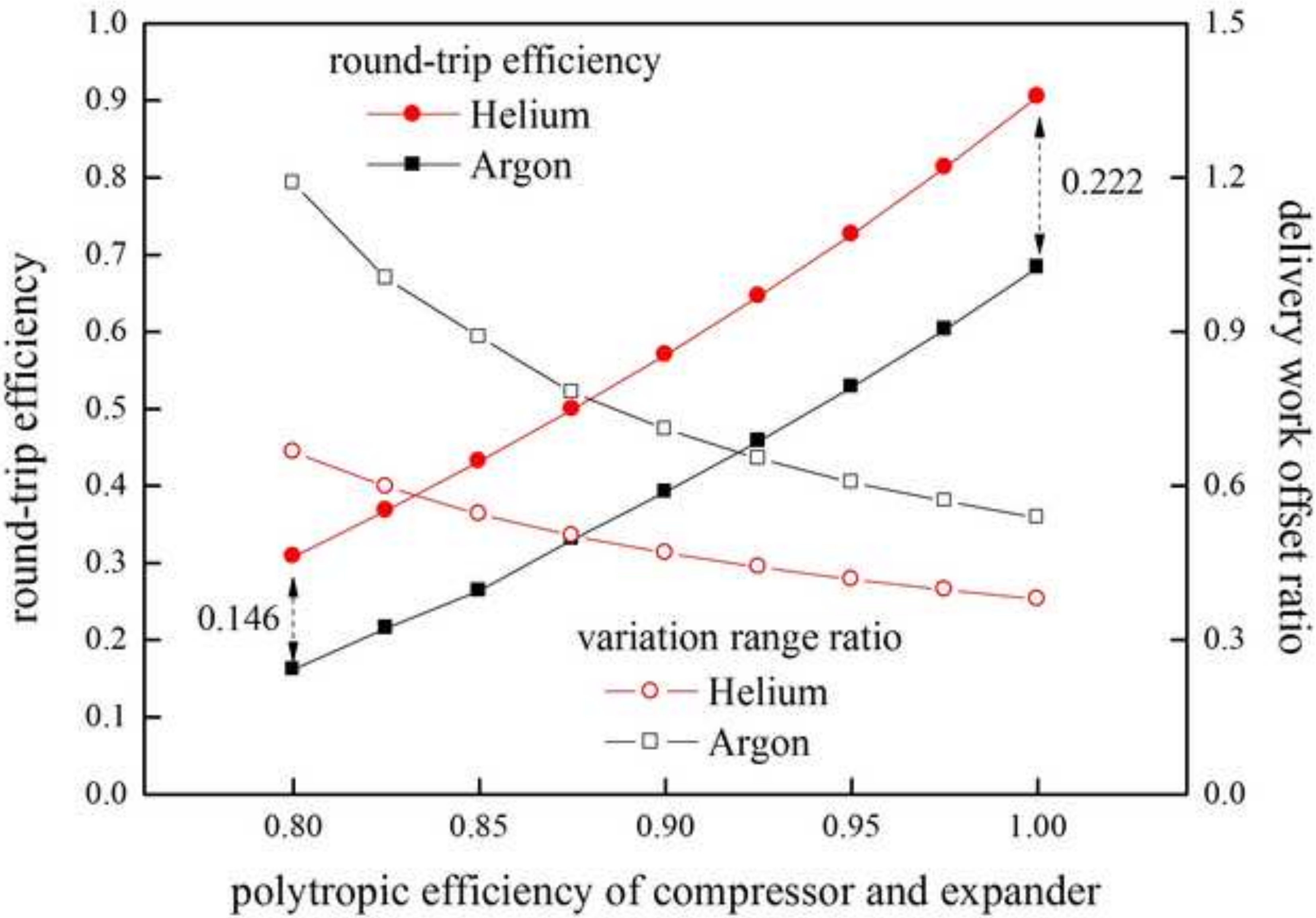

Figure 13a
Click here to download high resolution image

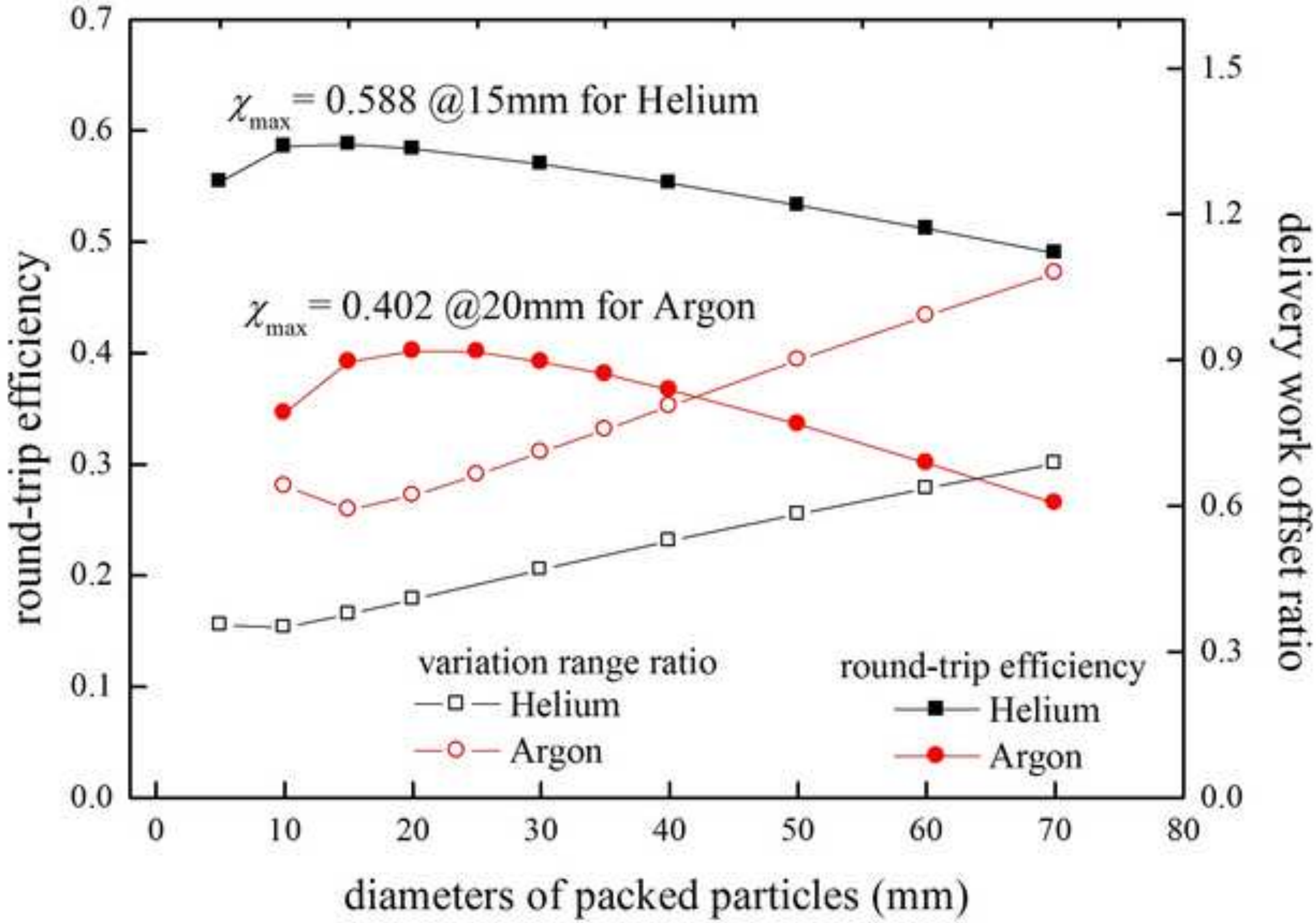

Figure 13b

Click here to download high resolution image

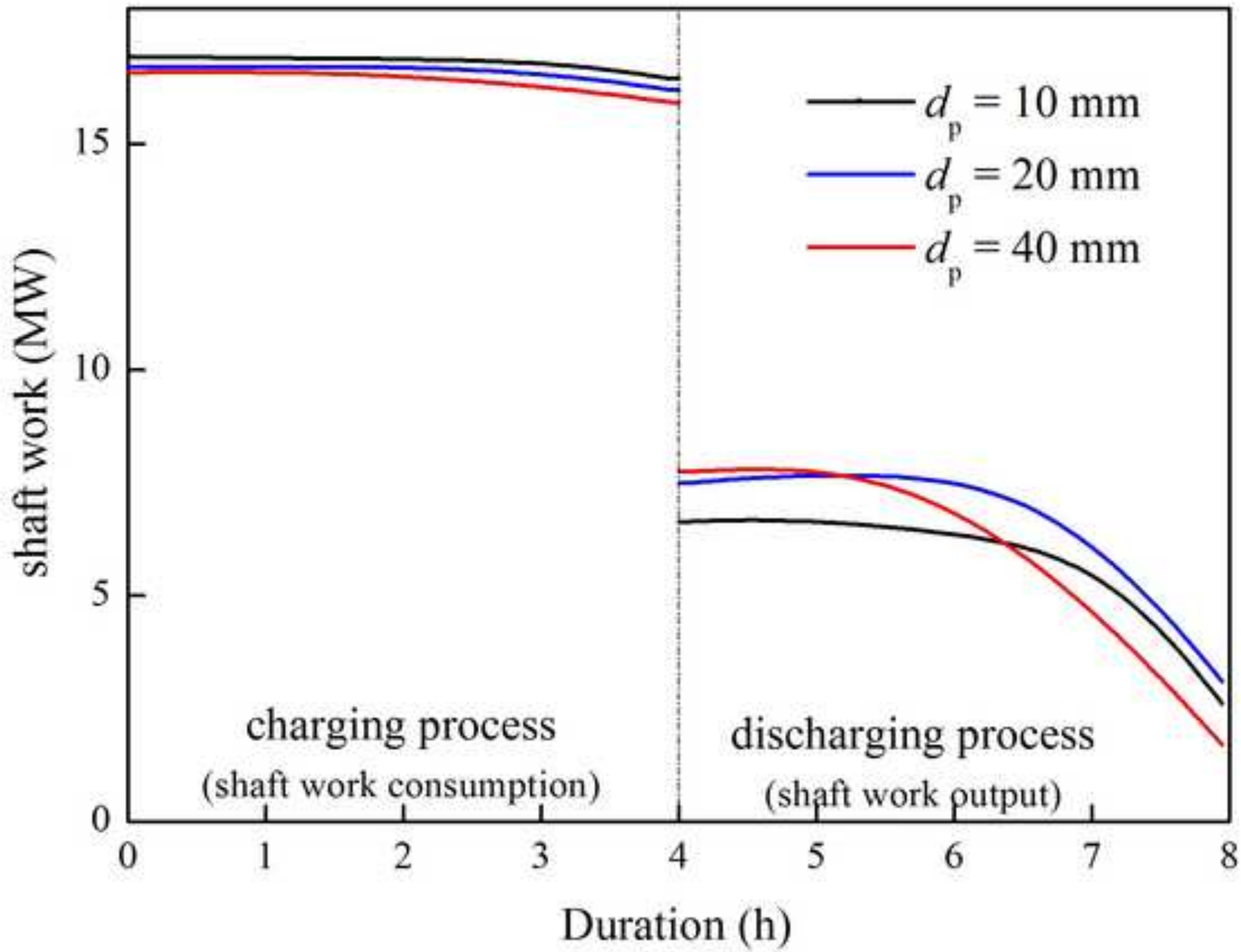

Figure 14a
Click here to download high resolution image

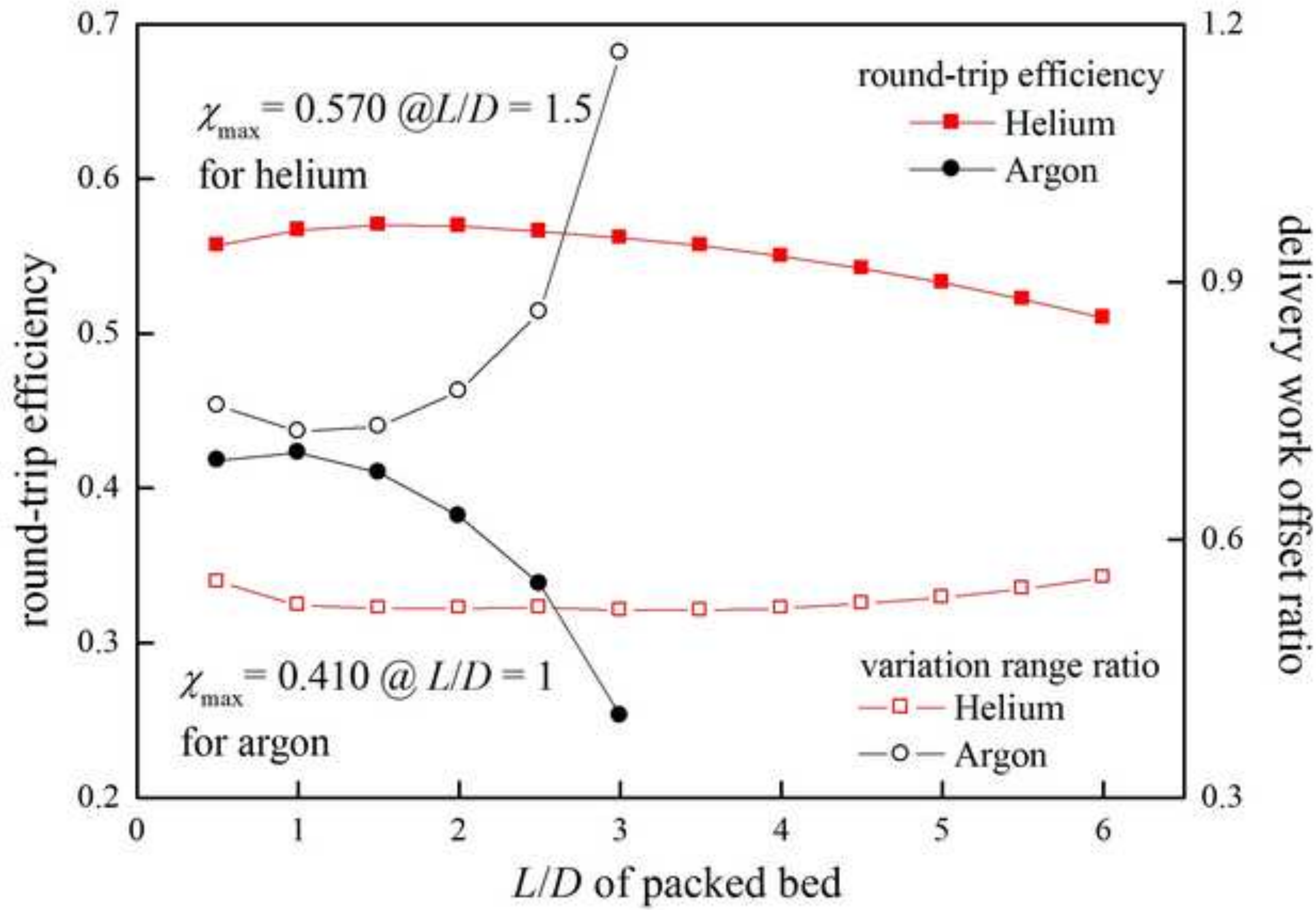

Figure 14b
Click here to download high resolution image

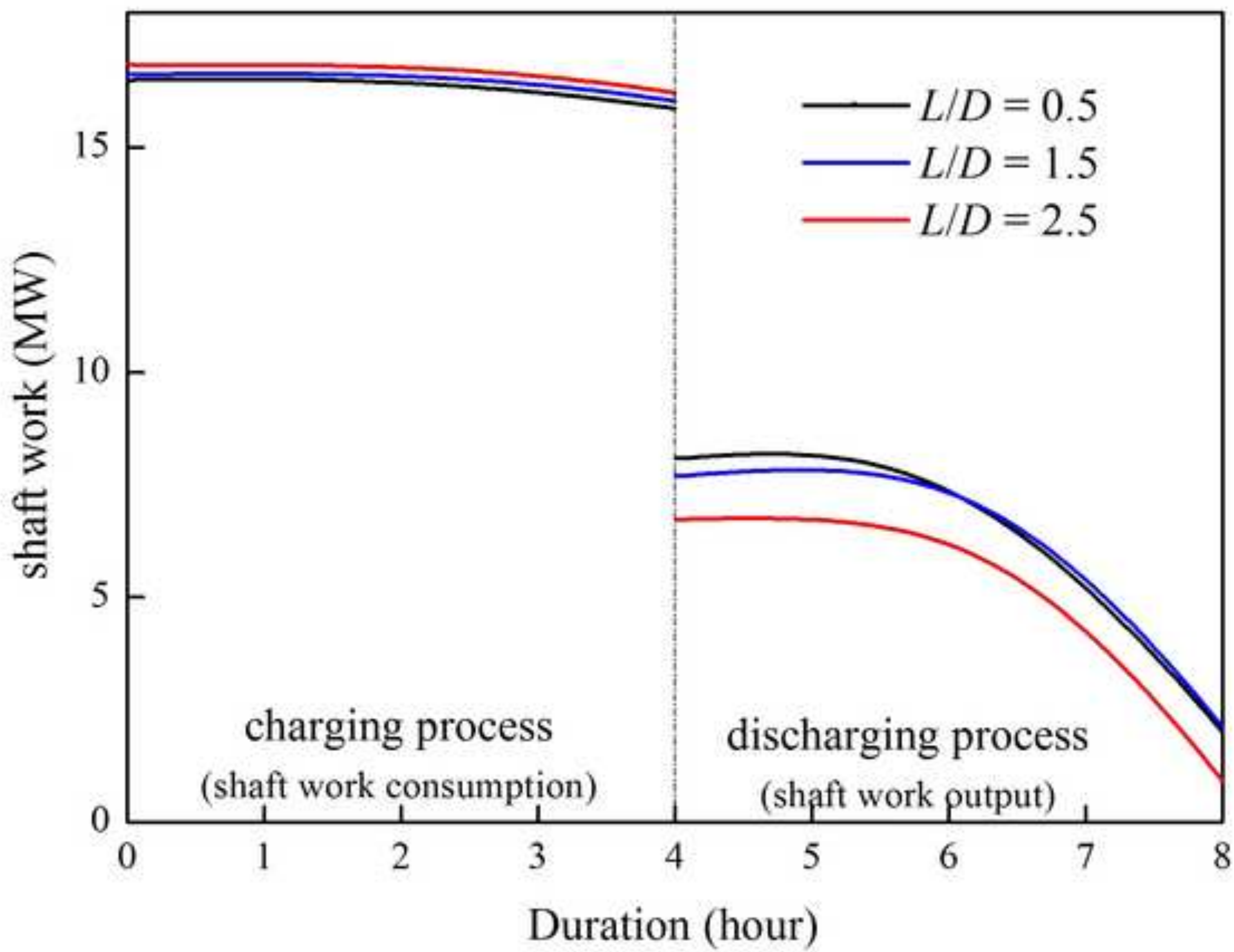

Figure 15
Click here to download high resolution image

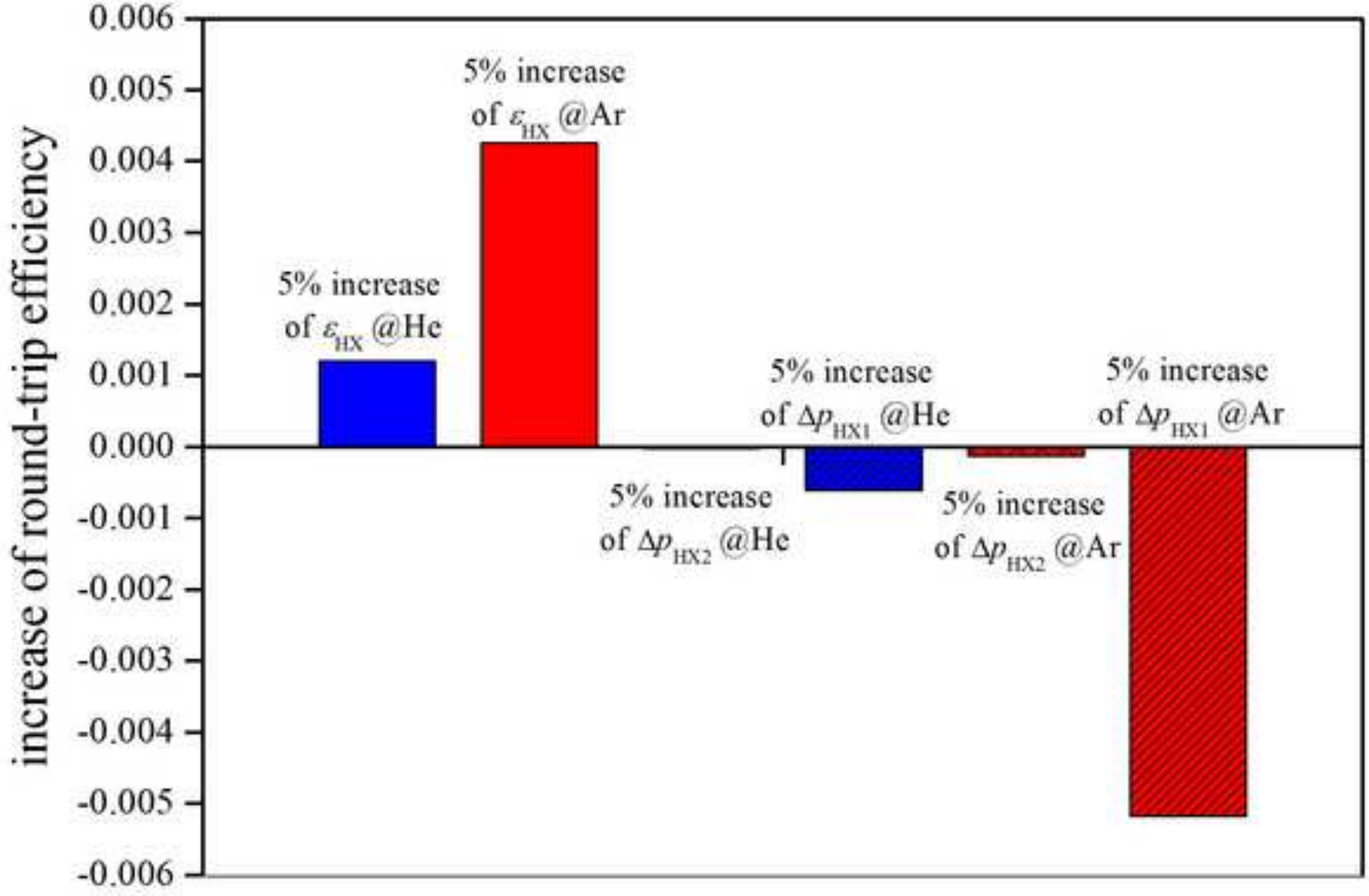

Figure 16a

Click here to download high resolution image

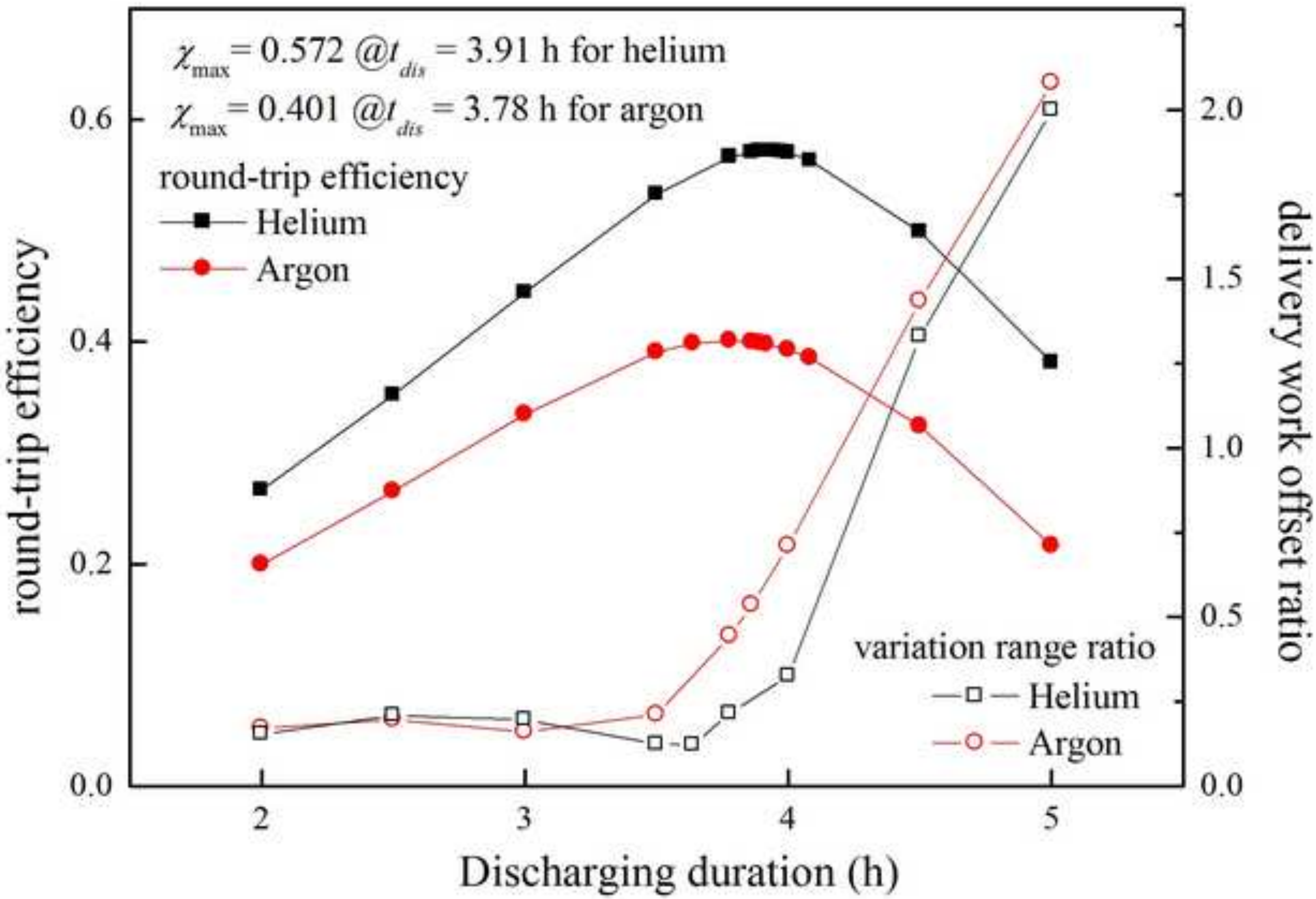

Figure 16b
Click here to download high resolution image

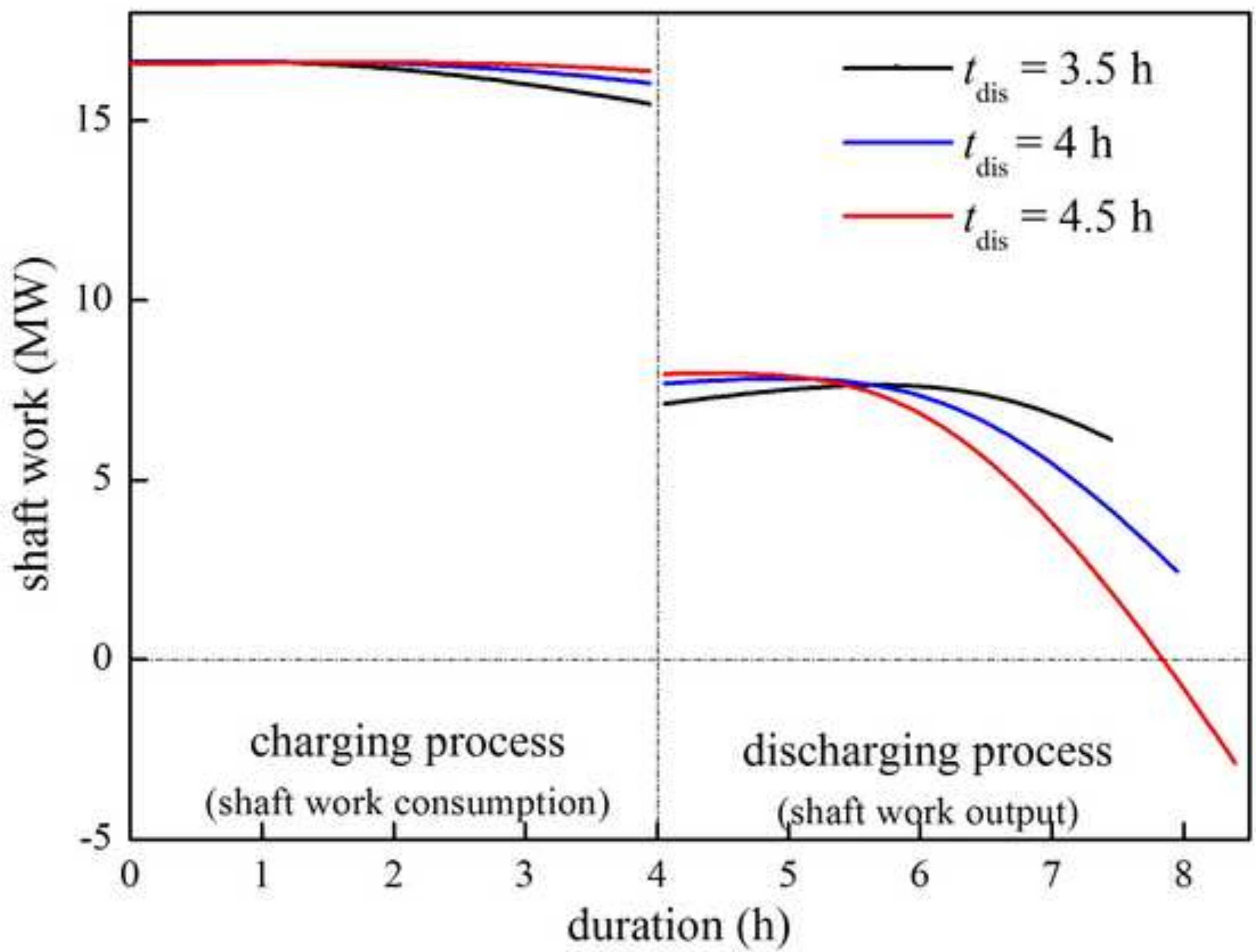

Figure 16c
Click here to download high resolution image

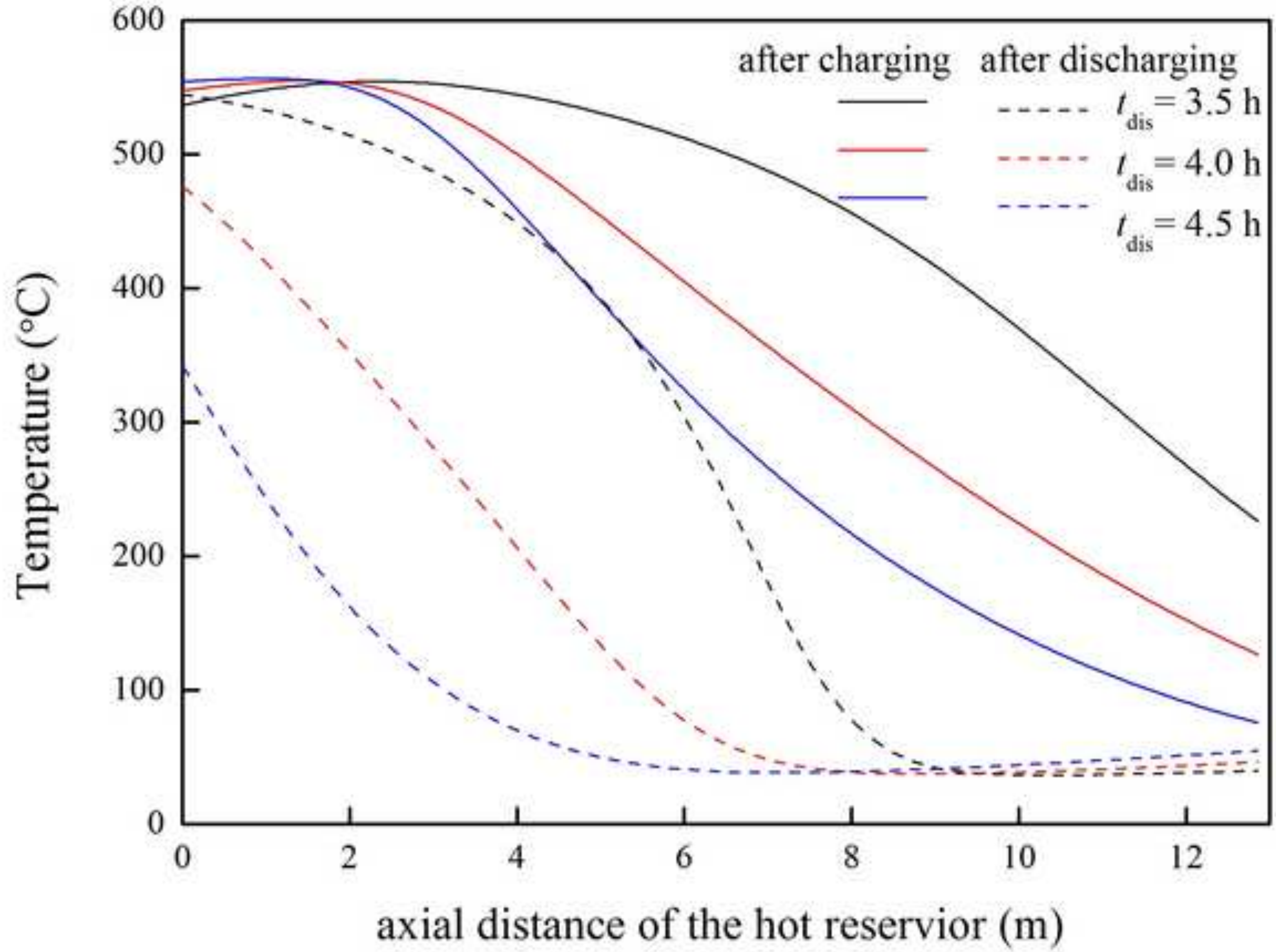

Table

Table 1 Designed parameters of PHES system of 10 MW discharging power

Working gas	HP Pressure (MPa)	LP Pressure (MPa)	Average $c_{p,g}$ (J/kg/K)	Mass flow rate (kg/s)	Polytropic efficiency	ε of HXs	$\triangle p$ of HP HXs (kPa)	$\triangle p$ of LP HXs (kPa)	Cooling water temperature (K)
Argon	1.05	0.105	525	85.1	0.9	0.9	3	20	300
Helium	1.05	0.105	5193	8.6	0.9	0.9	0.3	2	300

Table 2 Hot and cold reservoir details for 10 MW/4 h PHES system (the total volume is twice the minimum design volume)

Reservoir	Pressure (MPa)	Density of solid material (kg/m^3)	Porosity	Average d_p (mm)	Total Volume (m^3)	L (m)	D (m)
Heat	1.05	5175	0.35	30	460	10.96	7.31
Cold	0.105	5175	0.35	30	740	12.86	8.56

*Highlights

Highlights

- The transient analysis method for PTES system is proposed.
- The cyclic transient of 10MW/4h Joule-Brayton PTES is studied.
- Both the round-trip efficiency and delivery stability of the PTES are discussed.
- Helium has the overwhelming advantage above argon as the working gas.
- Impact of particle sizes and length to diameter ratio of packed bed was analyzed.